BIOFILM DISTRIBUTION IN A POROUS MEDIUM ENVIRONMENT EMULATING SHALLOW SUBSURFACE CONDITIONS

by

KaeLee Frances Massey

A thesis submitted in partial fulfillment
of the requirements for the degree

of

Master of Science

in

Chemical Engineering

MONTANA STATE UNIVERSITY
Bozeman, Montana

December 2021

DEDICATION

For my family and friends who have always encouraged me to push myself to be successful and given me unconditional support.

ACKNOWLEDGEMENTS

My utmost respect and gratitude go to Matthew Fields, who has been a constant source of encouragement and guidance throughout my experiences here at Montana State University. Thanks also go to my graduate committee for their efforts, advice, and guidance, Dr. Matthew Fields, Dr. Heidi Smith, and Dr. Robin Gerlach. I would also like to thank the members of the Fields' lab, past and present, for teaching a chemical engineering student how to think like a microbiologist. Thank you to everyone in the Center for Biofilm Engineering and the Chemical and Biological Engineering Department for all of your knowledge throughout the years.

I am grateful to the U.S. Department of Energy's ENIGMA program for financial and professional support throughout my graduate studies.

Thank you to my family and friends for their lasting support and encouragement throughout this process. I would also like to thank Kalyn Brown for always showing empathy, support, and bringing me coffee on the longest of days. Lastly, I would like to thank my two cats, Gizmo and Pico, for letting me hold them even when they don't want to be held.

TABLE OF CONTENTS

1. INTRODUCTION 1

A Need for Clean Water 1
The Shallow Subsurface Environment 1
Fluid Dynamics of the Shallow Subsurface Environment 3
Microorganisms in the Shallow Subsurface 4

2. BACKGROUND 10

Oak Ridge National Laboratory 10
Thesis Goals 12

3. BIOFILM DISTRIBUTION IN A POROUS MEDIUM REACTOR EMULATING SHALLOW SUBSURFACE CONDITIONS 13

Contribution of Authors and Co-Authors 13
Manuscript Information Page 15
Abstract 16
Introduction 17
Materials and Methods 21
Reactor Design and Construction 21
Sampling Protocols 23
Particle Size Distribution 24
Inoculum Sources and Preparation 25
Reactor Preparation 27
Reactor Sampling 28
Biomass Analysis - Protein 29
Total and Active Cell Enumeration 30
DNA Extraction, Sequencing, and Analysis 31
Epoxy Embedded and Imaging 32
Substrate Concentration Model 33
Results 36
Particle Size Distribution 36
Total Cell Protein 39
Cell Abundances – Porous Material 39
Planktonic Effluent Cell Abundances 41
Embedded Core and Confocal Imaging 42
Concentration Model 46
Microbial Community Analysis 47
Discussion 54
PBR Reactors 55

TABLE OF CONTENTS CONTINUED

Porous Media Visualization....56
Biomass and Cell Concentration....56
Diversity and Richness....58
Cell Localization Discussion....59
Conclusion....62

4. CONCLUSIONS....64

REFERENCES CITED....68

APPENDICES....75

APPENDIX A: Supplementary Information for Chapter 1....76
APPENDIX B: SGW Groundwater and Exo-Metabolite Composition....100
APPENDIX C: Characterization of a Packed Bed Reactor System at Field Relevant Flow Rates....104
APPENDIX D: Fluorescent Microsphere Bead Distribution in a Porous Medium Reactor Emulating Shallow Subsurface Conditions....125
APPENDIX E: Determining How Inoculating Methods Influence Biofilm Distribution in a Porous Medium Reactor....143

LIST OF TABLES

Table Page

1. Sediment samples collected from the FRC and used for particle size distribution analysis 25

2. Geochemical properties and flow paths of the three areas at the FRC 26

3. Field site area and well information for bug trap samples 27

4. Flow rate used for the experiment and its calculated hydraulic properties 28

5. Averaged molecular weights (g/mol), initial concentrations (µM), and estimated diffusion coefficients of the five different categories of substrates in the exo-metabolite solution 35

6. Average percentage of particle sizes measured from the sediment cores collected from the FRC 37

7. Average total protein and standard deviation for each reactor 39

8. Averaged BONCAT and total cell concentration (DAPI) for triplicates samples from each reactor 40

9. Averaged BONCAT and total cell concentration for each reactor as well as the calculated activity percentage for each reactor 41

10. Average planktonic cell concentration and standard deviation for each reactor 41

11. Summary of cell distance measurements from Confocal microscopy for each pH condition. 42

B.1. SGW groundwater media recipe 101

B.2. Salt solution recipe for SGW groundwater media 101

B.3. Exo-metabolite solution composition for SGW groundwater media 101

LIST OF TABLES CONTINUED

Table Page

C.1. Data summaries for the FRC background area 109

C.2. Low flow rate bromide sampling plan 111

C.3. High flow rate bromide sampling plan.....112

C.4. Reactor characteristics for bromide breakthrough experiments at the low flow 113

C.5. Hydrology of reactors for bromide breakthrough experiments at the low flow 114

C.6. Reactor characteristics for bromide breakthrough experiments at the high flow 118

C.7. Hydrology of reactors for bromide breakthrough experiments at the high flow 119

D.1. Data summaries for the FRC background area 130

D.2. Low flow rate fluorescent microsphere bead sampling plan 133

D.3. High flow rate fluorescent microsphere bead sampling plan.....134

D.4. Reactor characteristics for fluorescent microsphere breakthrough experiments at the low flow.....136

D.5. Fluorescent microsphere bead concentrations using FACS and direct counts 141

E.1. SGW media for Cupriavidus experiments 147

E.2. Flow rates for Cupriavidus experiments 147

E.3. Inoculation set up for Cupriavidus experiments.....148

LIST OF FIGURES

Figure Page

1. Conceptual illustration of representative shallow subsurface environment that includes the vadose, capillary fringe and saturated zones 3

2. Conceptual illustration of the different scales present in the shallow subsurface environment....5

3. Historical disposal of wastes on the Oak Ridge Reservation (ORR)....11

4. Diagram of the up-flow packed bed reactor designed and constructed for Chapter 1 experiment....22

5. Sampling timeline for Chapter 1 experiment....29

6. Depth profile of EB271....38

7. Volume density distribution of particle size from individual segments of EB271 38

8. Confocal images of reactor 1 that had a media pH of 7....43

9. Confocal images of reactor 2 that had a media pH of 6.3....44

10. Confocal images of reactor 3 that had a media pH of 4....45

11. Concentration model for all five substrate groups that are in the exo-metabolite solution....46

12. Concentration model of the amino acids, nucleotides, nucleosides, and osmolytes that are in the exo-metabolite solution. 47

13. Beta diversity PCoA plot for starting inoculum and sand samples collected from the porous media reactors 49

14. Principal Coordinate Analysis (PCoA) Bray-Curtis dissimilarity biplot by sample....50

15. Relative abundance plot for the starting inoculum and triplicate sand samples 52

LIST OF FIGURES CONTINUED

Figure Page

16. Shannon Index of β-diversity for all inocula and triplicate sand samples for each reactor 54

17. Hydraulic conductivity in respect to grain sizes. 66

A.1. Historical disposal of wastes from the operation of three industrial plant sites (K-25, Y-12, and ORNL) on the Oak Ridge Reservation (ORR)....77

A.2. Location of the contaminated areas, at the (BER) ORNL field research site 78

A.3. Diagram of the five different areas at the FRC and characteristics of the five areas including flow paths, pH levels, and contaminant level 79

A.4. Groundwater characteristics of the areas 1, 2, and 3 at the FRC 79

A.5. Former S-3 Ponds and current area at the Y-12 facility 80

A.6. Picture of bug trap next to a ruler to show the size....81

A.7. Individual value plot of cell distance measurements for each pH condition 82

A.8. Conditional residual plots for log-transformed cell distance measurements....83

A.9. Tukey pairwise comparison summary for log-transformed cell distance measurements....84

A.10. Individual value plot of cell/um for each pH condition 85

A.11. Conditional residual plots for cells/um 86

A.12. Tukey pairwise comparison summary for cells/um 87

LIST OF FIGURES CONTINUED

Figure Page

A.13. Individual value plot of total cell concentrations for each pH condition 88

A.14. Conditional residual plots for total cell concentrations. 89

A.15. Tukey pairwise comparison summary for total cell concentrations. 90

A.16. Individual value plot of BONCAT cell concentrations for each pH condition....91

A.17. Conditional residual plots for BONCAT cell concentrations. 92

A.18. Tukey pairwise comparison summary for BONCAT cell concentrations. 93

A.19. Individual value plot of planktonic cell concentrations for each pH condition....94

A.20. Conditional residual plots for planktonic cell concentrations. 95

A.21. Tukey pairwise comparison summary for planktonic cell concentrations. 96

A.22. Individual value plot of protein concentrations for each pH condition 97

A.23. Conditional residual plots for protein concentrations. 98

A.24. Tukey pairwise comparison summary for protein concentrations. 99

C.1. Diagram of the up-flow packed bed reactor for the bromide breakthrough curve study....106

C.2. Averaged breakthrough curve for the low flow rate 114

C.3. Bromide breakthrough curve, flow, and pressure for reactor 1 at the low flow rate 115

LIST OF FIGURES CONTINUED

Figure Page

C.4. Bromide breakthrough curve, flow, and pressure for reactor 2 at the low flow rate 116

C.5. Bromide breakthrough curve, flow, and pressure for reactor 3 at the low flow rate 117

C.6. Averaged breakthrough curve for high flow rate 119

C.7. Bromide breakthrough curve, flow, and pressure for reactor 1 at the high flow rate 120

C.8. Bromide breakthrough curve, flow, and pressure for reactor 2 at the high flow rate 121

C.9. Bromide breakthrough curve, flow, and pressure for reactor 3 at the high flow rate 122

C.10. Range of values of hydraulic conductivity and permeability for different sediments found in the subsurface 124

D.1. Diagram of the up-flow packed bed reactor for fluorescent microsphere bead study.....127

D.2. Averaged breakthrough curve for the fluorescent microsphere bead study.....137

D.3. Flow and pressure for reactor 1 for fluorescent microsphere bead study.....137

D.4. Bromide breakthrough curve for reactor 1 fluorescent microsphere bead study.....138

D.5. Flow and pressure for reactor 2 for fluorescent microsphere bead study.....138

D.6. Bromide breakthrough curve for reactor 2 fluorescent microsphere bead study.....139

LIST OF FIGURES CONTINUED

Figure Page

D.7. Flow and pressure for reactor 3 for fluorescent microsphere bead study....139

D.8. Bromide breakthrough curve for reactor 3 fluorescent microsphere bead study....140

D.9. Image of 1 µm fluorescent microsphere beads filtered onto a 0.2 µm membrane....141

D.10. Process for collecting and imaging fluorescent microsphere beads in a sand core....142

E.1. Diagram of the up-flow packed bed reactor for Cupriavidus experiments....145

E.2. Inoculation set up for Cupriavidus experiments....149

E.3. Protein measurements for each inoculation strategy for Cupriavidus experiments....154

E.4. Protein, DNA, and cells/g sand measurements for Cupriavidus experiment....155

E.5. Optical density (OD) (DO) measurements for all six reactors for Cupriavidus experiments....156

E.6. Dissolved oxygen (DO) measurements for all six reactors for Cupriavidus experiments....156

E.7. pH measurements for all six reactors for Cupriavidus experiments....157

E.8. Dissolved organic carbon (DOC) measurements for all six reactors for Cupriavidus experiments....157

ABSTRACT

Microorganisms in the terrestrial subsurface play important roles in nutrient cycling and degradation of anthropogenic contaminants, functions essential to the maintenance of healthy aquifers. Microorganisms have the potential to change the geochemical properties of the shallow terrestrial subsurface, and previous studies have uncovered significant roles microorganisms can play in groundwater processes, such as biogeochemical cycling. Much of the attention given to the shallow terrestrial subsurface has been focused on the effects of contamination and how microorganisms function in these systems, with far less emphasis on understanding how hydraulic properties influence subsurface microbial ecology. To fully understand how environmental factors impact microbial community dynamics, interactions, succession, colonization, and dispersal in the shallow subsurface environment it is essential to understand the link between microbiology and hydrology. In this thesis, an up-flow packed bed reactor (PBR) was designed to emulate select field conditions (*i.e.*, flow rate and particle size) observed at the Oak Ridge National Laboratory-Field Research Center (ORNL-FRC) to observe how environmental factors influences metabolic activity, community establishment, and cell distribution in a micropore environment. Furthermore, we developed methods to visualize the localization of active and non-active cells within the porous medium. The goals of this thesis were to 1) understand how environmental variables impact distribution and metabolic activity of microbial cells in the soil pore microenvironment at the FRC using native sediment bug trap material, 2) evaluate the hydraulic properties of the presented up-flow packed bed reactor (PBR), 3) observe how inert, non-charged particles distribute in a porous media environment, and 4) observe the biofilm distribution a microorganism isolated from the ORNL-FRC using different inoculation strategies. Overall, the data demonstrates that the presented reactor system accurately emulates field conditions and environmental factors (pH, particle size, average pore velocity) and the distribution of cells in *ex situ* conditions. The results of this thesis have implications for elucidating the impacts of environmental factors on metabolic activity and cell distribution in a field relevant reactor system.

INTRODUCTION

A Need for Clean Water

As of 2015, the United States uses approximately 322 billion gallons of water per day with the three largest water-use categories being irrigation, thermoelectric power, and public supply (Dieter, 2018), and with the projected upsurge in population it is projected that the water demand will continue to increase (MacDonald, 2010). Although 70% of the Earth's surface is covered in water, only a small portion of the water (approximately 1%) is available for human use (Danielopol et al. 2008; Griebler et al. 2014; Dennehy, Reilly and Cunningham 2015; Smith et al. 2018) with groundwater suppling about 95% of the Earth's available freshwater. Groundwater is an important resource for irrigation, industrial processes, and a source of recharge for lakes, rivers, and wetlands (Atekwana et al. 2009; Smith et al. 2018). In the face of increasing groundwater usage and historically poor management of many subsurface environments the fate of this resource is of growing concern. Thus, it is critical to fully understand how different environmental variables (i.e., changing hydrology, microbial activity, contamination effects, etc.) affect the terrestrial subsurface environment where groundwater exists as it is our main source of clean freshwater.

The Shallow Subsurface Environment

The terrestrial shallow, subsurface environment, located beneath weathered surface soil layers, and is comprised of sediments, rock, gas, pore water, and large reservoirs of groundwater (Atekwana et al. 2006). Solid phases of the subsurface environment are

constructed of weathered artifacts from parent material that are at various stages of development. The texture, porosity, and permeability of overlaying weathered sediments and surface soils are largely influenced by the mineral content and physiochemical properties of underlying parent sediment material (Berkowitz et al. 2004).

While estimates can vary, the shallow subsurface environment can extend from beneath the organic-matter rich soil layers (A and B horizons) to tens of meters deep eventually reaching bedrock (Atekwana et al. 2006; Pepper & Brusseau 2006; Chu et al. 2016; Smith et al. 2018). Shallow versus deep subsurface environments are differentiated based on the degree of hydrological connectivity to the surface (Toth 1963). Shallow subsurface environments have been characterized as being multilayered environments that can be comprised of the earth's crust, mineral ores, and aquifer environments (Jones et al. 2018).

Terrestrial subsurface porous habitats can be conceptually divided into three zones with respect to ground water flow and mixing. The first zone, the vadose zone including the capillary fringe, is variably saturated depending on infiltration episodes and the degree of vertical water table fluctuation (Smith et al., 2018). The vadose zone represents the upper most boundary of the subsurface and comprised of un-weathered and weathered materials (Smith et al. 2018). The capillary fringe is located at the interface of the saturated and vadose and is dynamic with varying physiochemical conditions due to water table fluctuations (Griebler and Lueders 2009; Smith et al. 2018). The second zone is the "shallow" groundwater zone, wherein groundwater flow can cause multi-directional flow that can result in greater mixing (Atekwana et al. 2009). The third zone is the "deeper" groundwater, or saturated zone, which lies below the depth affected by seasonal water table

fluctuations and has a more constant groundwater flow regime. The degree of mixing in the ‘deeper’ groundwater zone is related mainly to the ground water flow field.

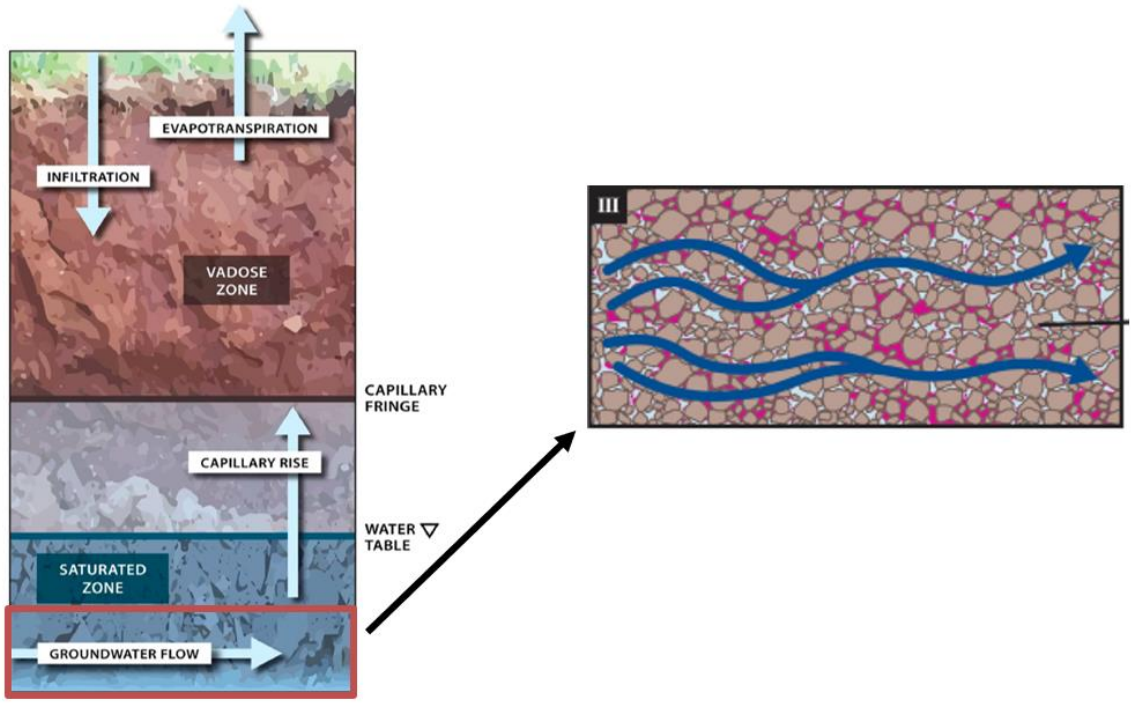

Figure 1. Conceptual illustration of representative shallow subsurface environment that includes the vadose, capillary fringe and saturated zones. Arrows depict the movement of water through infiltration, evapotranspiration, capillary rise and re-charge, and the movement of water within and between these zones. The saturated zone, or ‘deeper’ groundwater zone lies below the depth affected by seasonal water table fluctuations and has a more constant groundwater flow regime. Adapted from Smith et al., 2018.

Fluid dynamics of the shallow subsurface environment

The different characteristics of water (e.g., surface tension, cohesion, adhesion, and polarity) allow it to fill pore spaces, dissolve solutes, attach to subsurface products, and move through the subsurface (Brady and Weil, 2014). Subsurface water geochemistry (e.g., salinity, trace nutrients, metals, and pH) is largely dependent on the surrounding geology,

residence time of the environment, and the subsurface usage history (Brady and Weil, 2014). Furthermore, the surrounding geology greatly influences water movement and transport characteristics (e.g., porosity, permeability, hydraulic gradient, hydraulic conductivity). Groundwater flow in the terrestrial subsurface environment is driven by water flowing from high elevation to low elevation and from high pressure to low pressure. Gradients in potential energy drive groundwater flow which can be modeled by Darcy's law which states that the amount of water flowing through porous media depends on the energy driving the water flow and the hydraulic conductivity of the porous media.

Microorganisms in the Shallow Subsurface

Microorganisms in the shallow terrestrial subsurface have been demonstrated to be involved in various biogeochemical cycles (e.g., carbon, sulfur, nitrogen, and phosphorus cycles) and remain a highly relevant and understudied area of research that needs further investigation to better understand which biotic factors impact the fate and transport of nutrients (Thullner and Regnier, 2019; Anantharaman et al., 2016; Akob and Küsel, 2011). Expanding our current knowledge of how microorganisms distribute, function, and adapt to changing geochemical properties in the shallow subsurface environment will require a greater understanding of the structure of the shallow subsurface environment, including how porous media and flow can impact microbial distribution over time and space.

Studying subsurface microbial communities is complicated by the complexity of the terrestrial subsurface environment. It has been shown that microbial community dynamics and metabolic activity are influenced by environmental factors such as substrate flow and availability, as well as sediment and water chemistry (Liu *et al.* 2017). These factors vary

across geographic regions of differing sediment structure and saturation. Macropores between soil aggregates tend to promote increased substrate flow while micropores within individual soil aggregates retain water and accompanying substrates more tightly due to charge interactions (Figure 2). Similarly, finer aggregates tend to facilitate rapid drainage while coarser soils can create more tortuous paths. Sediment structure and water chemistry therefore play key roles in determining the preferential flow paths of substrates through the subsurface (O'Green 2013).

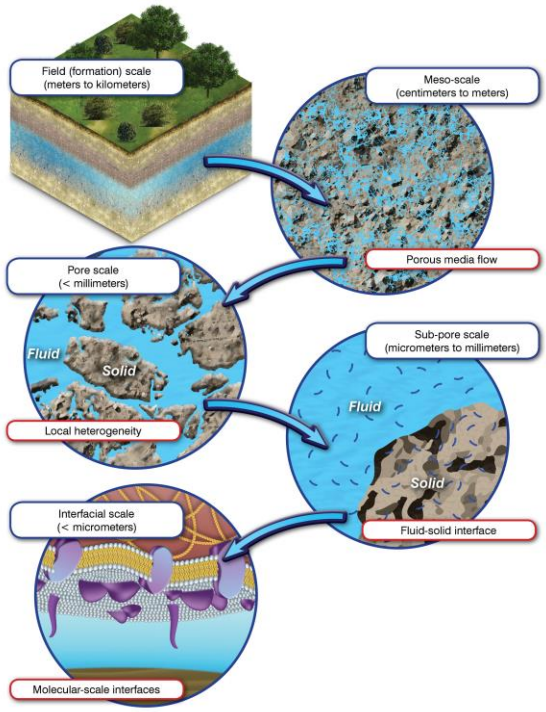

Figure 2. Conceptual illustration of the different scales present in the shallow subsurface environment. The largest scale is the field scale which can range from meters to kilometers. Porous media flow is observed in the meso-scale which ranges from centimeters to meters. The following scales, pore scale, sub-pore scale, and interfacial scale show fluid-solid interface of the shallow subsurface environment. At the sub-pore scale and interfacial scale, microorganisms interact with the fluid-solid interface either as free-living planktonic cells or attached to solid interfaces as singles cells or multicellular aggregates. Figure created by Jay Parson.

Microorganisms in the terrestrial subsurface make up approximately 40% of the total microbial biomass on Earth and often exist as diverse communities. These microbes can be observed as free-living planktonic cells or in association with soil structures as single cells or multicellular aggregates. Microorganisms can form multicellular communities that are held together by a self-produced extracellular matrix (Donlan 2002) termed biofilm. The mechanisms that different microorganisms utilize to form biofilms vary, often depending on environmental conditions and specific genetic attributes (López, Vlamakis, and Kolter, 2016). Biofilms can adhere to almost every surface, forming architecturally complex communities that can adapt to varying conditions. The shallow subsurface environment is an ideal environment for biofilms to form as it provides nutrients, moisture, and a large amount of colonizable surface area. However, the current lack of spatially resolved information limits our ability to make ecologically relevant conclusions about how environmental factors impact microbial community dynamics, interactions, succession, colonization, and dispersal in the shallow subsurface environment.

Interest in subsurface microorganisms and associated ecological function has increased largely due to the emerging need to assess groundwater quality for human use as well as for the potential to naturally remediate water systems that have been anthropogenically disturbed (*e.g.*, managed aquifer recharge systems) or contaminated from human practices (Anderson & Lovley, 1997; Chapelle, 2000; Langwaldt and Puhakka, 2000; Fields et al., 2006). Microorganisms have the potential to change the geochemical properties of the shallow terrestrial subsurface, and previous studies have uncovered significant roles microorganisms can play in groundwater processes, such as biogeochemical processes

(Chapelle, 2000) or fate and transport of metals and organic compounds (Anderson and Lovley, 1997**;** Fields et al., 2006; Hwang et al., 2009).

While much attention given to the shallow terrestrial subsurface has been focused on the effects of contamination and how microorganisms function in these systems, knowledge of how the hydraulic properties of the shallow terrestrial subsurface affect microbial distribution and growth have been far less studied. The hydraulic properties, including average pore velocity, porosity, hydraulic conductivity, and permeability can cause perturbations to an established microbial community. For example, average pore velocity can change the substrate flow and availability, and therefore, could impact the extent and rates of microbial activity in local environments.

In a porous media environment, the varying sizes of particles change the porosity, or void fraction, of the porous media environment. The porosity of the shallow subsurface environment can change with location and depth, largely dependent upon particle size distribution, composition, and mineralogy (Pepper & Brusseau 2006). The voids that fluid flows through are thought of as pore throats in which substrates and microorganisms are likely impacted by diffusivity and dispersivity. The varying sized pore throats cause preferential flow paths to occur in the shallow subsurface environment in which fluid flow will choose the path of least resistance. Thus, the porosity can change the average pore velocity of the shallow subsurface which ultimately influences the rate and distribution of substrates available for microorganisms. Additionally, the hydraulic conductivity of a porous media environment, the measure of its ability to transmit water when submitted to a hydraulic gradient, as well as the permeability, the property of a porous material that

determines how easily fluid flows through that material, are parameters of the shallow terrestrial subsurface environment that also impact the distribution of microbial biomass and activity. The hydraulic conductivity depends on fluid properties (e.g., saturation, viscosity, temperature, density, etc.) that can also directly impact microbial activity. Whereas permeability is an intrinsic property of a porous material (i.e., it only depends on properties such as pore size, tortuosity, and surface area). Saturated hydraulic conductivity is proportional to permeability. If the permeability of the shallow subsurface changes, the hydraulic conductivity of the shallow subsurface may also change. For example, if a porous material has a very small permeability, the hydraulic conductivity also decreases as it depends on the degree of saturation and the fluid's properties (i.e., density and viscosity). If the shallow subsurface environment had void fractions with smaller permeabilities in which fluid could not flow through, pockets of microorganisms, both planktonic and attached aggregates, could be restricted from necessary substrates in the fluid. Furthermore, if there were a geochemical perturbation to occur, such as increase in dissolved oxygen due to rainfall, the dissolved oxygen would likely be predominantly present in bigger pore throats because these flow paths are preferential due to less friction. Thus, some microorganisms would be exposed to an increase in dissolved oxygen, and some would not be exposed to an increase in dissolved oxygen, depending upon the distribution in the shallow subsurface. Because the hydraulic properties of the shallow subsurface ultimately determine the flow rate and distribution of different substrates, it is crucial to study the impacts of different hydraulic properties on microorganism's form, function, and metabolic activity.

Packed bed reactors (PBRs) are one of the most commonly used reactor systems in the chemical industry as the surface of the packing material can act as a catalytic surface for which reactions occur. Similar to chemical reactions, when using packed bed reactors to observe microbial growth in groundwater, the surfaces of the packing material mimic the surfaces of sediments found within the terrestrial subsurface, as well as provide a surface for microbial attachment. Packed bed reactors are the optimal (Taylor, 1990) reactor type to mimic porous media conditions as they provide the geometrical and transport properties desired when simulating environmentally relevant groundwater fluid flow conditions. Packed bed reactors can be used to study how different hydraulic properties (*i.e.*, flow rate, average pore velocity, permeability, etc.) influence metabolic activity and microbial distribution in a porous medium environment. Furthermore, packed bed reactors can be used to study microbial attachment to different porous media conditions, such as glass, sand, or sediment. Packed bed reactors allow for control over different hydraulic properties such as porosity, permeability, and hydraulic gradient. The porosity of the packing material for a packed bed reactor can be selected based on the packing material. Additionally, by controlling the flow rate, and by mimicking the particle size distribution of the field, desired hydraulic conductivities and permeabilities of packed bed reactors can be achieved. Other reactor types, such as batch, continually stirred tank reactors (CSTRs), and plug flow reactors (PFRs), do not provide the correct aspects to mimic porous media conditions. Furthermore, packed bed reactors can be easily built, there is greater surface area available for attachment the biofilm to attach to, and they are low maintenance.

BACKGROUND

Oak Ridge National Laboratory

The Oak Ridge Reservation (ORR) located in Oak Ridge, Tennessee is a U.S. Department of Energy facility that consists of three facilities: The Y-12 National Security Complex, Oak Ridge National Laboratory, and East Tennessee Technology Park. Originally established in the 1940's, the ORR was created during the Manhattan Project, and focused on developing a functional atomic weapon during World War II. The ORR was originally established to dispose of radioactive and non-radioactive materials that were utilized for nuclear weapons development. After the war, ORR continued to run a variety of activities related to research and production. Due to these activities, significant amounts of hazardous, radioactive, and mixed wastes were disposed at many sites throughout the reservation. One of the waste storage sites were the S-3 ponds that received mixed waste into four unlined ponds that later became the Oak Ridge National Laboratory-Field Research Center (ORNL FRC).

The mixed waste contaminates permeate throughout the subsurface, disrupting the microbial communities and geochemical cycling, leading to a widespread contamination in the area. As of 1989, the Environmental Protection Agency designated the ORR as a superfund site (epa.gov) requiring long-term remediation efforts. Current research at the ORNL-FRC entails understanding the impacts of contamination on the subsurface microbial communities, including the distribution and activity of microbial communities. Additionally, research is focused on understanding how both the contaminant materials and microbial life transport through the porous subsurface environment. A non-

contaminated area approximately 2 km away from any contaminated areas of the ORR, located in West Bear Creek Valley, with the same underlying hydrology and geology as the disposal site, was left untouched by industrial operations. As such, this area has become an essential field area for subsequent research regarding the effects of contamination on native microbial communities in ORR. Additionally, hundreds of field wells have been developed in both contaminated and non-contaminated areas, allowing for hydrological and biological field studies of the subsurface environment.

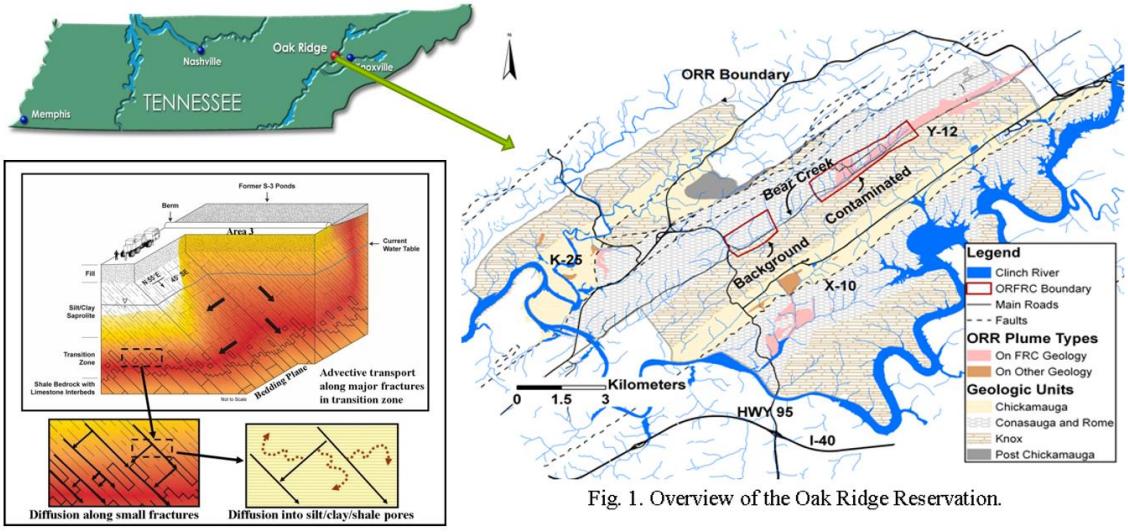

Fig. 1. Overview of the Oak Ridge Reservation.

Figure 3. Historic disposal of waste from the operation of three industrial plant sites (K-25, Y-12, and ORNL) on the Oak Ridge Reservation (ORR) have created extensive areas of subsurface contamination. Inorganic, organic, and radioactive wastes were released into thousands of unlined trenches, pits, ponds and streams by intentional disposal and accidental leaks and spills. These wastes have resulted in approximately 1,500 acres of contaminated ground water on the ORR (Fig. 1). Modified from Watson, Kostka, Fields, Jardine, 2004.

Thesis goals

The described work seeks to (*i*) understand how environmental variables impact the distribution and metabolic activity of microbial cells in the sediment pore microenvironment at the FRC. (*iI*) Develop methods for a packed bed reactor system that emulates field relevant conditions, (*iii*) and for collecting and processing an intact core taken from the PBR system for visualization of particle associated microbial cells. The reactor system and conditions were then tested with inoculum from three field samples that represent the gradient of pH levels (4.0 to 7.0) at the FRC to elucidate spatial distribution of microbial biomass and activity in a representative porous medium environment at the bench-scale. Methods development included processing the sub-core from the PBR for imaging intact cells. A more thorough understanding of how environmental variables impact the distribution and metabolic activity of microbial cells under field-relevant conditions provides improved parameter boundaries for developing models that can predict microbial function at field sites undergoing natural- and bio-stimulated remediation.

BIOFILM DISTRIBUTION IN A POROUS MEDIUM REACTOR EMULATING SHALLOW SUBSURFACE CONDITIONS

Contribution of Authors and Co-Authors

Manuscript(s) in Chapter(s) 1

Author: KaeLee F. Massey

Contributions: Performed literature review, synthesized ideas, maintained and sampled reactors, performed protein measurements, performed cell counts, performed epoxy embedding, created diffusion model, performed statistical analysis, wrote, and edited the manuscript

Co-Author: Heidi J. Smith

Contributions: Performed cell extraction and fixation, wrote methods, synthesized ideas, wrote and edited the manuscript

Co-Author: Al B. Cunningham

Contributions: Synthesized ideas, wrote and edited manuscript

Author: Hannah Dreesbach

Contributions: Confocal microscopy imaging and cell distance analysis, synthesized ideas, and performed cell counts

Co-Author: Luke J. McKay

Contributions: Performed bioinformatical analysis, created diversity and relative abundance plots, synthesized ideas

Co-Author: Yupeng Fan

Contributions: DNA extraction, library preparation and data processing

Co-Author: Ying Fu

Contributions: Miseq sequencing

Co-Author: Joy D. Van Nostrand

Contributions: Sample management

Co-Author: Jizhong Zhou

Contributions: Supervisor and PI to Yupeng Fan, Ying Fu, and Joy D. Van Nostrand

Co-Author: Katie F. Walker

Contributions: Performed field samplings, geochemical analysis, and data collection

Co-Author: Terry C. Hazen

Contributions: Supervisor and PI to Katie Walker

Co-Author: Matthew W. Fields

Contributions: PI, synthesized ideas, wrote and edited the manuscript

Manuscript Information

KaeLee F. Massey, Heidi J. Smith, Al B. Cunningham, Hannah Dreesbach, Luke J. McKay, Yupeng Fan, Ying Fu, Joy D. Van Nostrand, Jizhong Zhou, Katie F. Walker, Terry C. Hazen, Matthew W. Fields

Status of Manuscript:
__X__ Prepared for submission to a peer-reviewed journal
____ Officially submitted to a peer-reviewed journal
____ Accepted by a peer-reviewed journal
____ Published in a peer-reviewed journal

Abstract

Microorganisms have the potential to change the geochemical properties of the shallow terrestrial subsurface, and previous studies have uncovered significant roles that microorganisms can play in groundwater processes, such as biogeochemical processes. While much attention given to the shallow terrestrial subsurface has been focused on the effects of contamination and how microorganisms function in these systems, knowledge of the distribution of microbial biomass and activity related to hydraulic properties is less understood. In this study, an up-flow packed bed reactor (PBR) was designed to emulate select field conditions (*i.e.*, flow rate and particle size) at the Oak Ridge National Laboratory-Field Research Center (ORNL-FRC) and observe microbial biomass and activity distribution in a micropore environment. The PBR contained a porous medium of silica oxide particles (74-300 μm), and the size range was based upon particle size assessment of sediment material from the ORNL-FRC. The water phase of the system was a basal groundwater medium that contained low levels of sugars, amino acids, and nucleosides/nucleotides as the C and N sources that were based upon metabolomic characterization of sediment extracts. The inocula for the PBRs consisted of sediment material in samplers that were incubated down-well and retrieved from three FRC wells each at a distinct pH (4, 6.3, or 7). Following 4 months of incubation in the PBRs, biomass, cell concentrations, cell distribution, and microbial community analysis for each reactor were evaluated. The pH 4 reactor had the highest biomass and activity but had the lowest diversity amongst the pH conditions. The two circumneutral reactors (pH 7 and pH 6.3) both had lower biomass concentrations and activity but had microbial communities that

were more diverse than pH 4. Methods were also developed to enable the embedding and sectioning of an intact core from the PBRs, and this allowed visualization of cell localization within the porous medium. The reactors showed different trends in how microbial biomass was distributed through the porous medium as well as distances to other cells and/or cell aggregates. The measured distances were also compared to substrate concentrations over distances predicted by a model based upon diffusion coefficients for compound classes (*i.e.*, sugars, amino acids, nucleotides/nucleosides). Overall, the data and predictions demonstrated that under *ex situ* conditions meant to emulate porous media flow (*e.g.*, porosity, flow, particle size) at the ORNL-FRC, cells that are part of a diverse microbial community can be on average 20 to 80 µm apart with an average of 2 to 9 cells/particle. Based on diffusivity of potential substrates and measured distance ranges between cells, sugar levels could be approximately 5 to 20 µM whereas amino acids and nucleotides/nucleosides would be sub-micromolar between nearest cell/aggregate neighbors.

Introduction

As of 2015, the United States uses approximately 322 billion gallons of water per day with the three largest water-use categories being irrigation, thermoelectric power, and public supply (Dieter, 2018), and with the projected upsurge in population it is projected that the water demand will continue to increase (MacDonald, 2010). Although 70% of the Earth's surface is covered in water, only a small portion of the water (approximately 1%) is available for human use (Danielopol et al. 2008; Griebler et al. 2014; Dennehy, Reilly and Cunningham 2015; Smith et al. 2018) with groundwater suppling about 95% of the

Earth's and available freshwater. Groundwater is an important resource for irrigation, industrial processes, and a source of recharge for lakes, rivers, and wetlands (Atekwana et al. 2009; Smith et al. 2018). However, with an increasing demand for groundwater usage and a historically poor management of many subsurface environments, contamination in groundwater and subsurface soils and sediments has become a growing concern as it is not fully understood how contamination can affect the geochemical properties (i.e., pH, conductivity, total dissolved solids, etc.) of the groundwater in the terrestrial subsurface and thus the native microbial community that is established (Chapelle, 1993). Additionally, the potential of using native microbial communities for natural remediation of disturbed subsurface environments has gained interest in applied ecology (Holliger et al. 1997; Chakraborty et al. 2012).

The terrestrial shallow subsurface environment, located beneath vertically weathered surface soil layers, is comprised of sediments, rock, gas, pore water, and large reservoirs of groundwater (Atekwana et al. 2006). Solid phases of the subsurface environment are constructed of weathered artifacts from parent material that are at various stages of development. The texture, porosity, and permeability of overlaying weather sediments and surface soils are largely influenced by the mineral content and physiochemical properties of underlying parent sediment material (Berkowitz et al. 2004). Terrestrial subsurface porous habitats can be conceptually divided into three zones with respect to ground water flow and mixing. The first zone, the vadose zone including the capillary fringe, is variably saturated depending on infiltration episodes and the degree of vertical water table fluctuation (Jones et al. 2014). The second zone is the "shallow" groundwater zone,

wherein groundwater flow can cause multi-directional flow that can result in greater mixing (Atekwana et al. 2009). The third zone is the “deeper” groundwater, or saturated zone, which lies below the depth affected by seasonal water table fluctuations and has a more constant groundwater flow regime. The degree of mixing in the ‘deeper’ groundwater zone is related mainly to the ground water flow field.

While subsurface hydrology of groundwater aquifers has been well studied by hydrologists and hydrochemists (Chapelle, 2000; Griebler and Avramov, 2015), the relationship between hydrology in the shallow terrestrial subsurface and subsequent environment influences on metabolic activity and distribution of microbial communities is poorly understood. Previous work has shown that microbial community dynamics and metabolic activity can be influenced by environmental factors such as substrate flow and availability, as well as sediment and water chemistry (Liu *et al.* 2017). In the shallow terrestrial subsurface, microorganisms can be observed as free-living planktonic cells or in association with sediment structures as single cells or multicellular aggregates that can form biofilms. The shallow subsurface environment is an ideal environment for biofilms to form due to the presence of nutrients, moisture, and a large extent of surface area for microorganisms to attach. Interest in subsurface microorganisms and associated ecological function has increased largely due to the emerging need to assess groundwater quality for human use as well as for the potential to naturally remediate water systems that have been disturbed via engineering efforts (e.g., managed aquifer recharge systems) or contaminated from human practices (Anderson & Lovley, 1997; Chapelle, 2000; Langwaldt and Puhakka, 2000; Fields et al., 2006). Expanding our current knowledge on how

microorganisms colonize, function, and adapt to different conditions in the shallow subsurface environment will require a greater understanding of the organization of the shallow subsurface, including how sediment structure, substrate flow, and microbial distribution vary and interact spatially and temporally in the terrestrial subsurface.

Packed bed reactors (PBRs) are one of the most commonly used reactor systems in the chemical industry as the surface of the packing material can acts as a catalytic surface for which reactions occur. Similar to chemical reactions, when using packed bed reactors to observe microbial growth in groundwater, the surfaces of the packing material can mimic the surfaces of sediments observed within the terrestrial subsurface (*e.g.*, porous media). Packed bed reactors are the optimal reactor type to mimic porous media flow conditions as they provide the geometrical and transport properties desired when simulating environmentally relevant groundwater fluid flow conditions and allow for the control over different hydraulic properties (*i.e.*, flow rate, porosity, permeability). Therefore, packed bed reactors can be used to study how different hydraulic properties (*e.g.*, flow rate, average pore velocity, permeability) influence metabolic activity and microbial distribution in a porous medium environment.

The Oak Ridge Field Research Center (EOR-FRC), established by the U.S. Department of Energy (DOE), consists of several contaminated areas as well as a noncontaminated background site. Current research at the FRC entails understanding the impacts of contamination on the subsurface microbial communities, including overall structure-function relationships within microbial communities and changes over time and space in the shallow, subsurface environment. A clearer understanding of the sediment structure,

substrate flow, and the hydraulic properties of the shallow subsurface is necessary to understanding the growth, function, and adaptation of microorganisms in the shallow subsurface. The described study analyzed FRC native microbial communities at different pH levels in a developed porous medium reactor to ascertain the distribution of microbial biomass and activity in a micropore microenvironment.

Materials and Methods

Reactor Design and Construction

The up-flow packed bed reactor system described here is designed for laboratory bench-top use (total PBR volume ~ 257 mL) and can maintain an anoxic environment for all components upstream of the reactor column, the reactor column itself, and the effluent line. The system can be run at varying flow rates, including low flow rates that are representative of the shallow subsurface environment. Each reactor system has sampling ports at the top and bottom for injector or sampling. The sampling ports allow for temporal sampling of the planktonic phase. The size of the reactor was specifically designed to provide increased volume needed for sampling the void volumes and porous medium as well as for minimizing potential preferential flow paths. A schematic of the system is shown in Figure 4.

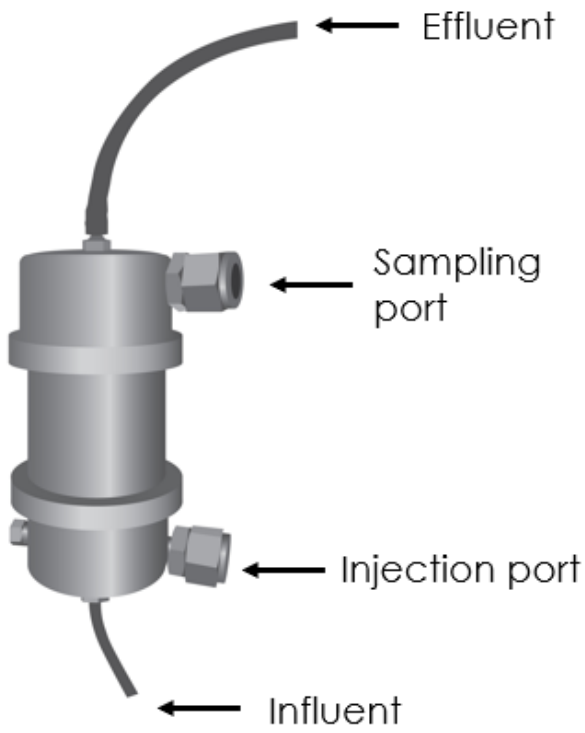

Figure 4. Diagram of the up-flow packed bed reactor designed and constructed. The reactor has an influent port at the bottom of the reactor and effluent exits the top of the reactor at the effluent port. Two septum ports were added to the reactor to easily inoculate the reactor and collect planktonic samples. The bottom septum port is used for inoculating the reactor and both ports can be used to collect planktonic samples.

The reactor column was constructed from type 316/316L stainless steel threaded pipe with a length of 3 inches, inner diameter of 2.067 inches, and a wall thickness of 0.154 inches. The threaded caps were 316 stainless steel with an outer diameter of 2.98 inches, a length of 1.77 inches, rated to a pressure of 150 psi. All components of the reactor body were bought from McMaster-Carr (Elmhurst, IL, USA). Holes were drilled into the side of both caps and 1/8-inch NPT threads were cut for the sampling port fittings. The bottom reactor cap (influent side) had two threaded holes, one located on the side for the sampling port and a second one located on the flat side of the cap for the influent port. The influent

port was fitted with a 1/16-inch barbed fitting for flow and attached to size 13 Masterflex® Norprene tubing. The second hole on the bottom cap was fitted with a septum port fitting for sampling and injection. The top reactor cap had drilled holes, one located on the side for sampling and a second one located on the top for the effluent flow. The drilled hole located on the side was fitted with a septum port fitting for sampling. The top hole of the top cap was fitted with a ¼-inch barbed fitting for effluent flow and attached to size 25 Masterflex® Norprene tubing. The reactor column can be packed with a variety of porous media, including sand, sediment, or glass beads. For the described experiments, the PBRs were packed with 380 g of a sand mix that contained sand particles whose diameter ranged from 75 to 300 µm.

The liquid medium reservoirs were 2-liter glass carboys, and the carboys were sealed with a butyl rubber stopper. The butyl rubber stopper was drilled to install a piece of glass tubing which was attached to Masterflex® Norprene tubing used to hold an oxygen-free gas purge. A second hole was drilled in the rubber stopper to hold 1/8-inch stainless steel tubing that was attached to Masterflex® Norprene tubing for the media influent line. The effluent flow was collected in 1 liter glass bottles.

Sampling Protocols

Liquid samples can be taken via septum sampling ports from the top and bottom caps of the reactor body, as well as the effluent reservoir. Additions and/or modifications to the system can also be made at any of these locations. Septum sampling port locations are designated in Figure 4. Destructive sampling at the end of the experiment provided

access for sampling the porous medium within the reactor body and the liquid within the void volume.

Particle Size Distribution

To replicate *in situ* particle size distribution in packed bed reactors, a sediment core from the FRC was analyzed using a Malvern Mastersizer 3000 to determine the particle size distributions (Moon et al., 2020). Sediment samples were run in duplicate to produce a total of 10 measurements for each depth corresponding to the sediment core. A separate group of sediment samples were treated with acetic acid to remove carbonates to compare the silt percentages within the sediment samples. To treat the sediment samples, 5 mL of 1 M NaOAc (pH of 5) was added to each sediment sample in the treated sample group. The mixture of sediment and acetic acid was shaken and sat at room temperature for 30 minutes. After 30 minutes, each treated sample was placed in a heating block set to 60 ℃ for 30 minutes. After 30 minutes, the samples were removed from the heating block and cooled at room temperature. After 30 minutes of sitting at room temperature, the treated samples were centrifuged at 4,000 rpm for 20 minutes or until the sample formed a solid puck at the bottom. The supernatant was removed from each treated sample and analyzed using the same settings for the untreated samples.

Sample ID	Sample Number	Depth bgs (cm)
EB271-02-01	2	114
EB271-02-02	3	137
EB271-02-03	4	147
EB271-03-01	5	206
EB271-03-02	6	229
EB271-03-03	7	257
EB271-04-01	8	297
EB271-04-02	9	320
EB271-04-03	10	343
EB271-04-04	11	363
EB271-05-01	12	383
EB271-05-02	13	401
EB271-05-03	14	418
EB271-05-04	15	439

Table 1. Sediment samples collected from the FRC and used for particle sized distribution analysis. The depth below the ground surface is listed for each sediment sample.

Inoculum Sources and Preparation

Bug-trap sediment (microbial samplers incubated down well for 2 months) was collected from one well in three different areas of the ORNL-FRC. A bug trap is an apparatus that is packed with porous material and has openings to allow both groundwater and source microbes to flow through allowing for the apparatus to entrap both planktonic

and attached microbes. The wells that bug-trap sediment was collected from were EU05 (Area 1), GW-835 (Area 2), and FW-106 (Area 3). These wells were selected for central location in each area as well as the diameter of the well that would allow for bug trap deployment. Additionally, these three areas were chosen based on the different geochemical properties and varying flow paths at the field site. Bug traps were constructed with 1 inch well screen and PVC caps, were filled with local sediment, and placed down-well in EU05 (Area 1), GW-835 (Area 2), or FW-106 (Area 3). The bug traps were placed at the screened interval in the saturated zone of each well and remained in the well for 8 weeks to establish an attached community. After retrieval, sediment (8 g) from each bug trap was collected and placed in a sterile 50 mL falcon tube. Samples were placed in a sealed shipment box that can maintain anoxic conditions and shipped overnight on blue ice. Upon arrival, 25 mL of respective growth medium was added to each bug trap sediment sample and vortexed to create a slurry. Using the inoculation port on the PBRs, the three separate reactors were inoculated with one slurry mixture to have a total of three reactors with a respective bug trap inoculum (EU05, GW835, or FW106, respectively).

Area	pH	Contaminant Level	Flow Path
1 (EU05)	5 - 8	Low	Gravel
2 (GW835)	6 - 8	Low	Limestone
3 (FW106)	3 - 7	High	Shale

Table 2. Geochemical properties and flow paths of the three areas that are studied in this project at the FRC.

To emulate field conditions, the growth media was based upon groundwater analysis of the FRC (Jenkins et. al, 2017). The groundwater media consisted of a salt solution, sodium bicarbonate, Wolfe's vitamins, Wolfe's minerals, and exo-metabolites. Each reactor received a different salt solution that was derived from groundwater measurements for each respective area. The exo-metabolite solution consisted of sugars, amino acids, nucleoside/nucleotides at concentrations based on groundwater analysis of the FRC (same for all three reactors; Jenkins et al., 2017). The exo-metabolite solution serves as the main source of nutrients for the microorganisms in this experiment. The pH of the groundwater media was adjusted to reflect each respective area. Thus, the groundwater media for reactor 1 had the pH adjusted to 7, reactor 2 had the pH adjusted to 6.3, and reactor 3 had the pH adjusted to 4.

Reactor	Field site area	Bug trap sample	Media pH	Nitrate Concentration
1	1	EU05	7	0.035 mM
2	2	GW-835	6.3	3.5 mM
3	3	FW-106	4	23 mM

Table 3. Field site area and well information that bug trap samples were collected from.

Reactor Preparation

Prior to the experimental run of the reactor systems, all Norprene tubing, reactor columns, liquid media reservoir, and effluent carboys were autoclaved. After sterilization, the reactor system was assembled aseptically. The reactor system was purged of atmospheric air, specifically targeting the removal of oxygen, using filtered 80% N_2/20%

CO_2. The pump was turned on to fill reactors with media before inoculating. After the entire reactor system was filled with media, the pump was paused, and all three reactors were inoculated from the bottom sampling port with the respective bug trap sediment slurry (~25 mL). The pump remained paused for 24 hours after inoculation to allow the bug trap inoculum to establish initial attachment to the porous medium. After 24 hours, the pump was started and set to 0.18 mL/min to achieve the desired flow rate of 0.048 mL/min. The PBR flow rate is representative of intermediate flow rates observed at the FRC (Watson, Kostka, Fields, Jardine, 2004). At this flow rate, the residence time in the PBRs was approximately 32 hours and had a hydraulic conductivity of 3.69E-05 m/s. Flow remained constant in the reactors for approximately 4 months.

Flow Rate (mL/min)	Residence Time (hr.)	Hydraulic Conductivity (m/s)	Permeability (m^2)	Porosity	Average Pore Velocity (m/s)
0.048	32	3.69E-05	3.35E-12	0.42	8.61E-07

Table 4. Flow rate used for the experiment and its calculated hydraulic properties.

Reactor Sampling

Planktonic samples were collected from each reactor once every couple weeks throughout the duration of the experiment. Approximately 2 mL of liquid of sample was collected from each reactor at each time point for microbial community analysis and analytes. On day 135, all three reactors were destructively sampled. Flow was stopped to all three reactors and both the influent and effluent lines were clamped. Planktonic samples were collected from the liquid headspace for cell concentrations, DNA extractions, and

glycerol stocks. The remaining liquid volume was drained from each reactor before opening the reactors to collect a sub-core by disconnecting the influent media line from the reactor and allowing the liquid to drain out of the influent port. Porous media samples were collected for glycerol stocks, enrichment slurries, DNA extractions, cell concentrations, and protein assays. Additionally, a sub-core was collected from each reactor column to be embedded with epoxy resin.

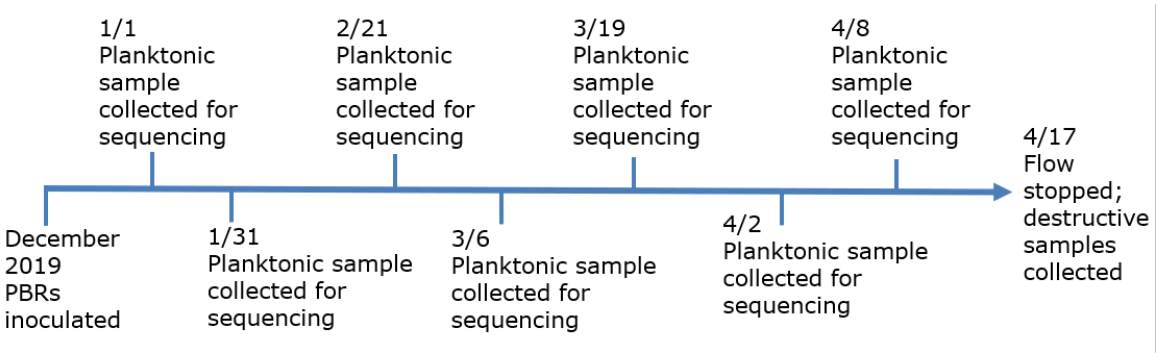

Figure 5. Sampling timeline for experiment.

Biomass Analysis - Protein. Approximately 5 mL of column material was collected and placed in a sterile 15 mL falcon tube for each reactor. For each protein sample, 0.5 mL of sterile water was added per mL of sand. The protein samples were stored at -80 ℃ for 24 hours and then allowed to thaw at room temperature. After fully thawed, the samples were vortexed and placed back into the -80 ℃ freezer for an additional 24 hours. After 24 hours, the samples were allowed to thaw fully and vortexed. Ensuring the samples were tightly sealed, the protein samples were then placed in a water bath at 100 ℃ for 30 minutes and vortexed. Protein was measured using the Qubit protein assay (Life Technologies, Carlsbad, CA). The porous material collected for each reactor was dried and weighed, and

the protein measurement was normalized to porous material dry weight. The protein concentrations for each pH condition were compared using a one-way ANOVA model with a factor of pH using the computer software package MINITAB (Minitab, State College, PA, USA).

Total and active cell enumeration. L-homopropargylglycine (HPG) was added to each media influent bottle 72 hours before the pump was turned off and destructive samples were taken. Planktonic and porous material samples were collected from each reactor to perform cell counts. For each reactor, solid material (1 g) was collected and fixed with 2% paraformaldehyde at room temperature for 1 hour. Samples were washed with a mixture of PBS and Tween to remove cells from the sand. The supernatant was collected for cell concentration analysis. Bioorthogonal Non-Canonical Amino Acid Tagging (BONCAT) was performed for each sample as previously described (Hatzenpichler & Orphan, 2015) and counterstained with DAPI to differentiate between total and active cells. Stained samples were filtered onto a 0.2 μm filter membrane to be analyzed via microscopy. Thirty fields of view were counted for each sample (Muthukrishnan, Govender, Dobretsov, & Abed, 2016). Porous material cell counts were performed in triplicate to calculate an average and standard deviation. For planktonic cell counts, sample (2 mL) from the liquid head space was collected from each reactor. The samples were fixed with formalin, stained with SYBR Gold, and filtered onto a 0.2 μm filter membrane to be analyzed via microscopy. The cell concentrations, both total and BONCAT active, for each pH condition were compared using a one-way ANOVA model with a factor of pH using the computer software package MINITAB (Minitab, State College, PA, USA).

DNA Extraction, Sequencing, and Analysis. Liquid reactor effluent samples (2 ml) and sand samples (2 g) were stored at -80°C before use. Microbial genomic DNA was extracted by a freeze-grinding method as described previously (Zhou and Tiedje, 1996) and purified by using DNeasy PowerSoil DNA isolation Kit (QIAGEN; bead tubes were not used). DNA quality was checked by NanoDrop, and double-strand DNA concentration was measured by Quant-iT™ PicoGreen™ dsDNA Assay Kit.

A two-step PCR amplification method was used for PCR product library preparation as described previously (Wu et al., 2015). In the first step PCR, the standard primers were used to amplify the V4 region of prokaryotic SSU rRNA genes (515F [5'-GTGCCAGCMGCCGCGGTAA-3'] and 806R [5'-GGACTACHVGGGTWT CTAAT-3']). In the second step PCR, phasing primers were designed and used to increase the base diversity in sequences of sample libraries. PCR amplification and purification were the same as reported previously (Wu et al. 2012), except amplification cycles (10 cycles in the first step and 20 cycles in the second step for 16S). Sample libraries were then sequenced by MiSeq platform (Illumina, San Diego, CA, USA) as described previously (Caporaso et al., 2012).

Qiime2 (version 2019.7) was used to perform the ASV-based processing. After barcode and primer sequences were trimmed with zero maximum error, sequencing data were processed by DADA2 to identify exact amplicon sequence variants (ASV). The ASVs were identified taxonomically based on the silva-132-99-515-806-nb-classifier. The ASV sequences were then used to build phylogenetic tree by FastTree (Price, Dehal, & Arkin, 2009; Price, Dehal, & Arkin, 2010).

Epoxy Embedding and Imaging

A sub-core (diameter = 1-inch, length = 4-inches) from each reactor were collected at the end of the experiment. Cores were collected using a sterile 5-inch-long plastic, hollow cylinder with a diameter of 1 inch. Once the cores were collected, each core was saturated with 2% paraformaldehyde and incubated at room temperature for 2 hours (fixation). After fixation, each core received a series of washes to remove moisture from the core prior to embedding. The washes that are used for the cores are in the following order: 1X PBS, 50% 1X PBS/50%ethanold, 20% 1X PBS/80% ethanol, 100% ethanol, 50% ethanol/50% LR white epoxy. After the 50% ethanol/50% LR white epoxy wash, the cores were saturated with LR white resin (LR white hard grade, catalyzed, Electron Microscopy Sciences) and placed in an incubator for 24 – 48 hours to allow the resin to set. Each of the LR white resin cores was cut into sections and imaged at multiple fields of view using Confocal Scanning Laser Microscopy. Cores were stained with SYBR Green, a nucleic acid stain (Invitrogen; Life Technologies) 1X final concentration and were rinsed after staining with 0.2 µm filter sterilized DI water three times to remove any excess stain. Core samples were imaged with a Leica TCS SP5 II confocal microscope using a 63X water immersion objective, 0.9 NA, WD 2.2 mm. Fluorophore excitation lasers and emission bandwidths are as follows: SYBR Green (ex 497/em 520) 488 nm excitation, 500–550 nm emission collection; 235 autofluorescence, 561 nm excitation, 580–700 nm emission collection. Three randomly selected images were collected to enumerate cellular biomass (SYBR green, autofluorescence, reflection). For each field of view, fluorescent images of the cells and reflection images of the exposed porous material surface were taken using the same Z-stack depth. Reflection images of the particles were then overlaid with

corresponding fluorescent image in Imaris (version 9.3.0; Bitplane). The circumference of a particle, the number of cells along that circumference, and the distances between observed cells were then measured using the segmented line tool in ImageJ. To improve visibility of the cells along the outline of each sediment particle, both an overlaid reflection/fluorescent image and a plain fluorescent image were imported into ImageJ and layered using the "Overlay" tool. The fluorescent image was set to an opacity of 70%. Throughout the measuring process, the overlaid fluorescent image could be turned on and off to confirm cell placement along the sediment particle boundary. The data was tabulated in Excel and the average distance between cells along a given sediment particle was determined. The measured distance between cells were log-transformed and analyzed using a mixed effects analysis of variance (ANOVA) with a fixed factor of pH. Random factors for the mixed effects model included image ID and particle ID, which was fit using the computer software package MINITAB (Minitab, State College, PA, USA).

Substrate Concentration Model

A concentration model was created to estimate the concentration of different substrates of the exo-metabolite solution at different distances. The concentration model was constructed using estimated diffusion coefficients of the substrates in the exo-metabolite solution as well as the known initial concentrations of the substrates in the exo-metabolite solution. The exo-metabolite mixture is comprised of sugars, amino acids, nucleotides, nucleosides and osmolytes. The concentration of each substrate is known for the exo-metabolite solution (Appendix B). However, to simplify the model and for the ease of representing each category of substrates, the concentrations for each category was

averaged. Using Equation 1, the concentration for each category of substrates was calculated at different lengths and time points. The equation is derived from Fick's Law and uses the initial concentration of the solute, C_0, distance, x, diffusion coefficient of the solute, D, and time, t, to calculate the concentration of the substrate. The complementary error function, erfc, is a mathematical function that is related to the normal, or Gaussian, distribution. Although some diffusion coefficients of the substrates could be found in the literature, most diffusion coefficients for small molecules remain unknown. Therefore, a method from Evans, Dal Poggetto, Nilsson, and Morris (2018) was used to calculate an estimated diffusion coefficient for each substrate category. The method uses a Matlab code that calculates the estimated diffusion coefficient using the Stokes-Einstein-Gierer-Wirtz equation. This method is based on viscosity scaling and effective density for the solute (Evans, Dal Poggetto, Nilsson, and Morris, 2018). The Matlab code produces a calculator, the SEGWE calculator, that can estimate the diffusion coefficient and hydrodynamic radius of the solute of interest. The parameters needed for calculating an estimated diffusion coefficient with this method include the temperature and molecular weight of the solute of interest. Additionally, the calculator has different options for the solvent that is used in the calculation. The molecular weights of the substrates in the exo-metabolite solution were averaged based on the substrate category. The temperature used for calculating the estimated diffusion coefficients was 293 Kelvin.

$$C(x,t) = C_0 * erfc\left(\frac{x}{2(D*t)^{0.5}}\right) \qquad Eqn\ 1$$

The estimated diffusion coefficients for the sugars, amino acids, nucleotides/nucleosides, and osmolytes were calculated to be 634 $\mu m^2/s$, 765 $\mu m^2/s$, 734

$\mu m^2/s$, 587 $\mu m^2/s$, 809 $\mu m^2/s$, respectively. The nucleotides and nucleosides were separated into two different categories based on their initial concentrations in the exo-metabolite solution. The nucleotide initial concentrations range from 0.52 µM to 4.5 µM, where all nucleoside initial concentrations are 0.52 µM. The diffusion coefficients increase with decreasing molecular weight. This is because the diffusion coefficient or, often, the relative diffusivity can be expressed in terms of the mass of the species, M, raised to an empirical power, α, as in Equation 2 (Evans, Dal Poggetto, Nilsson, and Morris, 2018).

$$D \propto M^{-\alpha} \qquad Eqn. 2$$

Substrate category	Average molecular weight (g/mol)	Average initial concentration (µM)	Estimated diffusion coefficient ($\mu m^2/s$)
Sugars	213.7	89.78	634
Amino acids	140.8	5.69	765
Nucleotides	154.0	1.064	734
Nucleosides	254.6	0.52	587
Osmolytes	124.7	0.52	809

Table 5. Averaged molecular weights (g/mol), averaged initial concentrations (µM), and estimated diffusion coefficient ($\mu m^2/s$) of the five different categories of substrates in the exo-metabolite solution.

Results

Particle Size Distribution

Results from depths corresponding to water table height were averaged to generate a representative particle size distribution from the saturated zone which indicated a 98.6% and 88.4% total particle size of 2-500 micrometers (μm) for the untreated and acetic acid treated sediment samples, respectively. This indicated that carbonates greatly influence the particle size corresponding to the silt and could influence the available surfaces for biofilms to form. Table 6 shows the particle size distribution results for both the untreated and treated sediment samples. For both the untreated and treated samples, the majority of the particle sizes were measured to be in the silt (2-50 μm) to medium sand range (250-500 μm). However, for the treated samples the percentages for the silt to the fine sand range decline, and for the medium sand range the percentage increases. Figure 6 shows the distribution of total sediment composition based on size classification for each depth of the sediment core. The total percentage for each particle size classification with each depth does not significantly vary except for the silt fraction. The silt fraction varies with each depth of the sediment but still remains to be the largest percentage of the total particle size. Based on these results, a sand mix containing particles ranging from 74 μm to 300 μm was used to pack the porous media reactors. This sand mix was chosen because it captures a significant portion of the particle size particularly for the saturated zone transition line observed in the FRC sediment. Although both the untreated and treated samples contained a large fraction of silt (2-50 μm), smaller sand particles were not used for the porous media reactors due to challenges associated with particles of this size in reactors, such as clogging.

Average % of particle size amongst **Untreated** saturated zones		Average % of particle size amongst Acetic Acid **Treated** saturated zones	
Fraction	% in	Fraction	% in
Clay (<2 µm)	1.2	Clay (<2 µm)	11.24
Silt (2 – 50 µm)	**50.55**	**Silt (2 – 50 µm)**	**37.58**
Very fine sand (50-100 µm)	**18**	**Very fine sand (50-100 µm)**	**10.1**
Fine sand (100-250 µm)	**21.87**	**Fine sand (100-250 µm)**	**17.76**
Medium sand (250-500 µm)	**6.98**	**Medium sand (250-500 µm)**	**11.72**
Coarse sand (500-1000 µm)	1.38	Coarse sand (500-1000 µm)	7.96
Very coarse sand (1000-2000 µm)	0.03	Very coarse sand (1000-2000) µm	3.1
Total sand (50-2000 µm)	48.25	Total sand (50-2000 µm)	50.64

Table 6. Average percentage of particle sizes measured from the sediment cores collected from the FRC. The majority of the particle sizes measured lie within the range of silt (2-50 µm) to the medium sand range (250-500 µm).

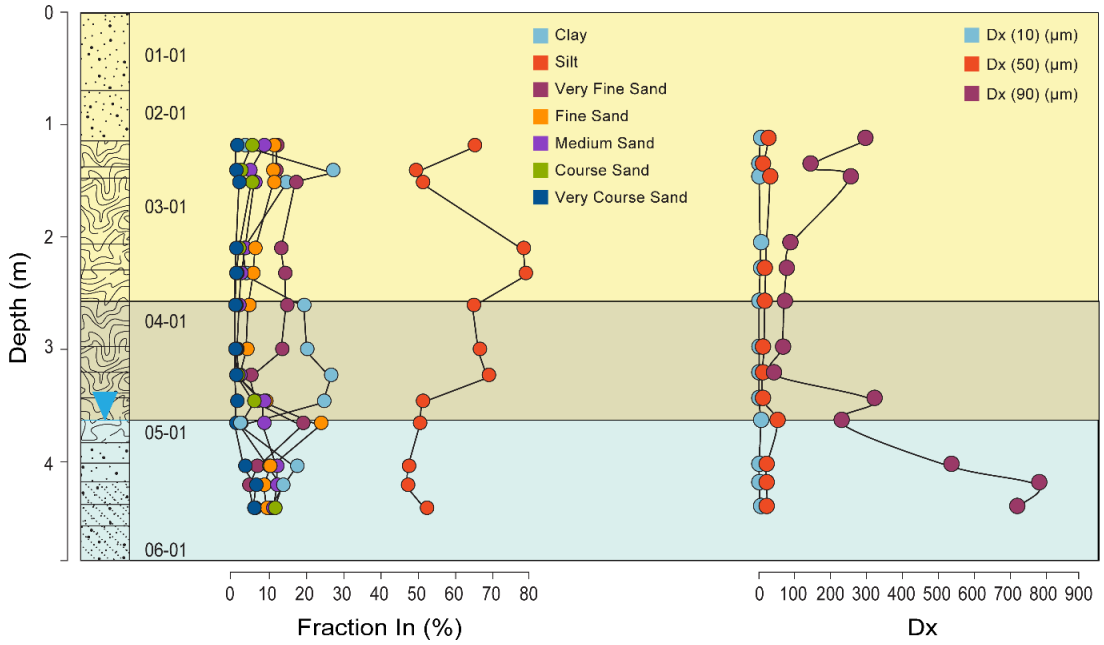

Figure 6. Depth profile of EB271 A.) distribution of total sediment composition based on size classification and B.) particle distribution by size. Dx(10) is the size of particles below which 10% of the samples lies, Dx(50) is the size of particles below which 50% of the samples lies, Dx(90) is the size of particles below which 90% of the samples lies, Dx(90) is the size of particles below which 90% of the sample lies.

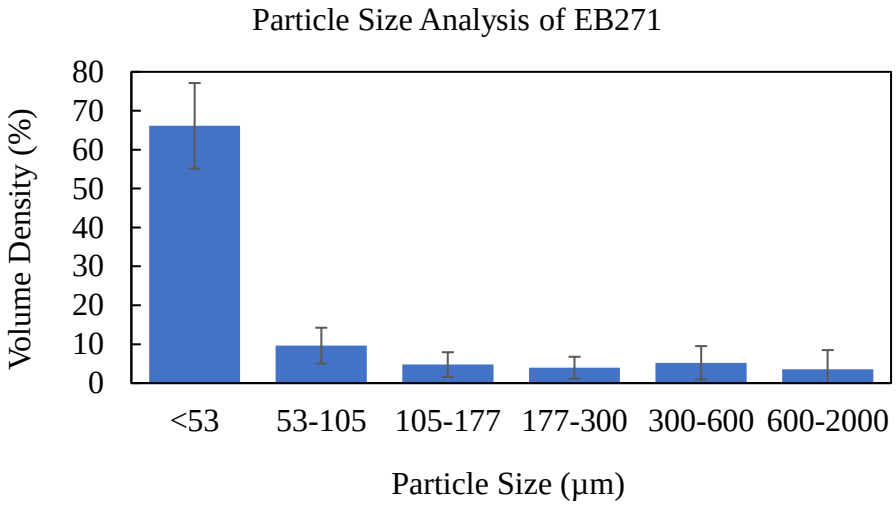

Figure 7. Volume distribution of particle size from individual segments of EB271. The majority of the volume density (> 60%) of the particles measured from all of the samples had a diameter of 53 µm or less.

Total Cell Protein

After the cores were collected from each reactor, the remaining porous material was homogenized for the remaining measurements including protein measurements. Protein measurements for each reactor were done in triplicate to calculate an average and were calculated on a µg protein per gram of porous material basis. The average total protein for pH 7, pH 6.3, and pH 4 was 12.69 µg/g sand, 13.03 µg/g sand, and 23.17 µg/g sand, respectively. pH 4 had the highest protein concentration of the three reactors indicating more attached biomass than the other two reactors that had a more circumneutral pH.

pH condition	Average Total Protein (µg/g sand)
7	12.69 ± 2.88
6.3	13.03 ± 0.52
4	23.17 ± 1.93

Table 7. Average total protein and standard deviation for each reactor.

Cell Abundances – Porous Material

After the cores were collected from each reactor, the remaining sand was homogenized for the remaining measurements including cell counts. Cell counts for each reactor were done in triplicate to calculate an average and standard deviation for both the BONCAT population and total cell population. The average BONCAT cell concentration and total cell concentration for pH 7 was 2.63E+07 cells/g sand and 1.93E+08 cells/g sand, respectively. The average BONCAT cell concentration and total cell concentration for pH 6.3 was 1.88E+07 cells/g sand and 3.18E+08 cells/g sand, respectively. The average

BONCAT cell concentration and total cell concentration for pH 4 was 4.12E+08 cells/g sand and 1.55E+09 cells/g sand, respectively. pH 4 had the highest cell concentration for both the BONCAT population and total cell population at an order of a magnitude higher than the populations of pH 7 and pH 6.3. Using the average BONCAT cell concentration and average total cell concentration for each reactor, the activity percentage was calculated. pH 4 had the highest activity percentage at 26.6% while pH 7 and pH 6.3 had an activity at 13.6% and 5.92%, respectively.

pH condition	Average DAPI cell concentration (cells/g sand)	DAPI standard deviation (cells/g sand)	Average BONCAT cell concentration (cells/g sand)	BONCAT standard deviation (cells/g sand)
7	1.93E+08	7.18E+07	2.63E+07	8.45E+06
6.3	3.18E+08	8.31E+07	1.88E+07	8.54E+06
4	1.55E+09	1.63E+09	4.12E+08	5.79E+08

Table 8. Averaged BONCAT and total cell concentration (DAPI) for triplicates samples from each reactor as well as the standard deviation for each type of cell count.

pH condition	Average DAPI cell count for triplicate samples (cells/g sand)	Average BONCAT cell count for triplicate samples (cells/g sand)	% of BONCAT cell count of total DAPI cell count
7	1.93E+08	2.63E+07	13.6
6.3	3.18E+08	1.88E+07	5.92
4	1.55E+09	4.12E+08	26.6

Table 9. Averaged BONCAT and total cell concentration for each reactor as well as the calculated activity percentage for each reactor.

Planktonic Effluent Cell Abundances

The average planktonic cell concentration for pH 7, pH 6.3, and pH 4 were 3.61E+07 cells/mL, 6.87E+07 cells/mL, and 5.45E+08 cells/mL, respectively. The planktonic cell counts for each of the reactors were significantly higher, whereas the cell count per solid material for pH 4 was significantly higher than pH 7 and pH 6.3. In terms of total bio-load for the reactors between porous medium and liquid, the vast majority of microbial biomass was associated with the porous medium (96-98%) when normalized to total biomass for each of the three reactors.

pH condition	Average planktonic cell concentration (cells/mL)	Standard deviation (cells/mL)
7	3.61E+07	5.20E+06
6.3	6.87E+07	1.00E+07
4	5.45E+08	3.84E+07

Table 10. Average planktonic cell concentration and standard deviation for each reactor.

Embedded Core and Confocal imaging

Three random fields of view were analyzed for each epoxy embedded core. For each field of view, fluorescent images of the cells and reflection images of the exposed porous material surface were taken using the same Z-stack depth. The circumference of a particle, the number of cells along that circumference, and the distances between observed cells were then measured using the segmented line tool in ImageJ. The total number of particles analyzed for each core are recorded in Table 11. The average distance between cells along a particle for pH 7, pH 6.3, and pH 4 were 79.07 ± 32.06 µm, 28.64 ± 29.36 µm, and 19.70 ± 107.3 µm, respectively. Due to variability in estimated distances between cells/aggregates likely due to heterogeneity of the porous medium, the average cell number per distance of particle circumference was estimated. The average cell/µm was significantly increased for pH 6.3 and pH 4 compared to pH 7, and this also coincides with the observed trend of increasing average cell number per particle as well as declining average distance between cells/aggregates for the three reactors, respectively.

pH Condition	Total # of particles analyzed	Average Cells/Particle	Average Cells/µm	Average distance between cells (µm)
7.0	15	2.13	0.0076	79.07
6.3	20	7.70	0.0268	28.64
4.0	19	9.32	0.0397	19.70

Table 11. Summary of cell distance measurements from Confocal microscopy for each pH condition.

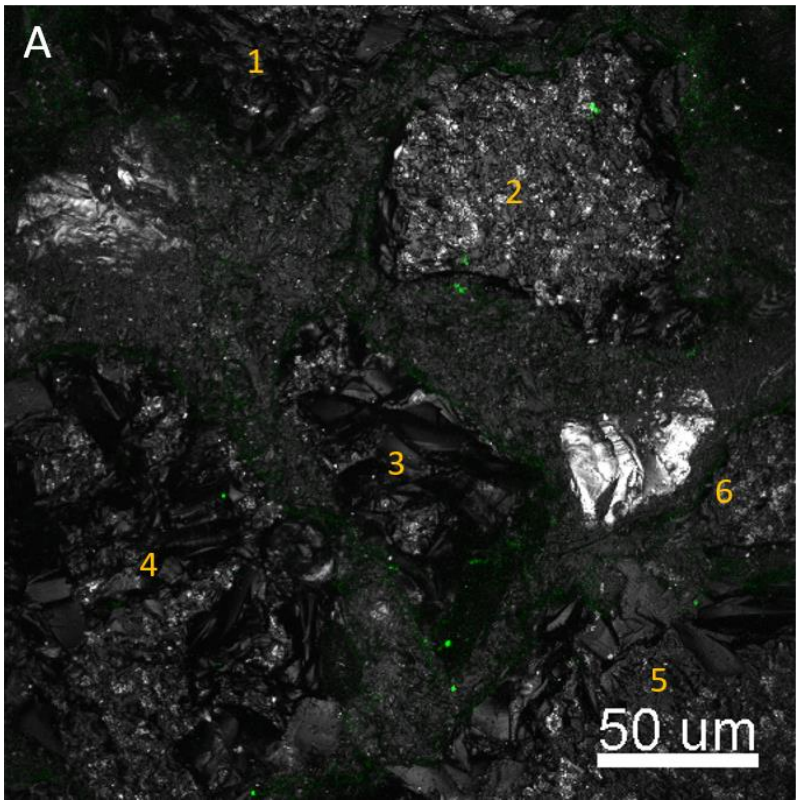

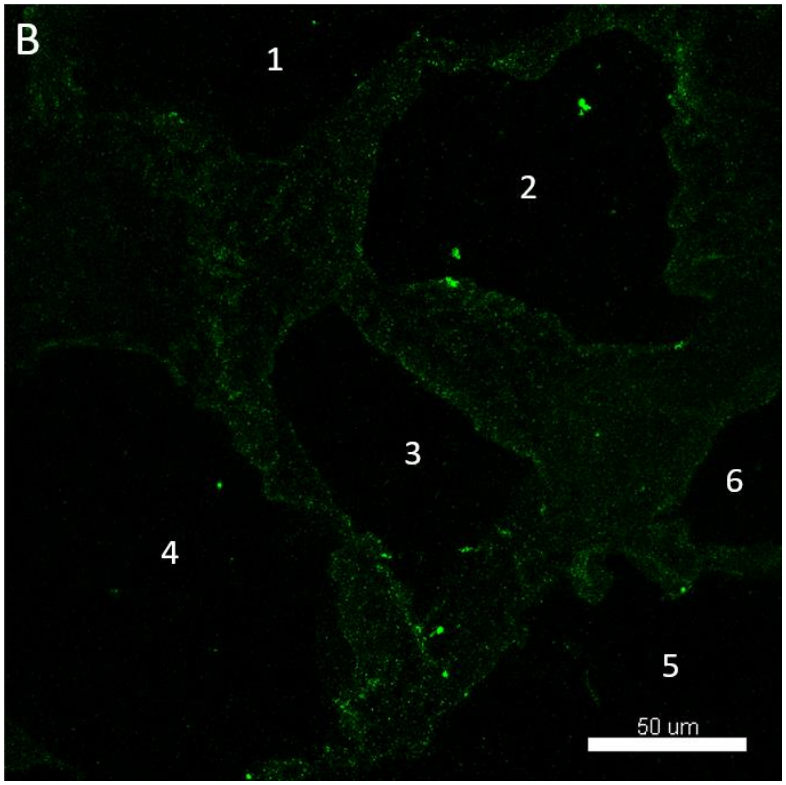

Figure 8. Confocal images of reactor 1 that had a media pH of 7. Representative confocal laser scanning microscopy images of sand with associated microbial communities and biofilm. (a) Green=SYBR Green stained microbes, grey=reflection of the sediment. (b), green =SYBR Green stained microbes. Sand particles are labeled by number.

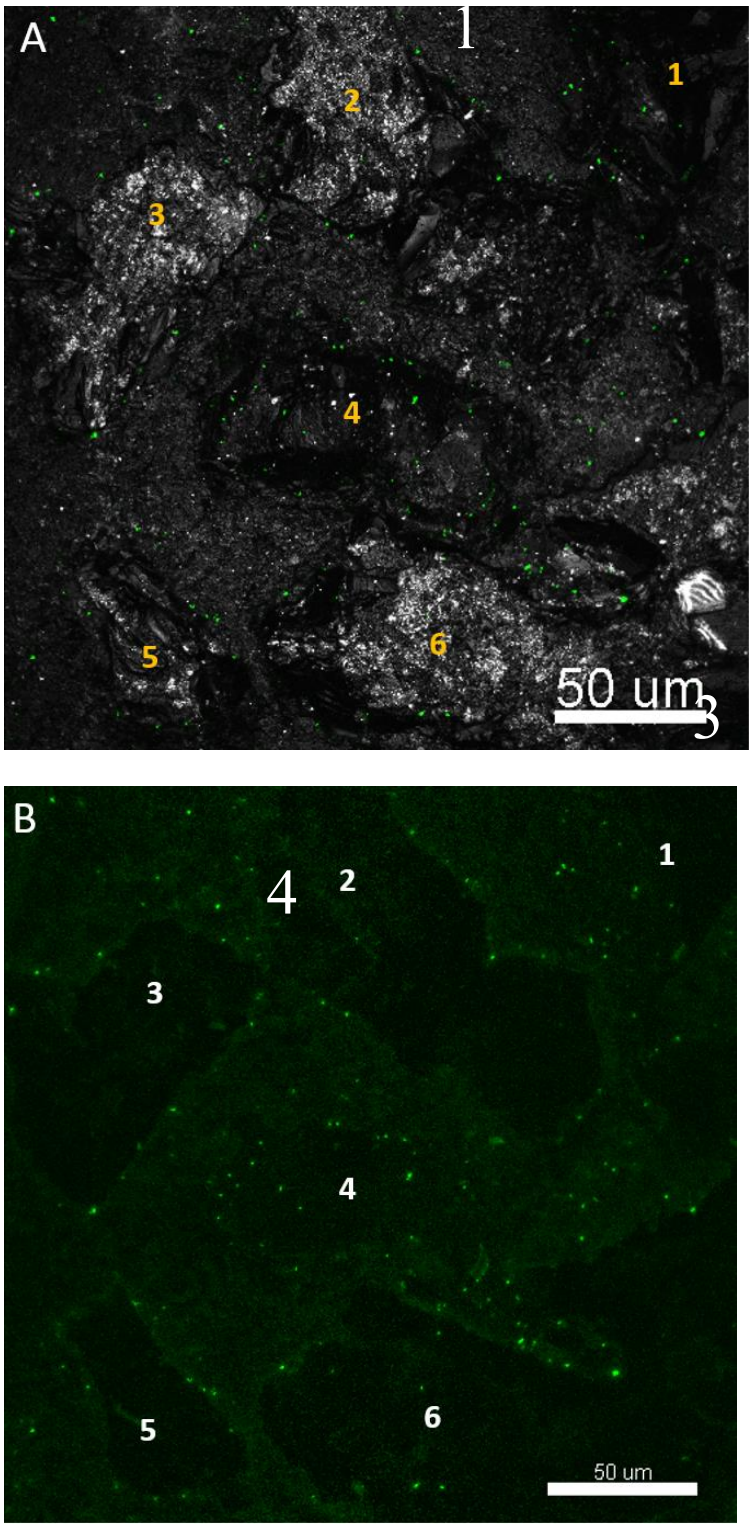

Figure 9. Confocal images of reactor 2 that had a media pH of 6.3. Representative confocal laser scanning microscopy images of sand with associated microbial communities and biofilm. (a) Green=SYBR Green stained microbes, grey=reflection of the sediment. (b), green =SYBR Green stained microbes. Sand particles are labeled by number.

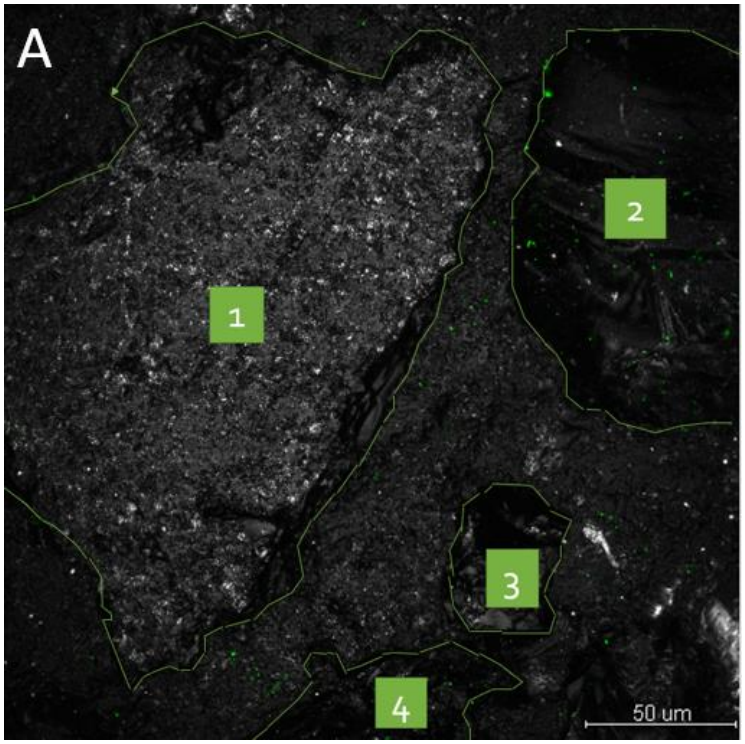

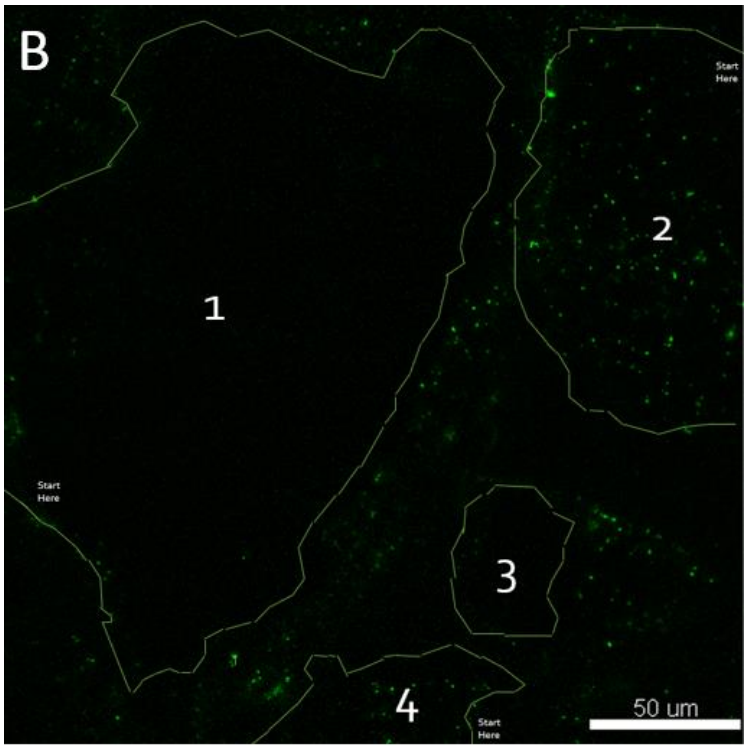

Figure 10. Confocal images of reactor 3 that had a media pH of 4. Representative confocal laser scanning microscopy images of sand with associated microbial communities and biofilm. (a) Green=SYBR Green stained microbes, grey=reflection of the sediment. (b), green =SYBR Green stained microbes. Sand particles are labeled by number. The green segment lines outlining the sand particles represent the measured distance between cells along a sand particle circumference.

Concentration Model

Using the calculated diffusion coefficients for each substrate group, the concentrations of each substrate group were calculated and graphed at increasing distances and time points. As seen in Table 5, the averaged initial concentration of the sugars is one order of magnitude greater than the amino acids and the nucleotides and is two orders of magnitude greater than the nucleosides and osmolytes. Since the sugars have a greater initial concentration and the smallest estimated diffusion coefficient, carbohydrate levels are higher over a greater distance (out to ~100 µm).

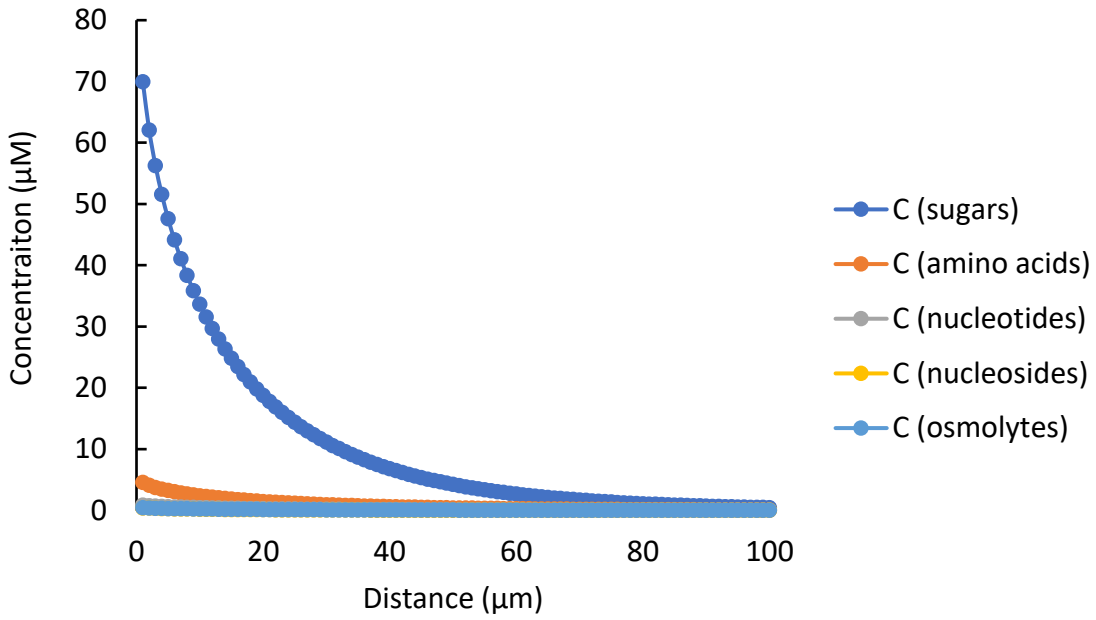

Figure 11. Concentration model for all five substrate groups that are in the exo-metabolite solution. The sugars have a much greater initial concentration compared to the four remaining groups and thus reach a concentration of zero at approximately 100 µm.

The sugars are removed from Figure 11 to be able to observe the concentrations of the four remaining groups at different distances more closely. Like the carbohydrate group,

the amino acids do not reach a concentration of zero until a distance of 100 µm. However, at 100 µm the concentration of the sugars group is approximately 0.45 µM whereas the concentration of the amino acids is 0.06 µM. For the three remaining groups, nucleotides, nucleosides and osmolytes, respective levels decline quickly over distance and are below 1 µM at approximately 40 µm.

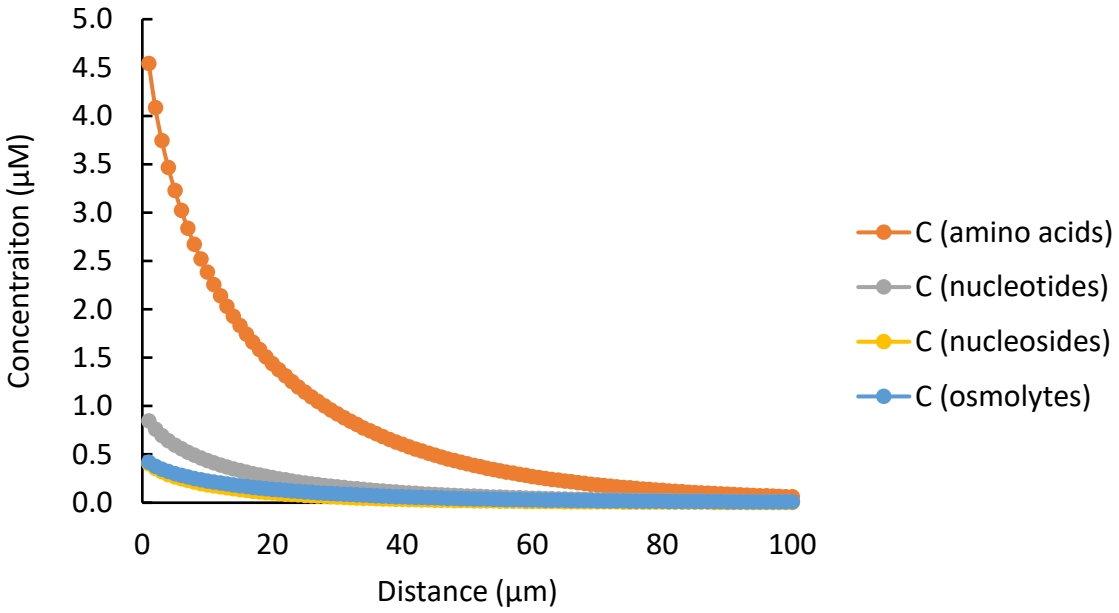

Figure 12. Concentration model of the amino acids, nucleotides, nucleosides, and osmolytes that are in the exo-metabolite solution. The sugars have been removed from this figure to be able to look at the trend of the four other substrate groups more closely.

Microbial Community Analysis

The microbial community composition for the starting inocula was distinct for each pH condition and from collected end point samples following four months of incubation (Figure 13). The starting inocula for pH 7 and pH 6.3 are slightly more similar than the starting inoculum for pH 4 and this coincides with the similar pH levels for Area 1 and 2

(pH 7 and pH 6.3) (Figure 13). Triplicate end-point samples for each pH condition clustered closely to each other indicating low variance between the samples (Figure 13). Following a four-month incubation, there is still dissimilarity in the microbial communities for each of the three pH conditions. The separation of pH 4 inoculum was explained by factor 1 on the x-axis and the pH 4 sand samples were further separated after the four-month incubation along the x-axis, likely a result of different starting populations selected under a lower pH (Figure 13). Likewise, pH 7 and pH 6.3 and respective reactor samples were further separated by factor2 along the y-axis (Figure 13). These results suggest that different populations present in the initial inocula drove the observed differences at the later time point.

In the Bray-Curtis plot (Figure 14), the starting inoculum for pH 7 and pH 6.3 are clustered more closely together than compared to the Jaccard plot because the Bray-Curtis analysis weighs the abundances of shared species. Similarly to the Jaccard plot, the pH 4 inocula is dissimilar from the inocula for pH 7 and pH 6.3. In the Bray-Curtis plot, the triplicate end-point reactor samples for pH 7 and pH 6.3 are much more similar to each othe. nd dissimilar from the pH 4 endpoint (Figure 14). The Jaccard and Bray-Curtis analyses indicate that each of the reactors started with unique populations that selected from unique compositions during the incubation period, but pH 7 and pH 6.3 were more similar to each other when the relative abundances of predominant groups were considered.

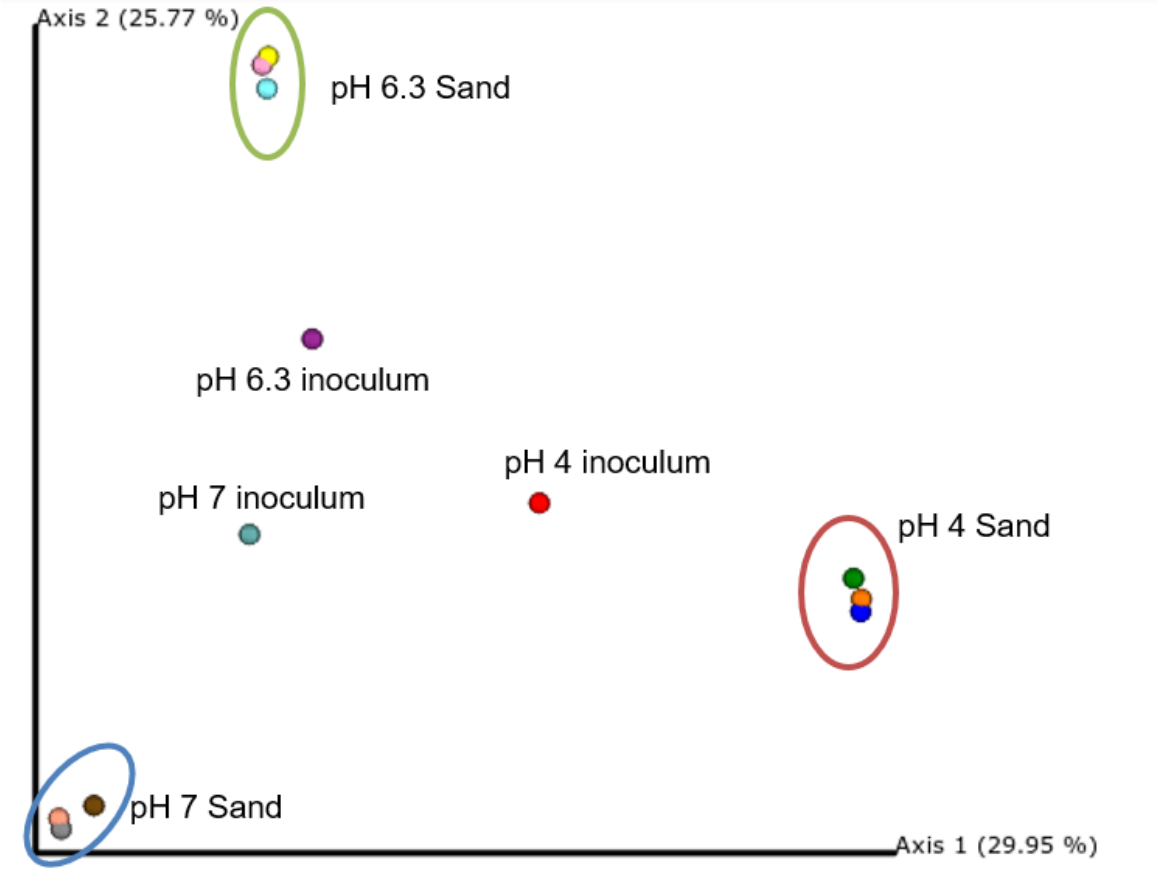

Figure 13. Beta diversity, Principal Coordinate Analysis (PCoA), plot for starting inoculum and sand samples collected from the porous media reactors. FW106 is the starting inoculum for the pH 4 condition, GW835 is the starting inoculum for the pH 6.3 condition, and EU05 is the starting inoculum for the pH 7 condition.

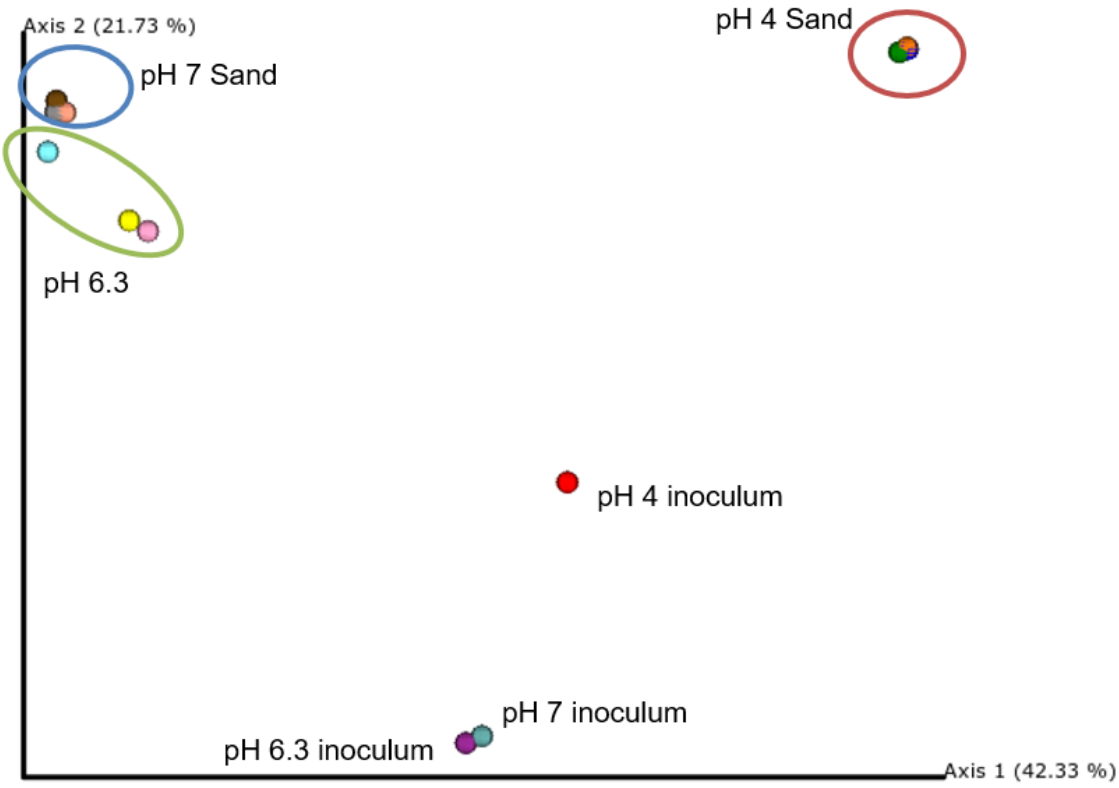

Figure 14. Principal Coordinate Analysis (PCoA) Bray-Curtis dissimilarity biplot by sample. FW106 is the starting inoculum for the pH 4 condition, GW835 is the starting inoculum for the pH 6.3 condition, and EU05 is the starting inoculum for the pH 7 condition.

Both circumneutral pH starting inocula (pH 7 and pH 6.3) have a large abundance of *Azoarcus* (~70% for pH 7 and ~27% for pH 6.3) and *Geothrix* (~5% for pH 7 and ~15% for pH 6.3). Additionally, the starting inoculum for pH 6.3 also had a large abundance of *Comomonadaceae* (~10%) and *Cellulomonas* (~18%), whereas the starting inoculum for pH 7 did not contain a large abundance of these genera. However, the relative abundance of both *Azoarcus* and *Geothrix* decreased in the end-point samples for both pH 7 and pH 6.3 (*Azoarcus* decreased by ~10-26%, *Geotrhix* decreased by ~3-12%). The triplicate sand samples for pH 7 and pH 6.3 have a large abundance of Enterobacteriaceae (~59% for pH

7 and ~34% for pH 6.3). However, the triplicate sand samples for pH 6.3 have a larger relative abundance of *Ochrobactrum* (~25%), while the triplicate sand samples for pH 7 have a larger relative abundance of *Azoarcus* (~10%).

The pH 4 inoculum was predominated by *Burkholderia*, *Rhodanobacter*, Burkholderia-Caballeronia-Paraburkholderia groups (4 groups comprising over 55% of the total community). The relative abundance of the Burkholderia-Caballernoia-Paraburkholderia group increased, by ~28%, in the end-point samples for pH 4 as compared to the starting inoculum for pH 4. Similarly, the relative abundance of *Rhodanobacter* and *Clostridium* in the sand samples for pH 4 increased by ~25% and ~18%, respectively as compared to the starting inoculum for pH 4. The inocula for pH 7 and pH 6.3 had higher diversity compared to pH 4 inoculum (Figure 16). After the 4-month incubation, all three pH samples had less diversity than the starting inocula but to a much lesser extent for pH 4 (7% decline in diversity versus ~20% decline in diversity for pH 7 and pH 6.3; Figure 16).

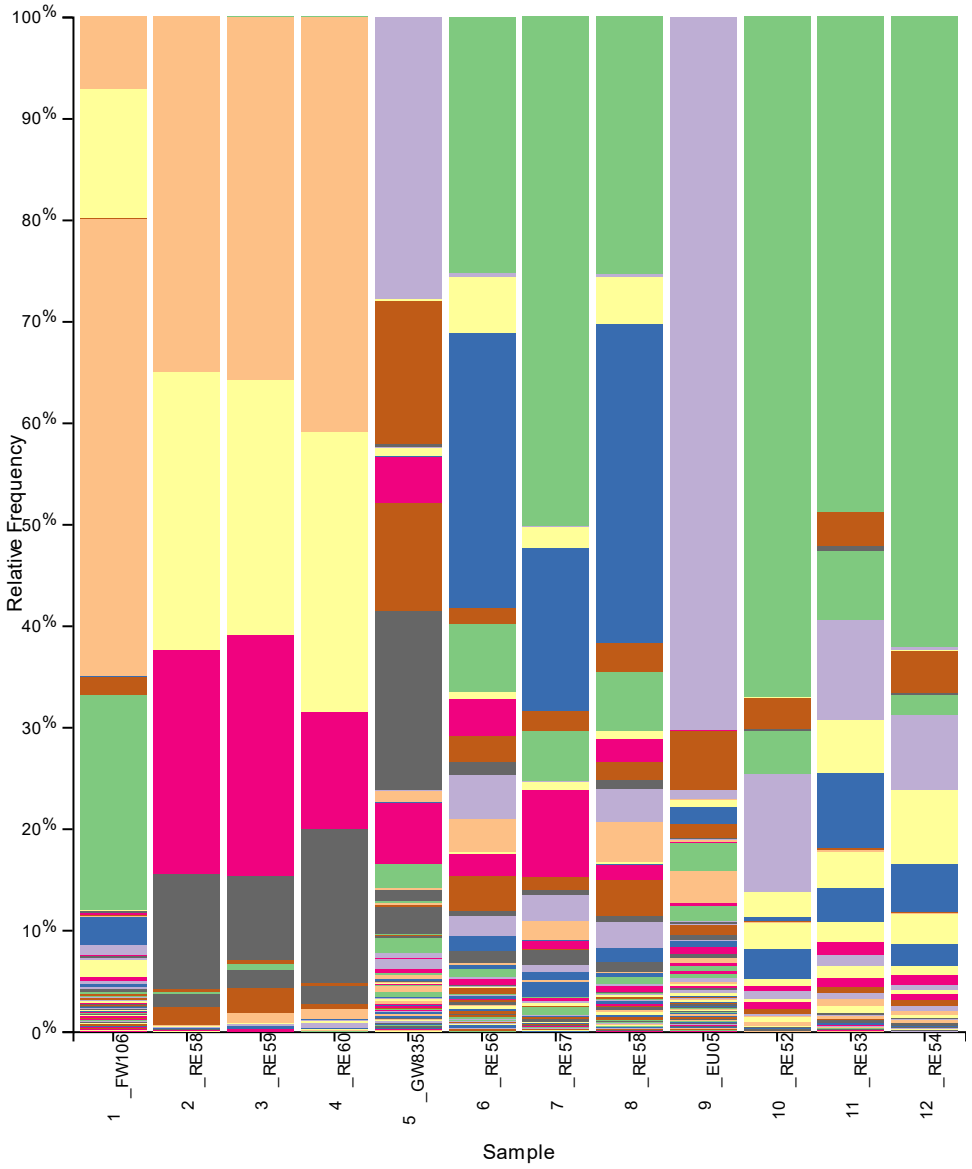
100%
90%
80%
70%
60%
50%
40%
30%
20%
10%
0%
Relative Frequency
1 _FW106
2 _RE58
3 _RE59
4 _RE60
5 _GW835
6 _RE56
7 _RE57
8 _RE58
9 _EU05
10 _RE52
11 _RE53
12 _RE54
Sample

Figure 15. Relative abundance plot for the starting inoculum and triplicate sand samples collected from each reactor. FW106 is the starting inoculum for reactor 3, GW835 is the starting inoculum for reactor 2, and EU05 is the starting inoculum for reactor 1. Samples 2 through 4 are the sand samples for pH 4, samples 6 through 8 are the sand samples for pH 6.3, and samples 10 through 12 are the sand samples for pH 7.

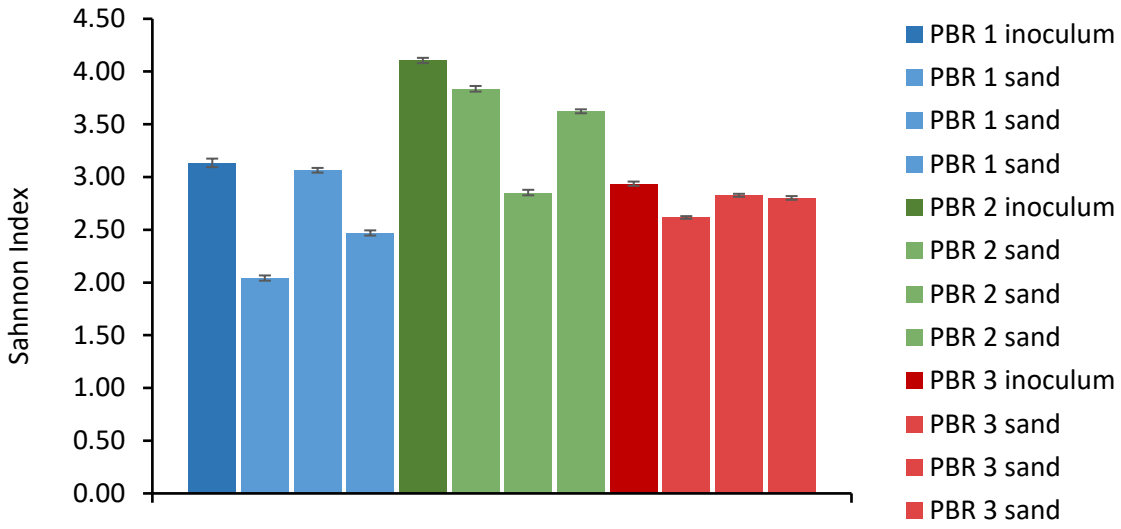

Figure 16. Shannon Index of β-diversity for all inocula and triplicate sand samples for each reactor.

Discussion

The shallow subsurface and the diverse microbial community play a vital role in sustaining life, both above and below the surface through major contributions to the geochemical properties of groundwater (Goldscheider et al., 2006). While much attention given to the shallow terrestrial subsurface has been focused on the effects of contamination and how microorganisms function in these systems (Fields et al., 2005; Zinger et al., 2012), the relationship between hydraulic properties and the indigenous microbial community have been far less studied. It is essential to understand how microbiology and hydrology of the shallow subsurface environment are linked to fully understand how environmental factors impact microbial community dynamics, interactions, succession, colonization, and dispersal in the shallow subsurface environment. In addition, the shallow subsurface

ecotones include both groundwater and porous media, and thus, both aqueous and solid media are important and unique niches that influence nutrient allocation, biomass distribution, and water quality. The current study focused on designing a reactor system that emulates select field conditions (*i.e.*, flow rate and particle size) observed at the Oak Ridge National Laboratory-Field Research Center (ORNL-FRC) to observe microbial biomass and activity distribution in a micropore environment with an inoculum that consisted of indigenous populations from both groundwater and sediments.

PBR Reactors

A flow rate of 0.048 mL/min was used in this study as a field relevant flow rate for the FRC (Watson, Kostka, Fields, & Jaridne, 2004). The hydraulic conductivity and permeability of the system are 3.69E-05 m/s and 3.35E-12 m^2, respectively. The hydraulic conductivity and permeability are both within the range of observed hydraulic properties of the field, with the hydraulic conductivity ranging from 10^{-4} to 10^{-6} m/s and the permeability ranging from 10^{-11} m^2 to 10^{-13} m^2 at the FRC (Watson, Kostka, Fields, Jardine, 2004). Additionally, the particle size distribution (75 µm to 300 µm) is similar to what is observed at the FRC with the majority of the particle size distribution ranging from the silt (2-50 µm) to medium sand range (250-500 µm). However, in this study particles with a diameter of less than 75 µm were not used due to the difficulty of using such small particles, such as clogging, as well as to prevent clogging of the influent line for the reactor set up. In previous studies it has been shown that particle size can impact microbial activity and distribution, with smaller grains (125-250 µm) having greater activity compared to larger grains (250-500 µm) (Alfreider, Krössbacher and Psenner, 1997). Particle size can impact

interstitial fluxes and mixing, ultimately influencing biofilm growth and activity, thus making it essential to have porous media that emulates the field of interest (Smith et al. 2018).

Porous Media Visualization

The epoxy embedded sand core method developed for this study allows for the visualization and measurement of cells in a field relevant porous media environment. The method allows for intact sand cores to be removed from the reactor system to visualize intact attached microbial communities post-fixation and embedding. Additionally, the method allows for the epoxy embedded sand core to be sectioned in both the vertical and horizontal axis giving the option to observe intact cells on multiple planes in the porous media. Similar methods have been used to show that bacterial cells are aggregated at the scale of a few micrometers, most likely due to the soil structure and the way bacterial cells reproduce (Raynaud and Nunan, 2014). Future work is planned to attempt the developed methods with field samples in order to elucidate the assembly and distribution of microbial communities *in situ* across subsurface zones.

Biomass and Cell Concentration

To understand how microorganisms exist and function in the terrestrial subsurface environment it is critical to observe both the planktonic and attached microbial community in order to determine how their functions differentiate. Cell concentrations were evaluated for both the planktonic and attached microbial communities. The total number of cells for the attached microbial community ranged from 1.93E+08 cells/g sand to 1.55E+09 cells/g

sand with pH 4 having the highest biomass. The total number of cells for the liquid fraction of the reactors ranged from 3.61E+07 cells/mL to 5.45E+08 cells/mL with pH 4 having the highest biomass. The total bio-load for pH 7, pH 6.3., and pH 4 was 6.23E+10 cells, 1.03E+11 cells, and 5.10E+11 cells, respectively. For all three pH conditions, the majority of the biomass was in the attached community accounting for 96-98%, whereas the planktonic fraction only accounted for 2-4% of the total biomass. A one-way ANOVA analysis with a factor of pH was performed on the protein concentrations and cell concentrations to determine the statistical difference between the three pH conditions. The protein concentration for pH 4 was significantly different from the circumneutral pH conditions (p-value = 0.002), but the circumneutral pH conditions were not significantly different from each other (p-value = 0.976; Figures A22-24). Similarly, the total attached cell concentration of pH 4 was significantly different from the two circumneutral pH conditions (p-value < 0.05), and the circumneutral pH conditions were not significantly different from each other (p-value = 0.270; Figures A13-A15). However, when the attached BONCAT cell concentrations were compared, the difference in the median cell concentrations was significantly different between pH 4 and pH 6.3 (p-value 0.016; Figures A16-A18). The attached BONCAT cell concentration for the pH 7 reactor was not significantly different from the pH 6.3 reactor or the pH 4 reactor (p-value = 0.767 and 0.071, respectively). When the planktonic cell concentrations of the three different pH conditions were compared, all three pH conditions were significantly different from each other (p-value < 0.05 for all comparisons; Figures A19-A21). Previous studies have shown

similar biomass concentrations for an *in situ* attached microbial community of 10^8 cells/g soil from an agricultural environment (Raynaud and Nunan, 2014).

Diversity and Richness

It is well known that the shallow subsurface harbors a large fraction of total microbial biomass on the planet (approximately 40%) with an immense level of diversity (Whitman, Coleman and Weibe 1998; Griebler and Lueders 2009; McMahon and Parnell 2014). However, there is limited information detailing the exact relationship between microbial diversity, environmental parameters, and hydrological processes between groundwater and porous media in the subsurface (Smith et al., 2018). The described study focused on the diversity of established microbial communities in a field relevant porous medium environment at field relevant pH and nitrate levels. The inocula for pH 7 and pH 6.3 had higher diversity compared to pH 4 inoculum After the 4-month incubation, all the reactor samples had less diversity than the starting inocula but to a much lesser extent for pH 4 (7% decline in diversity versus ~20% decline in diversity for pH 7 and pH 6.3, Figure 16). Higher diversity was observed in the pH 7 and pH 6.3 inocula, and likewise, pH 7 and pH 6.3 had higher sampled diversity that was significantly different from pH 4 (Bray-Curtis and Jaccard). The two circumneutral reactors (pH 7 and pH 6.3) were predominated by a mixture of sequences indicative of low G+C Gram-positive bacteria as well as α-, β-, and γ-Proteobacteria and had more similar community structure with each other compared to pH 4. The pH 4 inoculum was predominated by *Burkholderia*, *Rhodanobacter*, Burkholderia-Caballeronia-Paraburkholderia groups (4 groups comprising over 55% of

total), most likely driven by low pH and high nitrate levels (Hemme et al., 2010; Hemme et al., 2015). The *Burkholderia* and *Rhodanobacter*-like sequences were not observed at significant levels in the pH 7 and pH 6.3 nor in pH 7 and pH 6.3. It is interesting that despite similar reactor conditions (particles, flow rate, C/N sources, dissolved oxygen), the three pH conditions supported very different levels of microbial biomass and diversity akin to observations in the field driven by pH and nitrate. Future work is planned to use the developed methods to ascertain the distribution of microbial biomass *in situ*.

Cell Localization Discussion

The distribution of microorganisms in porous environments, like the shallow subsurface, is a consequence of both extrinsic processes (*e.g*., pore size; pH; flow rate) that likely impact microbial dispersal as well as intrinsic processes (*e.g*., cellular reproduction; attachment/detachment, motility) that can impact aggregation. However, it is likely that intrinsic processes are related to extrinsic processes, as the probability of growth is greater where external conditions are more suitable for growth (*i.e*., presence of metabolites) or attachment/detachment is impacted by dispersivity, permeability, and the presence of multi-valent cations. Yet, the pores and aggregates are continuously changing due to biogeochemical processes and physical processes (Schlüter and Vogel, 2016), which could impact the pore size distributions of the shallow subsurface. Sediment pores can have discrete microenvironments with distinct activities and conditions (Keil and Mayer 2014) that are likely attributed to areas of high metabolic activities or "hot spots and hot moments' (McClain et al., 2003). Thus, understanding the role of hydrological flow paths in

distributing reactants, metabolites, and cells is crucial for predicting when and where microbial communities will exist, be active/dormant, and aggregate or disperse.

In this study, the visualization and measurement of cells along the circumference of a sand particle were analyzed for three pH conditions (4, 6.3, 7). pH 4 had the smallest average distance between cells on or along the circumference of a particle. When comparing the means for all three conditions using a Tukey pairwise comparison, there was not a statistical difference between the three conditions for the average distance between cells (p-value > 0.05 for all comparisons; Figure A8 and Figure A9). However, when the cell distances were normalized to the particle circumference, pH 6.3 and pH 4 were significantly different from pH 4 (p-values < 0.05 for both comparisons; Figure A10 and Figure A11).

pH 4 had the highest number of cells per gram of porous medium (1.6×10^9 cells/g) that was 5-fold and 8-fold higher than pH 6.3 and pH7, respectively. Interestingly, pH 4 had the highest BONCAT cell counts, and in pH 4 almost 30% of attached cells were active (compared to 6 and 13% for the other reactors). pH 4 also had higher cell counts in the planktonic phase. pH 6.3 and pH 7 had significantly higher average cell numbers per µm of particle circumference distance. Particle size, flow rate, and organic C and N sources were the same for all three reactors; however, in order to emulate field conditions for respective areas, the pH, nitrate, and inocula differed for the three pH conditions. Based upon previous work, the gradients of pH and nitrate have significant impacts on the

microbial communities and activities at the FRC and likely drive community differences (Fields et al., 2005; Fields et al., 2006; Smith et al., 2015).

The reactors showed different trends in the average distance between cells and/or cell aggregates along a particle. The measured distances were also compared to substrate concentrations over distances predicted by a model based upon diffusion coefficients for compound classes (*i.e.*, sugars, amino acids, nucleotides/nucleosides). Based on the concentration model in terms of the average distance between cells for each reactor, sugars and amino acids could be at levels (10s of µM) that could impact physiological responses between cells on a particle due to the larger concentrations in the exo-metabolite mix. However, in pH 7, the average distance between cells on a particle was 79 µm. Thus, nucleosides, nucleotides and osmolytes would likely not be exchanged between cells on a particle at the pH condition of 7. For pH 6.3 and pH 4, all five substrate groups would likely be able to be exchanged between cells on a particle because the estimated average distance between cells was 28 µm and 19 µm, respectively.

It is interesting to note that pH 4 had the lowest pH and highest nitrate levels similar to sites in Area 3 (such as FW106) and had the highest biomass, cell numbers, and activity levels. pH 4 also had the shortest distances between cells as well as the highest density of cells per particle or per particle circumference. These observations coincide with observations from the field that show high cell counts from FW106 and other similar wells with high nitrate and low pH (T.C. Hazen, personal communication), and demonstrate the selection of adapted populations over approximately 70 years. Despite the conditions of low pH and high nitrate levels being considered stressful, higher levels of attached biomass

with more even biomass distribution on particles was observed for pH 4 (and somewhat pH 6.3). Previous models have predicted that flow conditions could select for slower attached growth in porous media (Coyte et al., 2016), and this could partially explain our observations with pH 4 conditions and the slower flow rate of 0.048 mL/min in the porous medium reactor system. The slower growth associated with low pH and higher nitrate could allow a more even distribution of attached biomass under the tested flow conditions, and likewise, potentially faster growth in the higher pH conditions (where there was also higher diversity) caused a less even distribution of biomass that could be more analogous to the paradigm of "hot spots and hot moments". The pH 4 condition also had higher numbers of active cells as determined via BONCAT, and it is important to note that the BONCAT estimate is based upon an "active" cell that is translationally-active and does not provide a direct measurement of activity per se.

Conclusion

In conclusion, environmental factors influence bacterial diversity and metabolic activity in the shallow subsurface. However, most studies observe how environmental factors influence microorganisms in batch studies rather than in a system that emulates the shallow subsurface and flow in porous medium. This study created a reactor system that emulates the shallow subsurface and allows for modification of different parameters of interest such as solid matrices and hydraulic properties. We also developed a method to visualize the localization of active and non-active cells within the porous medium. Overall, the data and predictions demonstrated that under *ex situ* conditions, cells that are part of a diverse microbial community can be on average 20 to 80 µm apart with an average of

0.0076 to 0.0397 cells/μm for representative sites with varying pH and nitrate levels at the FRC. Based on diffusivity of potential substrates and measured distance ranges between cells, sugar levels could be approximately 5 to 20 μM whereas amino acids and nucleotides/nucleosides would be sub-micromolar between nearest cell/aggregate neighbors. Future work will include elucidating the impacts of average pore velocity on targeted metabolic interactions between different predominant populations as well as determining the distribution of biomass and activity *in situ*.

CONCLUSIONS

With 99% of the 1% of water usable for human use located in groundwater, global demands for natural subsurface resources continues to grow at increasing rates. However, we currently lack a thorough understanding of how minerals (Kesler, 2007), clean and potable water (Jackson and Smith, 2014), and extraction and utilization of underground resources (Tilman et al., 2011) impact the ecosystems of the shallow subsurface. Interest in subsurface microorganisms and associated ecological function has increased largely due to the emerging need to assess groundwater quality for human use as well as for the potential to naturally remediate water systems that have been disturbed via engineering efforts (e.g., managed aquifer recharge systems) or contaminated from human practices (Anderson & Lovley, 1997; Chapelle, 2000; Langwaldt and Puhakka, 2000; Fields et al., 2006). Expanding our current knowledge of how microorganisms form, function, and adapt to changing geochemical properties in the shallow subsurface environment will require a greater understanding of the structure of the shallow subsurface environment, including how sediment structure, substrate flow, and microbial distribution vary and interact over space in the terrestrial subsurface. The work presented in this thesis aimed towards designing a reactor system that could emulate field relevant conditions (e.g., particle size, porosity, average pore velocity, hydraulic conductivity, and permeability).

While much attention given to the shallow terrestrial subsurface has been focused on the effects of contamination and how microorganisms function in these systems, knowledge of how the hydraulic properties of the shallow terrestrial subsurface influence microbial distribution and function have been far less studied. The hydraulic parameters of

the shallow subsurface can influence microbial growth or inhibit it. For example, where there are larger particle grains, which also can correspond to a more porous and more permeable flow path, there is a higher hydraulic conductivity, or the ease with which a fluid can flow through that material. In areas of larger hydraulic conductivities, metabolites and reactants can be transferred more easily to the microbial communities, including both planktonic and attached microbial communities. However, in areas that are mostly comprised of smaller particles, lower hydraulic conductivities typically exist. The lower hydraulic conductivity of these areas limits the transport of metabolites and reactants. Furthermore, if there are biofilms attached to particles in areas with lower hydraulic conductivity the attached microbial community can decrease the porosity and permeability of the flow path. Thus, understanding how hydraulic parameters and microbial activity are linked is crucial for modeling how microorganisms exist in the shallow subsurface, as well as understanding how perturbations will impact microbial communities in the shallow subsurface.

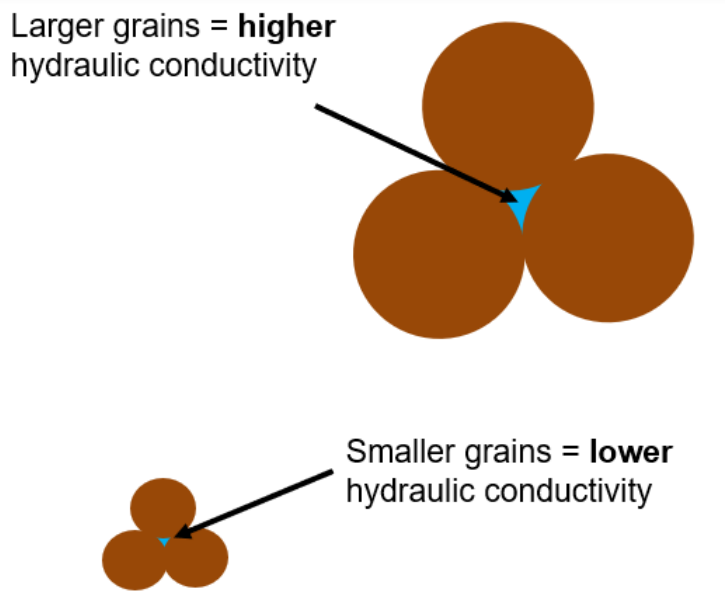

Figure 17. Hydraulic conductivity in respect to grain sizes.

On an ecosystem scale, there is limited information regarding the exact relationship between microbial diversity, environmental parameters, and biogeochemical processes between groundwater and porous media of the terrestrial subsurface. Furthermore, there are multiple scales that the terrestrial subsurface exists at (field scale to interfacial scale) but little is known about how microbially relevant scales ultimately impact field scale behavior and function. Few studies have determined the proper scale to emulate to define these relationships (microbially relevant scale to field scale). The packed bed reactor system presented in this thesis simulates the pore scale (< millimeters) at which porous media flow and local heterogeneity occurs, the sub-pore scales (micrometers to millimeters) where fluid-solid interfaces occur, and the interfacial scales (<micrometers) at which molecular-scale interfaces occur. The reactor system designed and presented can simulate the pore scale to the interfacial scale that exists in the terrestrial subsurface which

allows us to observe how the heterogeneity of porous media impacts microbial activity, as well as study how the planktonic community and attached community differ in a field relevant environment. Furthermore, visualizing and analyzing individual cells in both the planktonic and attached fractions have been developed for the reactor system at hand.

In conclusion, the system presented in this thesis can be used to study how different environmental factors and hydraulic properties affect microbial communities in a porous media environment. The results presented in this thesis contribute to the collective understanding of subsurface microbial activity in the terrestrial subsurface environment. Additionally, the presented results have field-relevant implications for isolation and modeling of microbial populations within the terrestrial shallow subsurface at the FRC.

REFERENCES CITED

Akob, D. M., & Küsel, K. (2011). Where microorganisms meet rocks in the Earth's Critical Zone. *Biogeosciences*, *8*(12), 3531-3543.

Alfreider, A., Krössbacher, M., & Psenner, R. (1997). Groundwater samples do not reflect bacterial densities and activity in subsurface systems. *Water Research*, *31*(4), 832-840.

Anantharaman, K., Brown, C. T., Hug, L. A., Sharon, I., Castelle, C. J., Probst, A. J., ... & Banfield, J. F. (2016). Thousands of microbial genomes shed light on interconnected biogeochemical processes in an aquifer system. *Nature communications*, *7*(1), 1-11.

Anderson, R. T., & Lovley, D. R. (1997). Ecology and biogeochemistry of in situ groundwater bioremediation. *Advances in microbial ecology*, 289-350.

Atekwana, E. A., & Slater, L. D. (2009). Biogeophysics: A new frontier in earth science research: Review of Geophysics, 47. *RG4004*.

Atekwana, E. A., Werkema, D. D., & Atekwana, E. A. (2006). Biogeophysics: The effects of microbial processes on geophysical properties of the shallow subsurface. In *Applied hydrogeophysics* (pp. 161-193). Springer, Dordrecht.

Berkowitz, B., Silliman, S. E., & Dunn, A. M. (2004). Impact of the capillary fringe on local flow, chemical migration, and microbiology. *Vadose Zone Journal*, *3*(2), 534-548.

Caporaso, J. G., Lauber, C. L., Walters, W. A., Berg-Lyons, D., Huntley, J., Fierer, N., ... & Knight, R. (2012). Ultra-high-throughput microbial community analysis on the Illumina HiSeq and MiSeq platforms. *The ISME journal*, *6*(8), 1621-1624.

Coyte, K. Z., Tabuteau, H., Gaffney, E. A., Foster, K. R., & Durham, W. M. (2017). Microbial competition in porous environments can select against rapid biofilm growth. *Proceedings of the National Academy of Sciences*, *114*(2), E161-E170.

Brady, N. C., Weil, R. R., & Brady, N. C. (2010). Elements of the nature and properties of soils.

Chakraborty, R., Wu, C. H., & Hazen, T. C. (2012). Systems biology approach to bioremediation. *Current Opinion in Biotechnology*, *23*(3), 483-490.

Chapelle, F. H. (1993). Ground-Water Microbiology and Geochemistry: New York, NY, JohnWiley and Sons.green

Chapelle, F. H. (2000). The significance of microbial processes in hydrogeology and geochemistry. *Hydrogeology Journal*, *8*(1), 41-46.

Cho, S. J., Kim, M. H., & Lee, Y. O. (2016). Effect of pH on soil bacterial diversity. *Journal of Ecology and Environment*, *40*(1), 1-9.

Chu, H., Sun, H., Tripathi, B. M., Adams, J. M., Huang, R., Zhang, Y., & Shi, Y. (2016). Bacterial community dissimilarity between the surface and subsurface soils equals horizontal differences over several kilometers in the western Tibetan Plateau. *Environmental Microbiology*, *18*(5), 1523-1533.

Danielopol DL, Griebler C, Gunatilaka A et al. Incorporation of groundwater ecology in environmental policy. In: Quevauviller P (ed). Groundwater Science and Policy. Cambridge: Royal Society of Chemistry, 2008, 671–89.

Dennehy, K. F., Reilly, T. E., & Cunningham, W. L. (2015). Groundwater availability in the United States: the value of quantitative regional assessments. *Hydrogeology Journal*, *23*(8), 1629-1632.

Dieter, C. A. (2018). *Water availability and use science program: Estimated use of water in the United States in 2015*. Geological Survey.

Donlan, Rodney M. "Biofilms: microbial life on surfaces." *Emerging infectious diseases* vol. 8,9 (2002): 881-90. doi:10.3201/eid0809.020063

Evans, R., Dal Poggetto, G., Nilsson, M., & Morris, G. A. (2018). Improving the interpretation of small molecule diffusion coefficients. *Analytical chemistry*, *90*(6), 3987-3994.

Fetter, C. W. (2018). *Applied hydrogeology*. Waveland Press.

Fields, M. W., Yan, T., Rhee, S. K., Carroll, S. L., Jardine, P. M., Watson, D. B., ... & Zhou, J. (2005). Impacts on microbial communities and cultivable isolates from groundwater contaminated with high levels of nitric acid–uranium waste. *FEMS Microbiology Ecology*, *53*(3), 417-428.

Fields, M. W., Bagwell, C. E., Carroll, S. L., Yan, T., Liu, X., Watson, D. B., ... & Zhou, J. (2006). Phylogenetic and functional biomakers as indicators of bacterial community responses to mixed-waste contamination. *Environmental science & technology*, *40*(8), 2601-2607.

Fierer, N., & Jackson, R. B. (2006). The diversity and biogeography of soil bacterial communities. *Proceedings of the National Academy of Sciences*, *103*(3), 626-631.

Goldscheider, N., Hunkeler, D., & Rossi, P. (2006). Microbial biocenoses in pristine aquifers and an assessment of investigative methods. *Hydrogeology Journal*, *14*(6), 926-941.

Griebler, C., & Avramov, M. (2015). Groundwater ecosystem services: a review. *Freshwater Science*, *34*(1), 355-367.

Griebler, C., & Lueders, T. (2009). Microbial biodiversity in groundwater ecosystems. *Freshwater Biology*, *54*(4), 649-677.

Griebler, C., Malard, F., & Lefébure, T. (2014). Current developments in groundwater ecology—from biodiversity to ecosystem function and services. *Current opinion in biotechnology*, *27*, 159-167.

Hatzenpichler, R., & Orphan, V. J. (2015). Detection of protein-synthesizing microorganisms in the environment via bioorthogonal noncanonical amino acid tagging (BONCAT). In *Hydrocarbon and Lipid Microbiology Protocols* (pp. 145-157). Springer, Berlin, Heidelberg.

Hemme, C. L., Deng, Y., Gentry, T. J., Fields, M. W., Wu, L., Barua, S., ... & Zhou, J. (2010). Metagenomic insights into evolution of a heavy metal-contaminated groundwater microbial community. *The ISME journal*, *4*(5), 660-672.

Hemme, C. L., Tu, Q., Shi, Z., Qin, Y., Gao, W., Deng, Y., ... & Zhou, J. (2015). Comparative metagenomics reveals impact of contaminants on groundwater microbiomes. *Frontiers in microbiology*, *6*, 1205.

Holliger, C., Gaspard, S., Glod, G., Heijman, C., Schumacher, W., Schwarzenbach, R. P., & Vazquez, F. (1997). Contaminated environments in the subsurface and bioremediation: organic contaminants. *FEMS Microbiology Reviews*, *20*(3-4), 517-523.

"How We Use Water." *EPA*, Environmental Protection Agency, www.epa.gov/watersense/how-we-use-water.

Hwang, C., Wu, W., Gentry, T. J., Carley, J., Corbin, G. A., Carroll, S. L., ... & Fields, M. W. (2009). Bacterial community succession during in situ uranium bioremediation: spatial similarities along controlled flow paths. *The ISME journal*, *3*(1), 47-64.

Jackson, P. M., & Smith, L. K. (2014). Exploring the undulating plateau: the future of global oil supply. *Philosophical Transactions of the Royal Society A: Mathematical, Physical and Engineering Sciences*, *372*(2006), 20120491.

Jenkins, S., Swenson, T. L., Lau, R., Rocha, A. M., Aaring, A., Hazen, T. C., ... & Northen, T. R. (2017). Construction of viable soil defined media using quantitative metabolomics analysis of soil metabolites. *Frontiers in microbiology*, *8*, 2618.

Jones, A. A., & Bennett, P. C. (2014). Mineral microniches control the diversity of subsurface microbial populations. *Geomicrobiology Journal*, *31*(3), 246-261.

Jones, R. M., Goordial, J. M., & Orcutt, B. N. (2018). Low energy subsurface environments as extraterrestrial analogs. *Frontiers in microbiology*, *9*, 1605.

Keil, R. G., & Mayer, L. M. (2014). Mineral matrices and organic matter. Treatise on Geochemistry. Eds. HD Holland, KK Turekian.

Kesler, S. E. (2007). Mineral supply and demand into the 21st century. In *proceedings for a workshop on deposit modeling, mineral resource assessment, and their role in sustainable development. US Geological Survey circular* (Vol. 1294, pp. 55-62).

Langwaldt, J. H., & Puhakka, J. A. (2000). On-site biological remediation of contaminated groundwater: a review. *Environmental pollution*, *107*(2), 187-197.

Liu, Y., Liu, C., Nelson, W. C., Shi, L., Xu, F., Liu, Y., ... & Zachara, J. M. (2017). Effect of water chemistry and hydrodynamics on nitrogen transformation activity and microbial community functional potential in hyporheic zone sediment columns. *Environmental science & technology*, *51*(9), 4877-4886.

López, D., Vlamakis, H., & Kolter, R. (2010). Biofilms. *Cold Spring Harbor perspectives in biology*, *2*(7), a000398. https://doi.org/10.1101/cshperspect.a000398.

McClain, M. E., Boyer, E. W., Dent, C. L., Gergel, S. E., Grimm, N. B., Groffman, P. M., ... & Pinay, G. (2003). Biogeochemical hot spots and hot moments at the interface of terrestrial and aquatic ecosystems. *Ecosystems*, 301-312.

MacDonald, G. M. (2010). Water, climate change, and sustainability in the southwest. *Proceedings of the National Academy of Sciences*, *107*(50), 21256-21262.

McMahon, S., & Parnell, J. (2014). Weighing the deep continental biosphere. *FEMS Microbiology Ecology*, *87*(1), 113-120.

Moon, J. W., Paradis, C. J., Joyner, D. C., von Netzer, F., Majumder, E. L., Dixon, E. R., ... & Hazen, T. C. (2020). Characterization of subsurface media from locations up-and down-gradient of a uranium-contaminated aquifer. *Chemosphere*, *255*, 126951.

Muthukrishnan, T., Govender, A., Dobretsov, S., & Abed, R. M. (2017). Evaluating the reliability of counting bacteria using epifluorescence microscopy. *Journal of Marine Science and Engineering*, *5*(1), 4.

O'Green, A.T. (2013) Soil Water Dynamics. *Nature Education Knowledge*, *4*(5).

Pepper, I. L., & Brusseau, M. L. (2019). Physical-chemical characteristics of soils and the subsurface. *Environmental and pollution science*, 9-22.

Price, M. N., Dehal, P. S., & Arkin, A. P. (2009). FastTree: computing large minimum evolution trees with profiles instead of a distance matrix. *Molecular biology and evolution*, *26*(7), 1641-1650.

Price, M. N., Dehal, P. S., & Arkin, A. P. (2010). FastTree 2–approximately maximum-likelihood trees for large alignments. *PloS one*, *5*(3), e9490.

Raynaud, X., & Nunan, N. (2014). Spatial ecology of bacteria at the microscale in soil. *PloS one*, *9*(1), e87217.

Schlüter, S., & Vogel, H. J. (2016). Analysis of soil structure turnover with garnet particles and X-ray microtomography. *PLoS One*, *11*(7), e0159948.

Smith, H. J., Zelaya, A. J., De León, K. B., Chakraborty, R., Elias, D. A., Hazen, T. C., Arkin, A.P., Cunningham, A.B., & Fields, M. W. (2018). Impact of hydrologic boundaries on microbial planktonic and biofilm communities in shallow terrestrial subsurface environments. *FEMS microbiology ecology*, *94*(12), fiy191.

Smith, M. B., Rocha, A. M., Smillie, C. S., Olesen, S. W., Paradis, C., Wu, L., ... & Hazen, T. C. (2015). Natural bacterial communities serve as quantitative geochemical biosensors. *MBio*, *6*(3), e00326-15.

Taylor, S. W. (1990). *Transport of substrate and biomass in porous media with application to in-situ bioremediation of organic contaminants in groundwater*. Princeton University.

Thullner, M., & Regnier, P. (2019). Microbial controls on the biogeochemical dynamics in the subsurface. *Reviews in Mineralogy and Geochemistry*, *85*(1), 265-302.

Tilman, D., Balzer, C., Hill, J., & Befort, B. L. (2011). Global food demand and the sustainable intensification of agriculture. *Proceedings of the national academy of sciences*, *108*(50), 20260-20264.

Toth, J. (1963). A theoretical analysis of groundwater flow in small drainage basins. *Journal of geophysical research*, *68*(16), 4795-4812.

Watson, D. B., Kostka, J. E., Fields, M. W., & Jardine, P. M. (2004). The Oak Ridge field research center conceptual model. *NABIR Field Research Center, Oak Ridge, TN*.

Whitman, W. B., Coleman, D. C., & Wiebe, W. J. (1998). Prokaryotes: the unseen majority. *Proceedings of the National Academy of Sciences*, *95*(12), 6578-6583.

Wu, L., Wen, C., Qin, Y., Yin, H., Tu, Q., Van Nostrand, J. D., ... & Zhou, J. (2015). Phasing amplicon sequencing on Illumina Miseq for robust environmental microbial community analysis. *BMC microbiology*, *15*(1), 1-12.

Zhou, J., Bruns, M. A., & Tiedje, J. M. (1996). DNA recovery from soils of diverse composition. *Applied and environmental microbiology*, *62*(2), 316-322.

Zinger, L., Gobet, A., & Pommier, T. (2012). Two decades of describing the unseen majority of aquatic microbial diversity. *Molecular ecology*, *21*(8), 1878-1896.

APPENDICES

APPENDIX A

SUPPLEMENTARY INFORMATION FOR CHAPTER 1

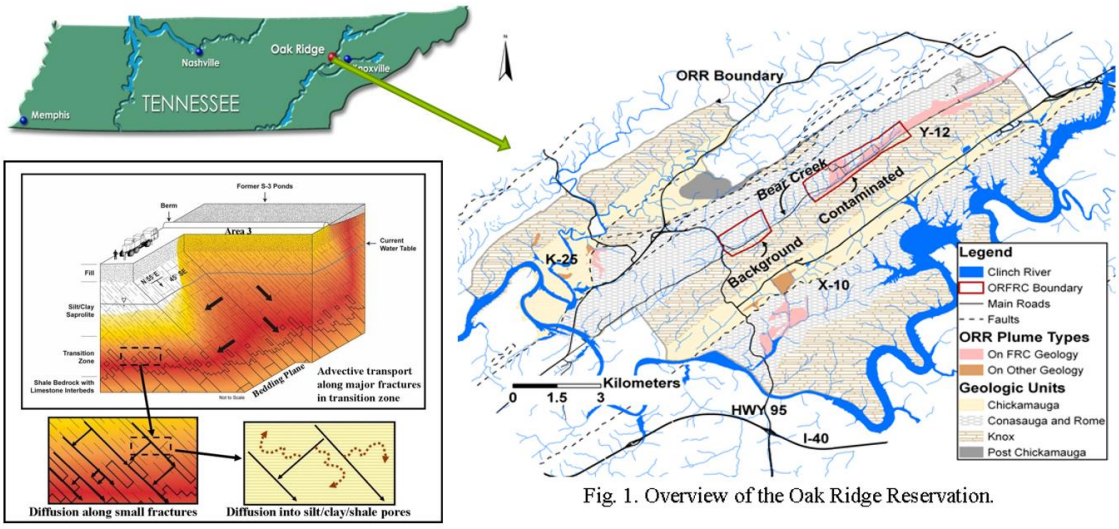

Fig. 1. Overview of the Oak Ridge Reservation.

Figure A1. Historical disposal of wastes from the operation of three industrial plant sites (K-25, Y-12, and ORNL) on the Oak Ridge Reservation (ORR) have created extensive areas of subsurface contamination. Inorganic, organic, and radioactive wastes were released into thousands of unlined trenches, pits, ponds and streams by intentional disposal and accidental leaks and spills. These wastes have resulted in approximately 1,500 acres of contaminated ground water on the ORR (Fig. 1).

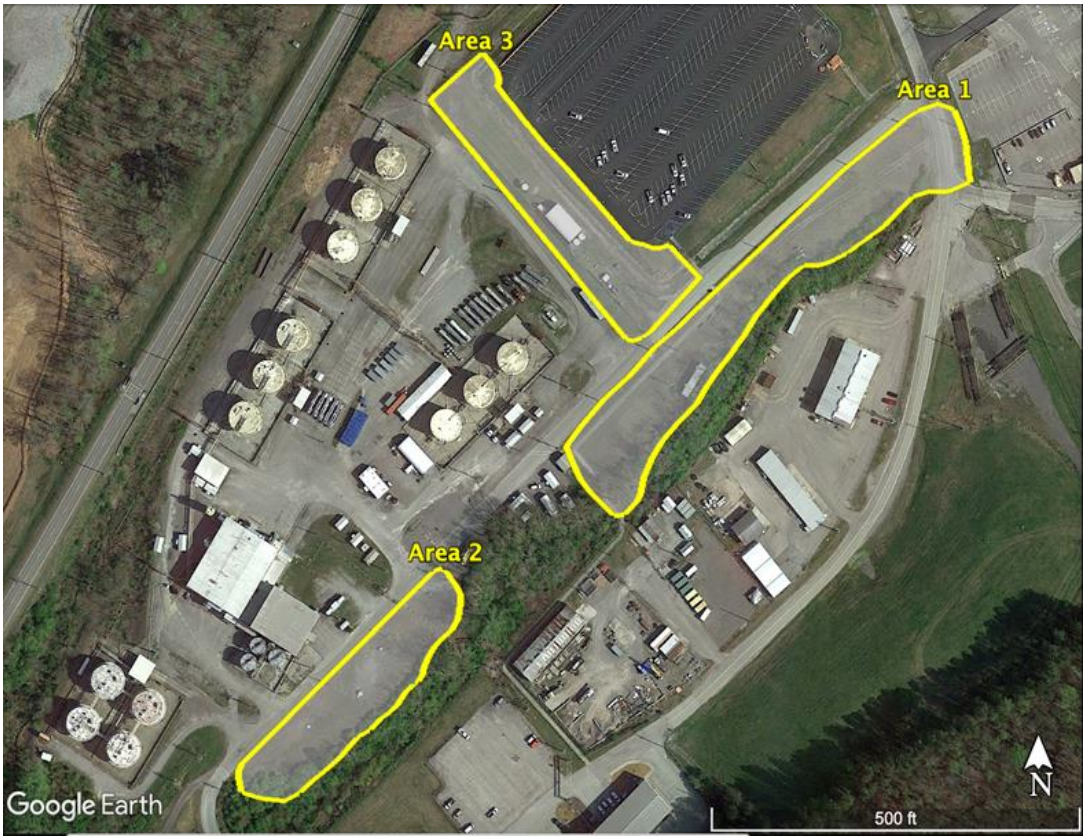

Figure A2. Location of the contaminated areas, at the Biological and Environmental Research (BER) ORNL field research site

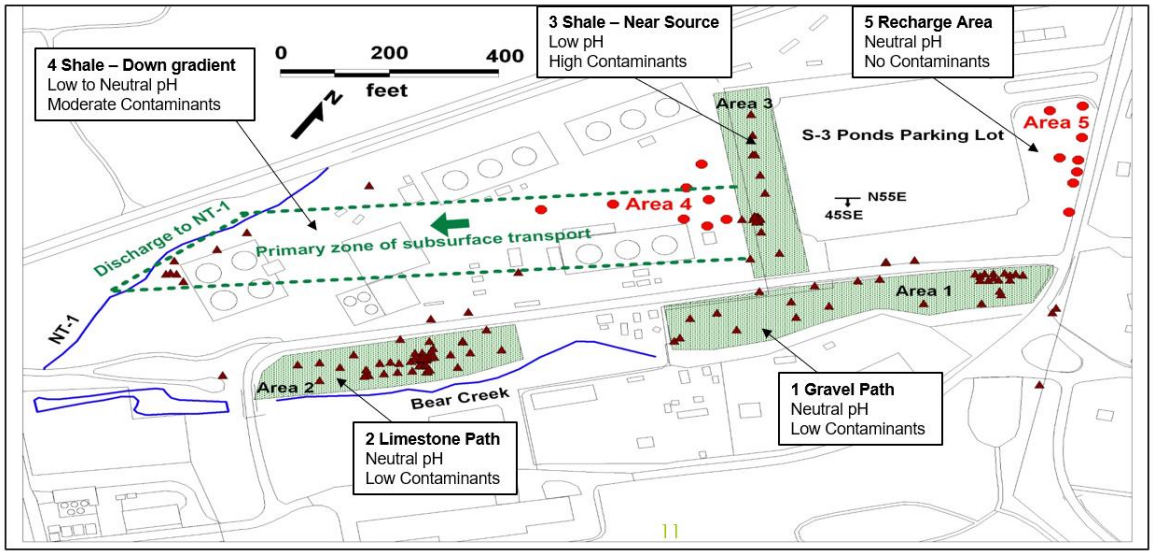

Figure A3. Diagram of the five different areas at the FRC and characteristics of the five areas including flow paths, pH levels, and contaminant level.

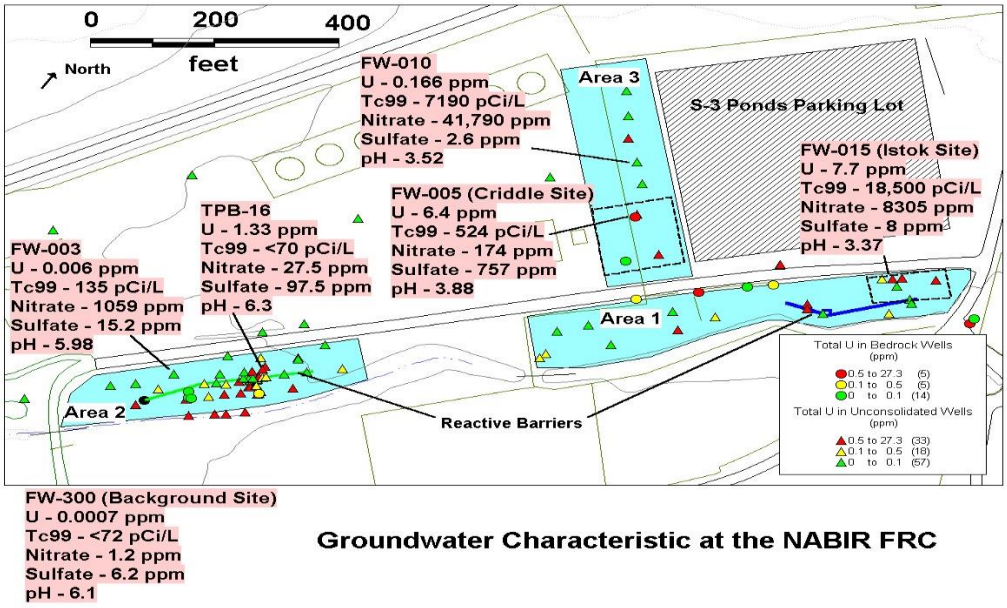

Figure A4. Groundwater characteristics of the areas 1, 2, and 3 at the FRC.

Figure A5. Former S-3 Ponds and current area at the Y-12 facility

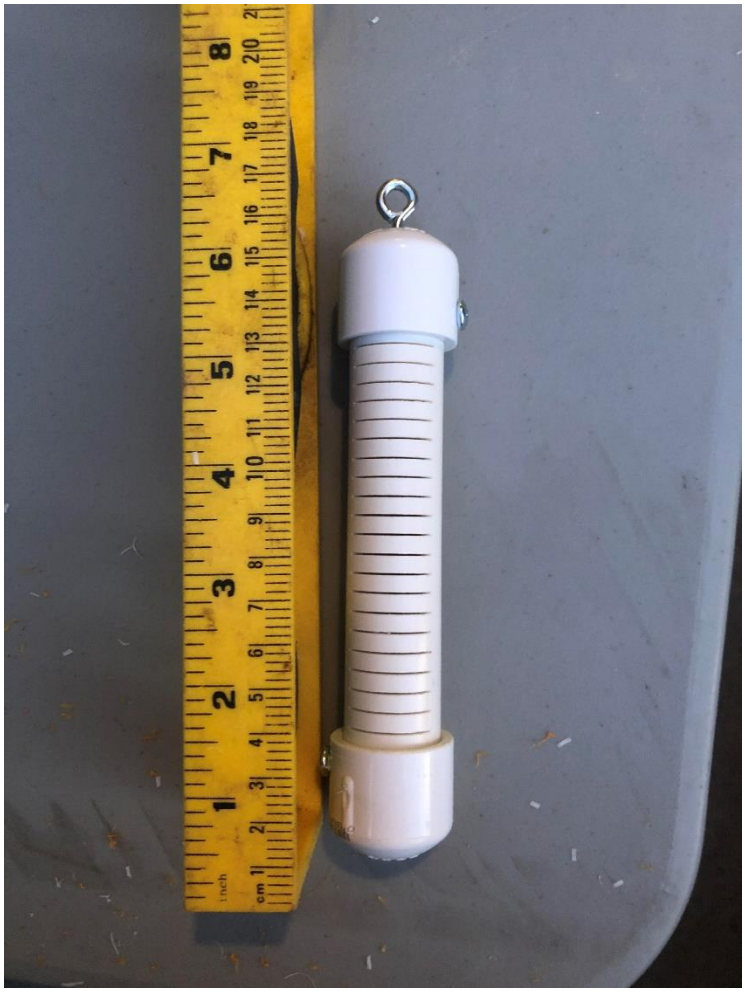

Figure A6. Picture bug trap next to a ruler to show the size

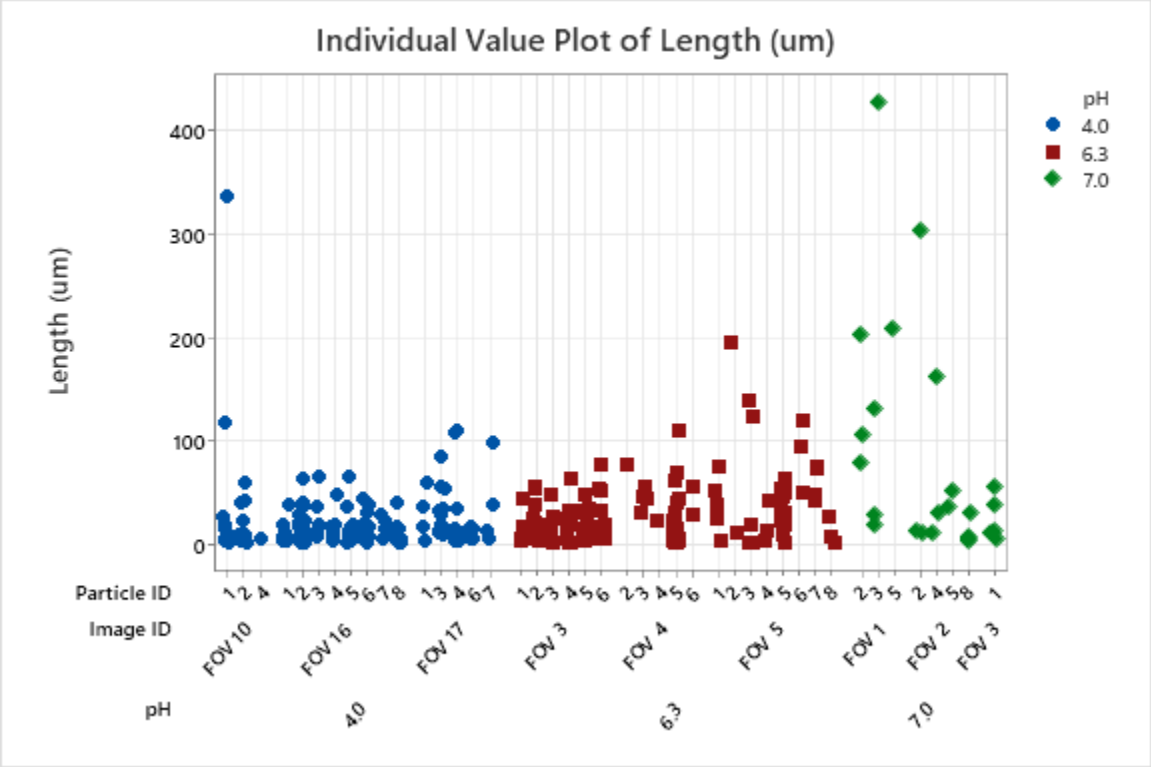

Figure A7. Individual value plot of cell distance measurements for each pH condition. The cell distance measurements are grouped by pH, particle ID, and image ID.

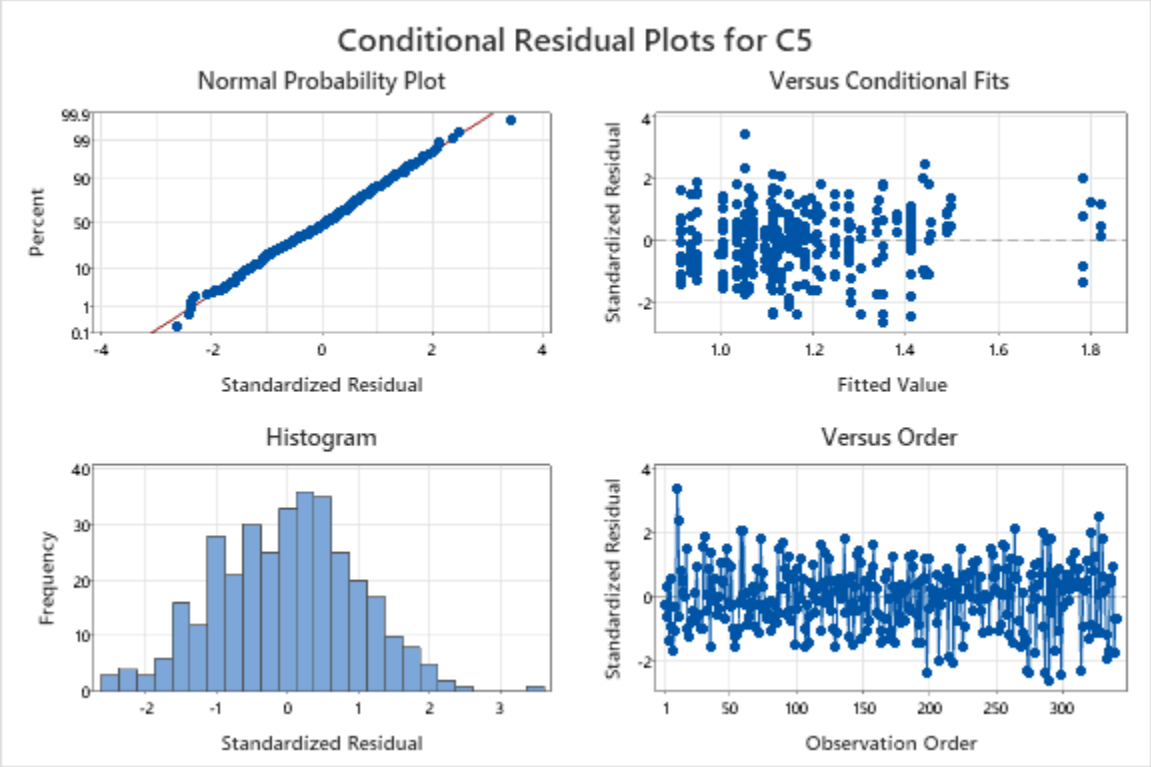

Figure A8. Conditional residual plots for log-transformed cell distance measurements.

Tukey Pairwise Comparisons: pH

Grouping Information Using the Tukey Method and 95% Confidence

pH	N	Mean	Grouping
7.0	25	1.55259	A
6.3	146	1.32526	A
4.0	170	1.07057	A

Means that do not share a letter are significantly different.

Tukey Simultaneous Tests for Differences of Means

Difference of pH Levels	Difference of Means	SE of Difference	DF	Simultaneous 95% CI	T-Value	Adjusted P-Value
6.3 - 4.0	0.255	0.154	3.5527	(-0.220, 0.729)	1.66	0.296
7.0 - 4.0	0.482	0.178	6.2100	(-0.068, 1.032)	2.71	0.080
7.0 - 6.3	0.227	0.167	15.7629	(-0.289, 0.743)	1.36	0.417

Individual confidence level = 97.79%

Figure A9. Tukey pairwise comparison summary for log-transformed cell distance measurements.

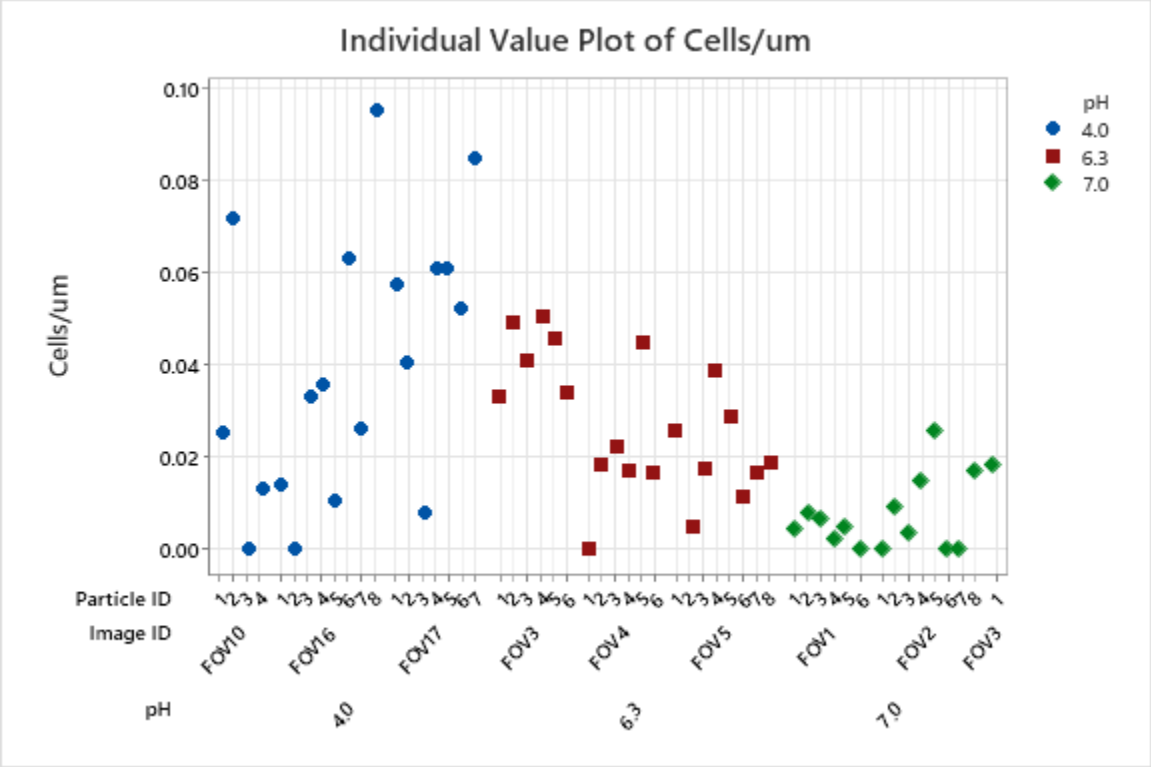

Figure A10. Individual value plot of cell/um for each pH condition. The cell distance measurements are grouped by pH, particle ID, and image ID.

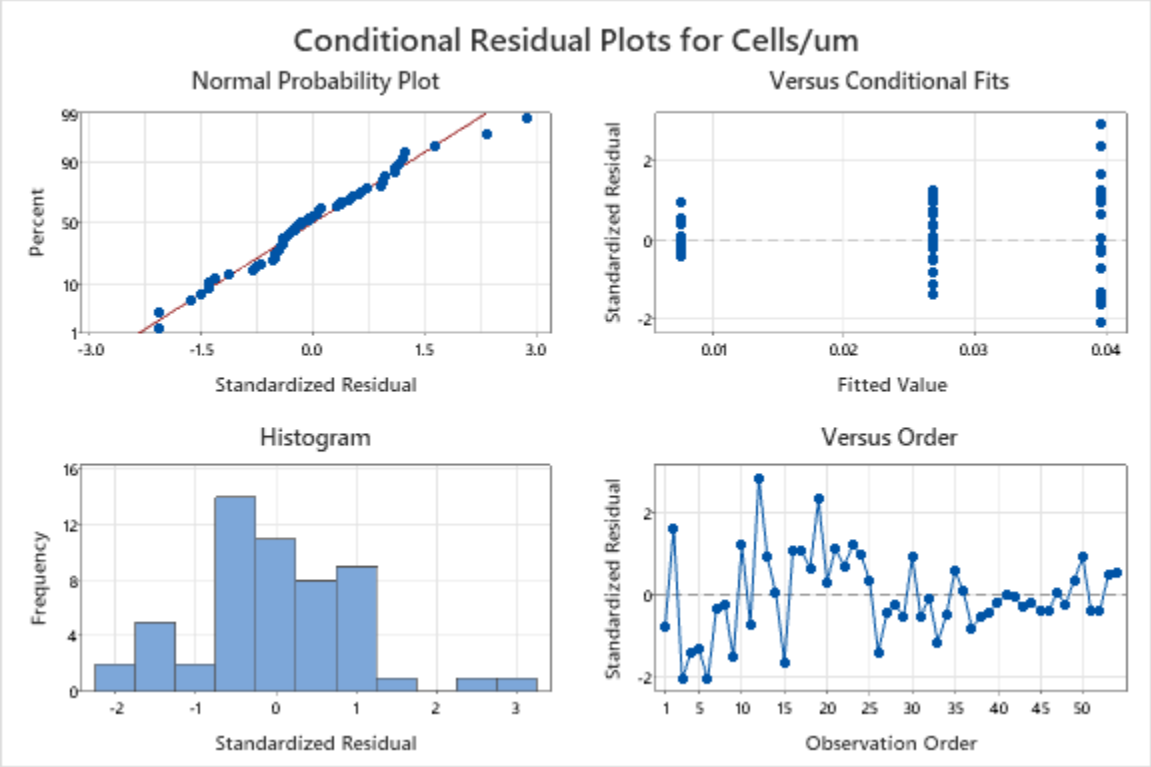

Figure A11. Conditional residual plots for cells/um.

Tukey Pairwise Comparisons: pH

Grouping Information Using the Tukey Method and 95% Confidence

pH	N	Mean	Grouping
4.0	19	0.0396561	A
6.3	20	0.0267614	A
7.0	15	0.0075610	B

Means that do not share a letter are significantly different.

Tukey Simultaneous Tests for Differences of Means

Difference of pH Levels	Difference of Means	SE of Difference	DF	Simultaneous 95% CI	T-Value	Adjusted P-Value
6.3 - 4.0	-0.01289	0.00633	51	(-0.02818, 0.00239)	-2.04	0.114
7.0 - 4.0	-0.03210	0.00683	51	(-0.04857, -0.01562)	-4.70	0.000
7.0 - 6.3	-0.01920	0.00675	51	(-0.03550, -0.00291)	-2.84	0.017

Individual confidence level = 98.06%

Figure A12. Tukey pairwise comparison summary for cells/um.

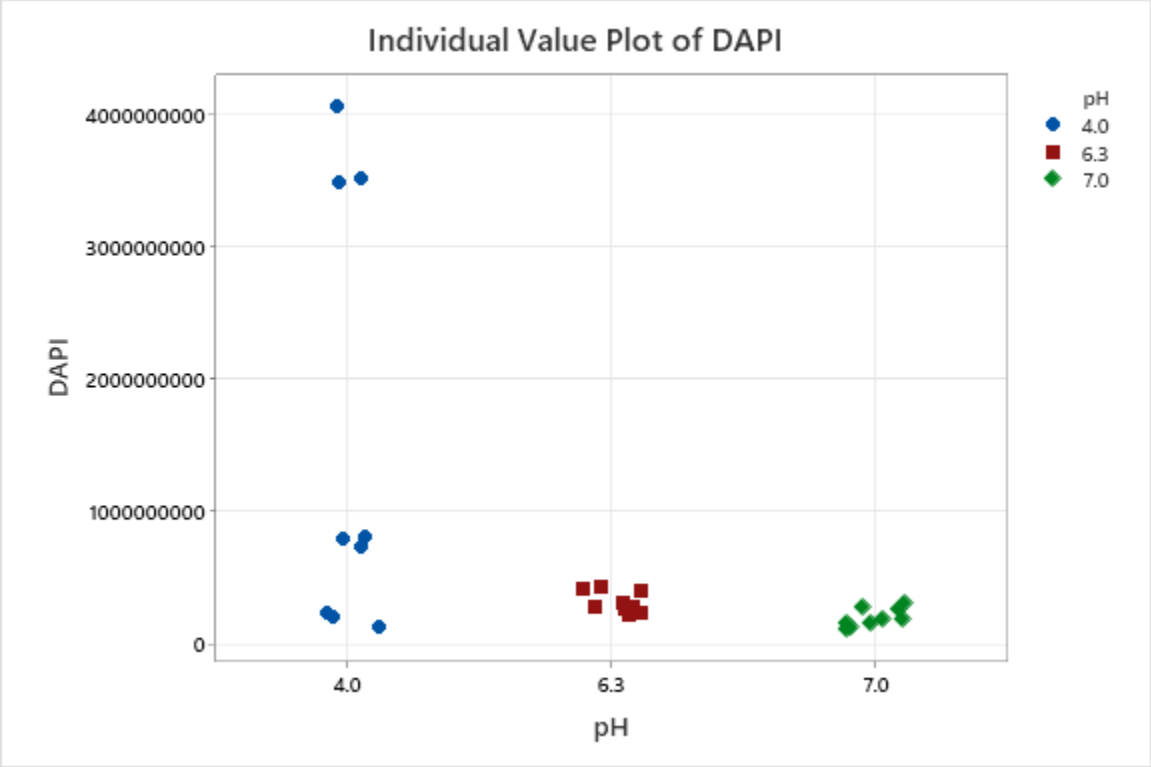

Figure A13. Individual value plot of total (DAPI) cell concentrations for each pH condition.

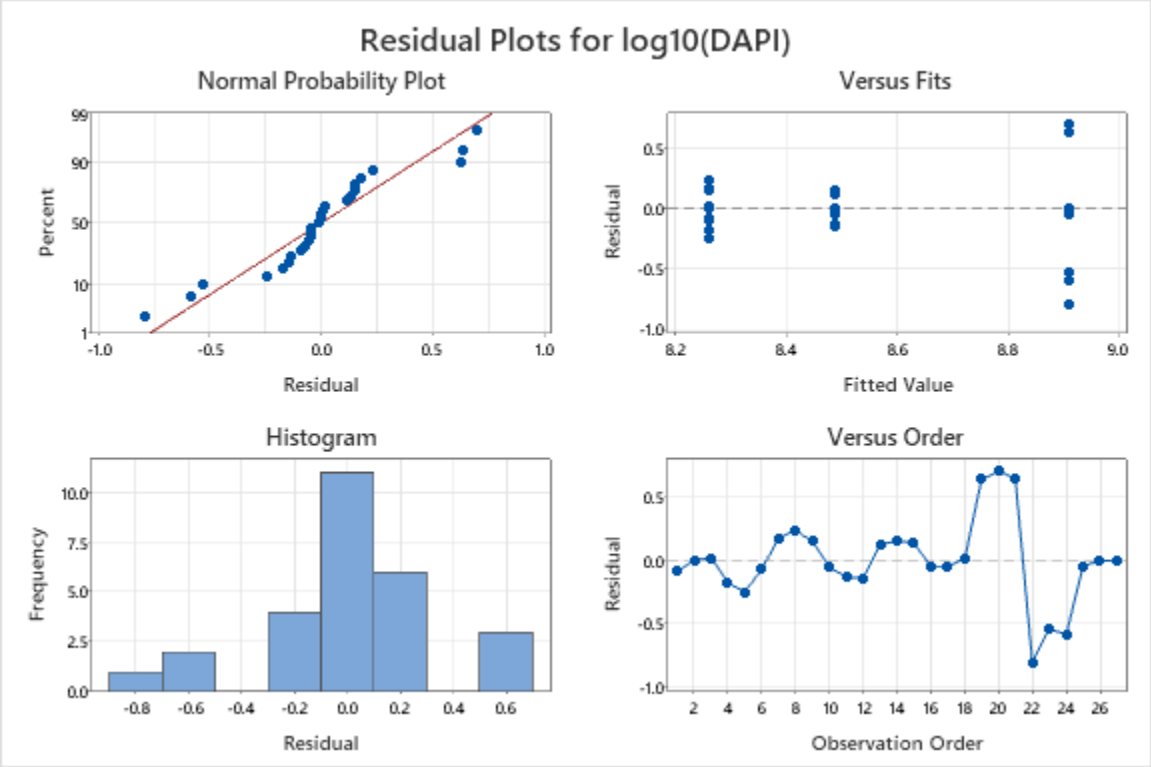

Figure A14. Conditional residual plots for total (DAPI) cell concentrations for three pH conditions.

Tukey Pairwise Comparisons

Grouping Information Using the Tukey Method and 95% Confidence

pH	N	Mean	Grouping
4.0	9	8.909	A
6.3	9	8.4897	B
7.0	9	8.2598	B

Means that do not share a letter are significantly different.

Tukey Simultaneous Tests for Differences of Means

Difference of Levels	Difference of Means	SE of Difference	95% CI	T-Value	Adjusted P-Value
6.3 - 4.0	-0.419	0.163	(-0.826, -0.012)	-2.57	0.043
7.0 - 4.0	-0.649	0.163	(-1.056, -0.242)	-3.98	0.002
7.0 - 6.3	-0.230	0.163	(-0.637, 0.177)	-1.41	0.352

Individual confidence level = 98.02%

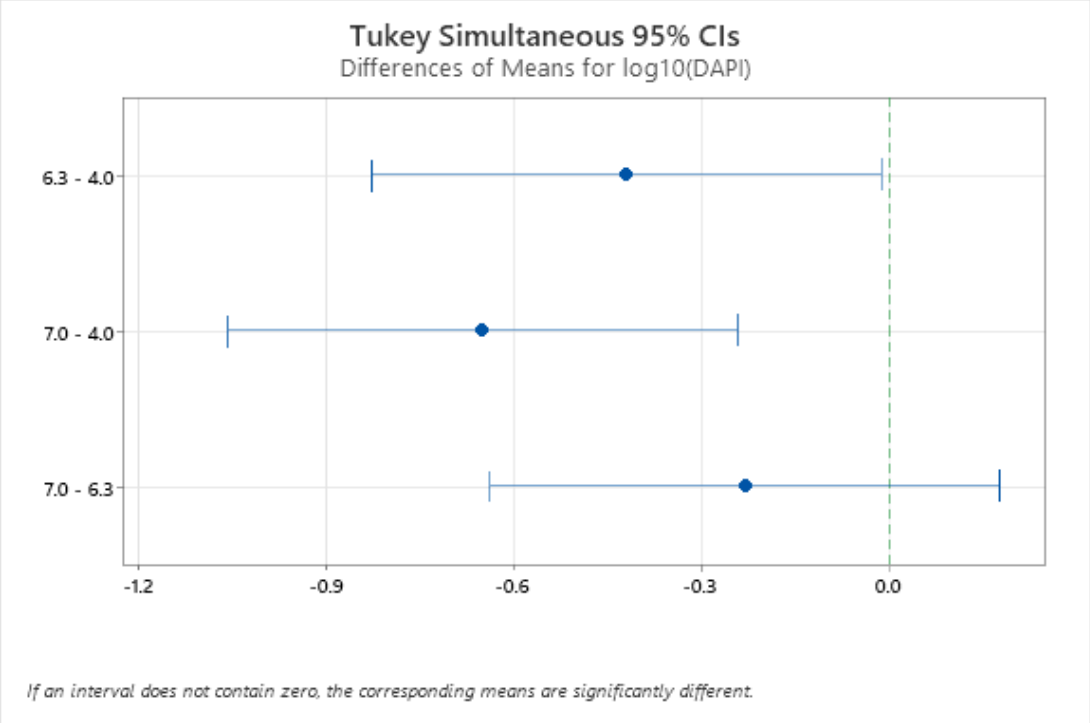

Figure A15. Tukey pairwise comparison for the total cell (DAPI) concentrations for the three pH conditions.

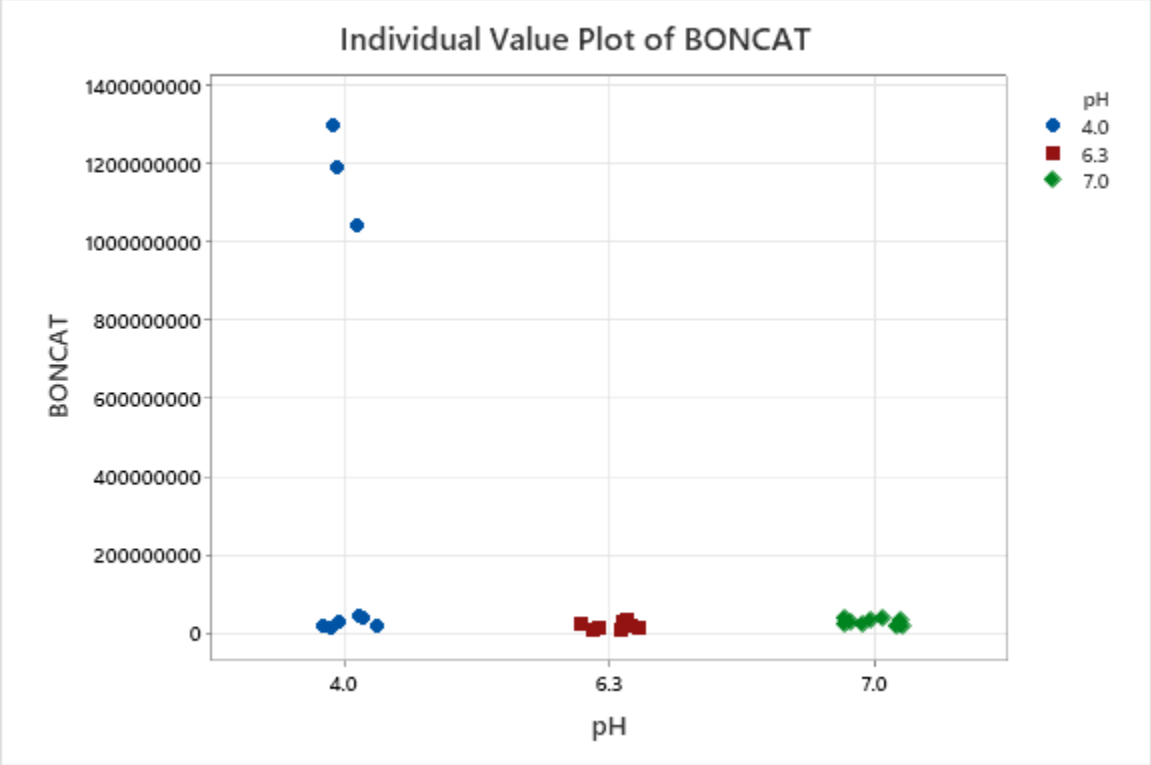

Figure A16. Individual value plot of BONCAT cell concentrations for each pH condition.

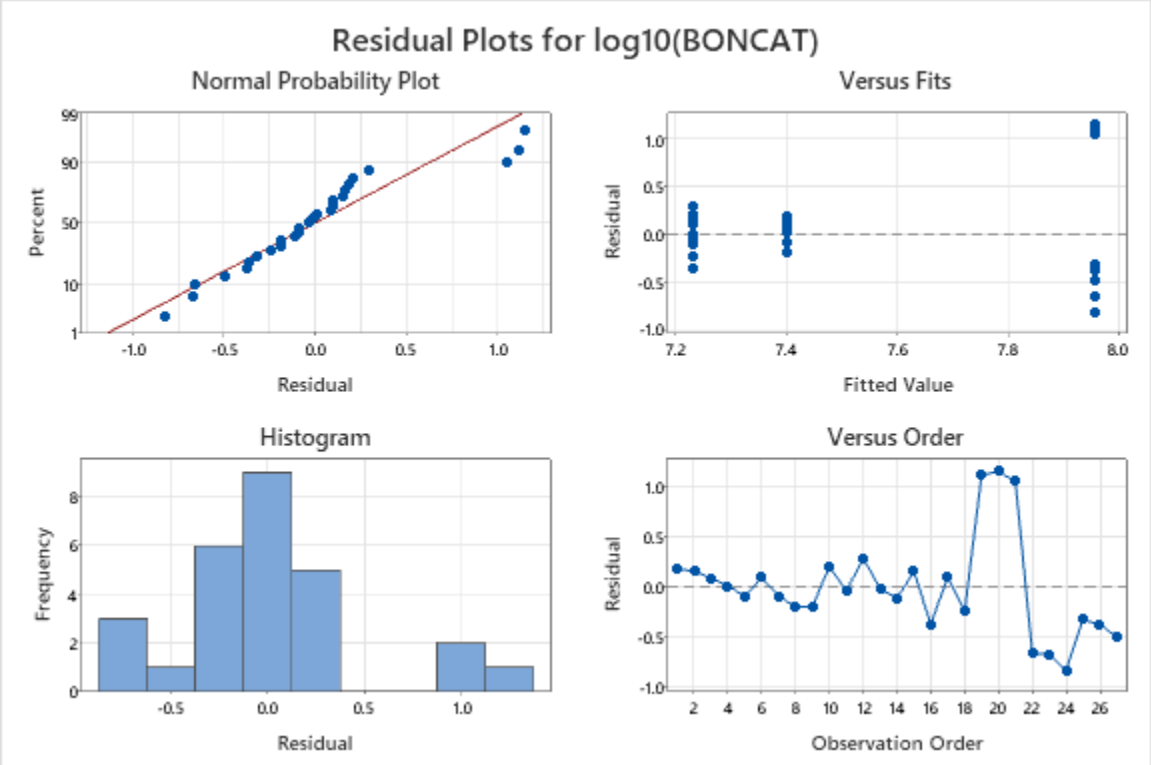

Figure A17. Conditional residual plots for BONCAT cell concentrations for three pH conditions.

Tukey Pairwise Comparisons

Grouping Information Using the Tukey Method and 95% Confidence

pH	N	Mean	Grouping	
4.0	9	7.960	A	
7.0	9	7.3993	A	B
6.3	9	7.2313		B

Means that do not share a letter are significantly different.

Tukey Simultaneous Tests for Differences of Means

Difference of Levels	Difference of Means	SE of Difference	95% CI	T-Value	Adjusted P-Value
6.3 - 4.0	-0.728	0.241	(-1.330, -0.127)	-3.02	0.016
7.0 - 4.0	-0.560	0.241	(-1.162, 0.041)	-2.33	0.071
7.0 - 6.3	0.168	0.241	(-0.433, 0.769)	0.70	0.767

Individual confidence level = 98.02%

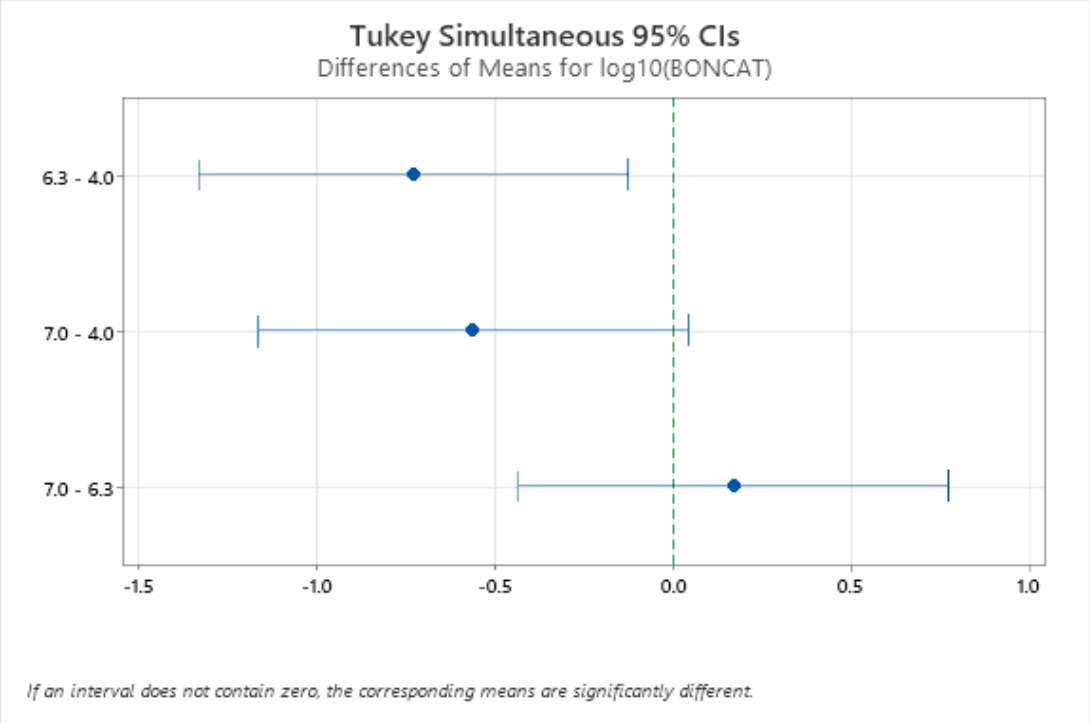

Figure A18. Tukey pairwise comparison for the BONCAT concentrations for the three pH conditions.

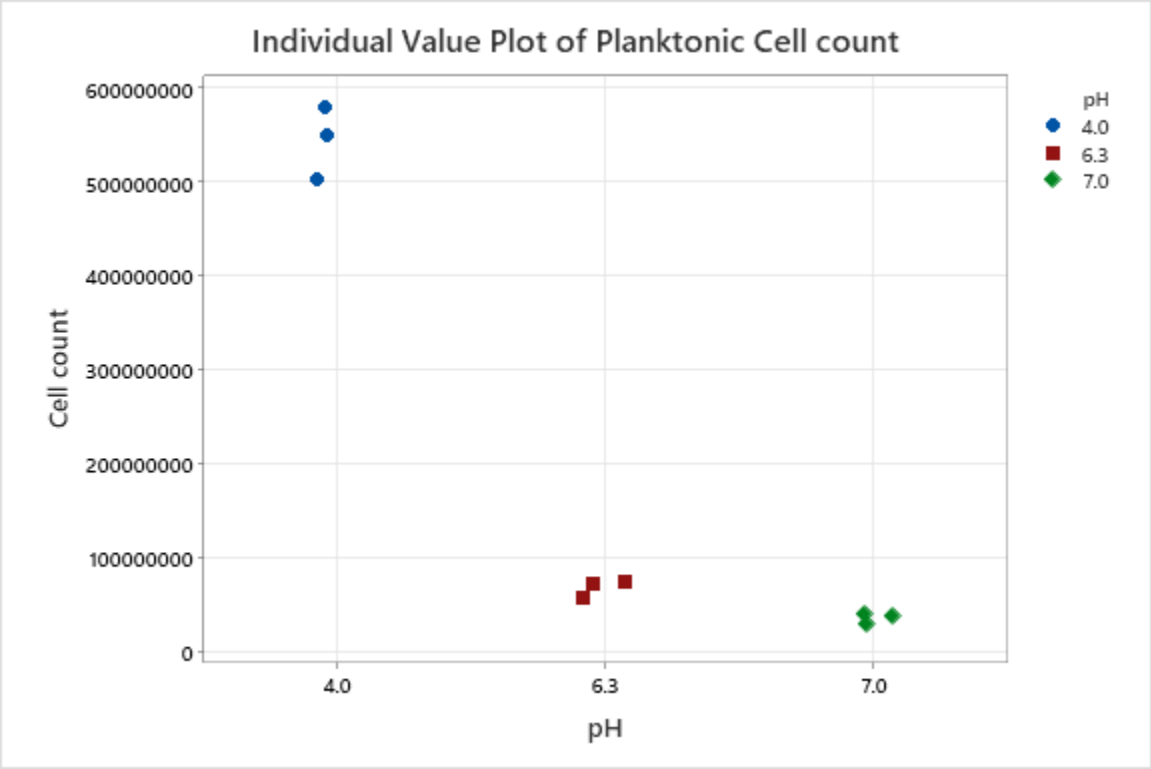

Figure A19. Individual value plot of planktonic cell concentrations for each pH condition.

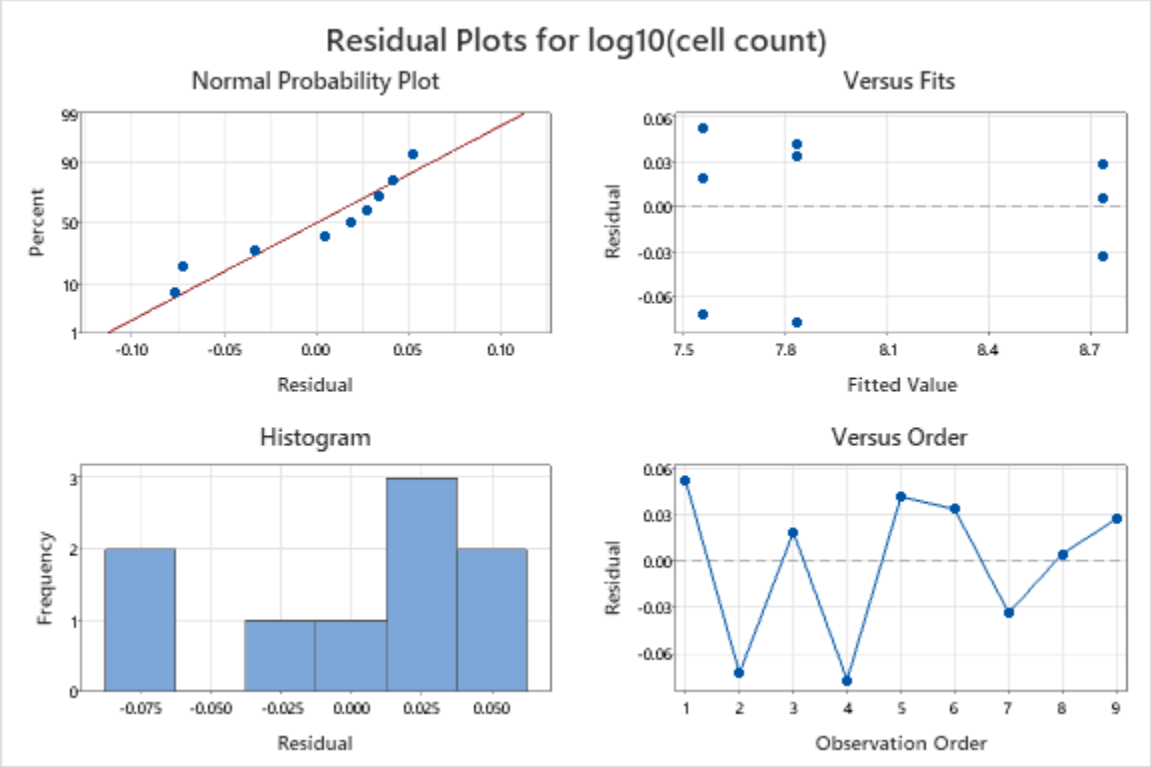

Figure A20. Conditional residual plots for planktonic cell concentrations for three pH conditions.

Tukey Pairwise Comparisons

Grouping Information Using the Tukey Method and 95% Confidence

pH	N	Mean	Grouping
4.0	3	8.7354	A
6.3	3	7.8335	B
7.0	3	7.5543	C

Means that do not share a letter are significantly different.

Tukey Simultaneous Tests for Differences of Means

Difference of Levels	Difference of Means	SE of Difference	95% CI	T-Value	Adjusted P-Value
6.3 - 4.0	-0.9019	0.0461	(-1.0433, -0.7605)	-19.58	0.000
7.0 - 4.0	-1.1811	0.0461	(-1.3225, -1.0397)	-25.64	0.000
7.0 - 6.3	-0.2792	0.0461	(-0.4206, -0.1378)	-6.06	0.002

Individual confidence level = 97.80%

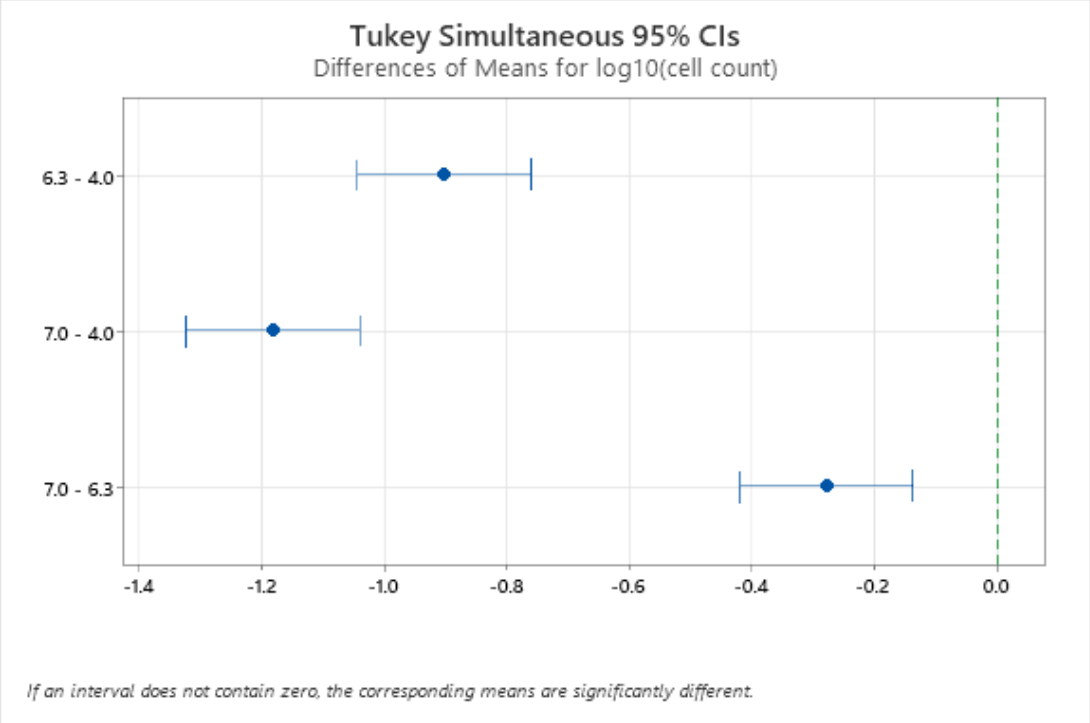

Figure A21. Tukey pairwise comparison for the planktonic cell concentrations for the three pH conditions.

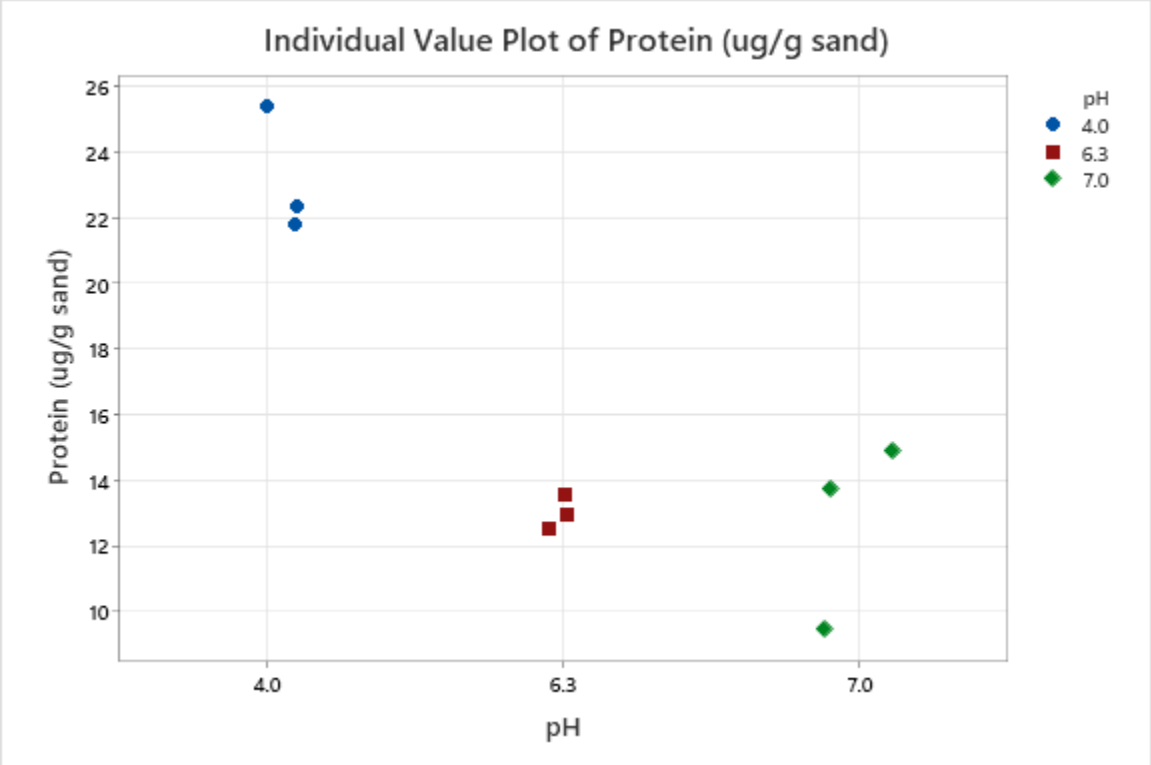

Figure A22. Individual value plot of total protein concentrations for each pH condition.

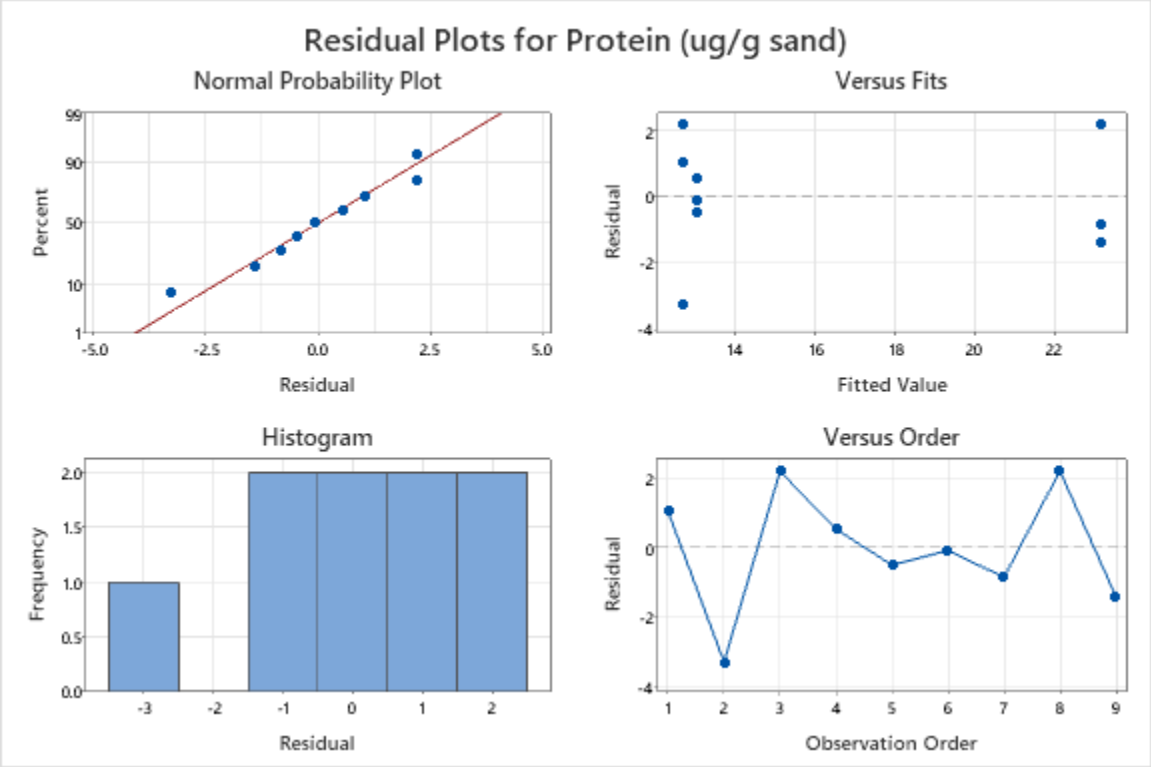

Figure A23. Conditional residual plots for total protein concentrations for three pH conditions.

Tukey Pairwise Comparisons

Grouping Information Using the Tukey Method and 95% Confidence

pH	N	Mean	Grouping
4.0	3	23.17	A
6.3	3	13.033	B
7.0	3	12.69	B

Means that do not share a letter are significantly different.

Tukey Simultaneous Tests for Differences of Means

Difference of Levels	Difference of Means	SE of Difference	95% CI	T-Value	Adjusted P-Value
6.3 - 4.0	-10.14	1.65	(-15.21, -5.06)	-6.13	0.002
7.0 - 4.0	-10.48	1.65	(-15.56, -5.41)	-6.34	0.002
7.0 - 6.3	-0.35	1.65	(-5.42, 4.73)	-0.21	0.976

Individual confidence level = 97.80%

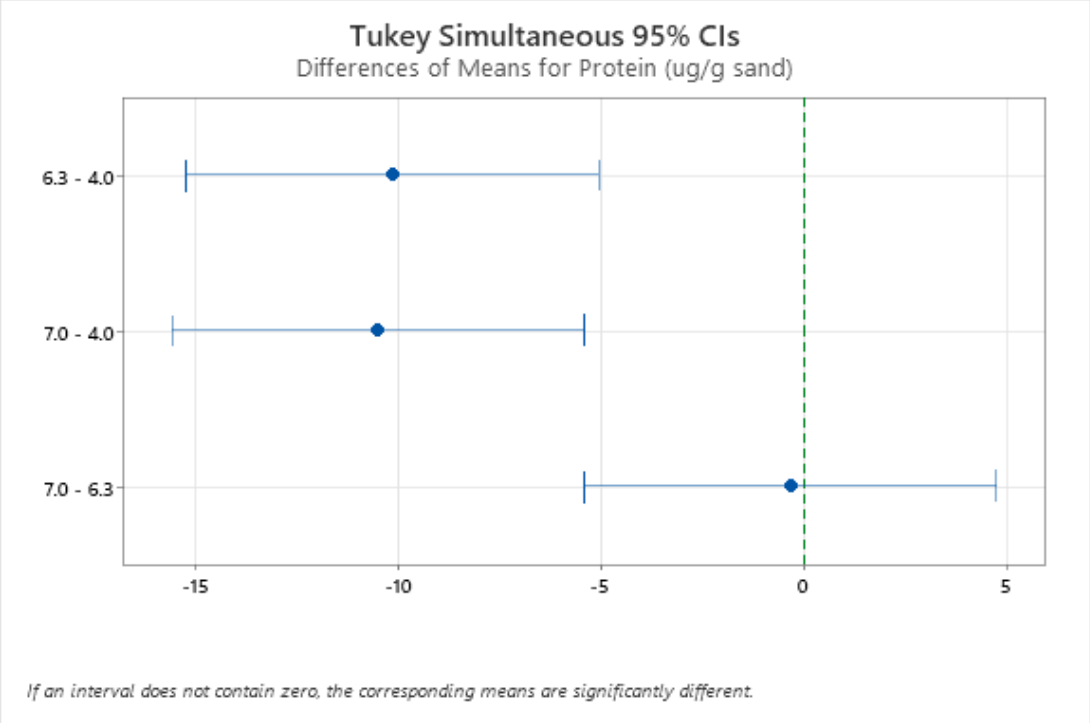

Figure A24. Tukey pairwise comparison for the total protein concentrations for the three pH conditions.

APPENDIX B

SGW GROUNDWATER RECIPE AND EXO-METABOLITE COMPOSITION

Component	Concentration
Salt Solution	50X
NaHCO3	11.5 g/L
Wolfe's Vitamins (100X)	10 mL/L (1X)
Wolfe's Minerals (100X)	10 mL/L (1X)
Exo-metabolites (100X)	2X

Table B1. SGW groundwater media recipe

Salt Solution	Respective Area	Potassium phosphate (KH2PO4) Concentration	Sodium bicarbonate (NaHCO3) Concentration	Sodium Nitrate (NaNO3) Concentration
1	1	0.15 g/L	2.5 g/L	3 mg/L
2	2	0.15 g/L	2.5 g/L	0.303 g/L
3	3	0.15 g/L	2.5 g/L	1.97 g/L

Table B2. Salt solution recipe for SGW groundwater media.

Exo-metabolite Composition				2X Concentration	2X Concentration
Name	Class	Formula	MW	Conc (µM)	mg/L
Mannitol	hexose alcohol	C6H14O6	182.1718	176.1	32.08
Glucose	hexose	C6H12O6	180.1559	164.96	29.718
Fructose	hexose	C6H12O6	180.1559	161.3	29.06
Trehalose	dihexose	C12H22O11	342.2965	112.36	38.46
Arabinose	pentose	C5H10O5	150.1299	41.52	6.234
Maltose	dihexose	C12H22O11	342.2965	33.08	11.324
Arabitol	pentose alcohol	C5H12O5	152.1458	21.04	3.202
Leucine	amino acid	C6H13NO2	131.1729	12	1.574
Isoleucine	amino acid	C6H13NO2	131.1729	12	1.574
Glycine	amino acid	C2H5NO2	75.0666	8	0.6

Arginine	amino acid	C6H14N4O2	174.2012	8	1.394
Proline	amino acid	C5H9NO2	115.1305	8	0.922
Threonine	amino acid	C4H9NO3	119.1192	8	0.952
Lysine	amino acid	C6H14N2O2	146.1876	8	1.17
Phenylalanine	amino acid	C9H11NO2	165.1891	8	1.322
Mannose	hexose	C6H12O6	180.1559	7.88	1.42
Uridine	nucleotide	C9H12NO6	230.1947	4.5	1.036
Carnitine	amino acid derivative	C7H15NO3	161.1989	4	0.644
Asparagine	amino acid	C4H8N2O3	132.1179	4	0.528
Serine	amino acid	C3H7NO3	105.0926	4	0.42
Valine	amino acid	C5H11NO2	117.1463	4	0.468
Tyrosine	amino acid	C9H11NO3	181.1885	4	0.724
Tryptophan	amino acid	C11H12N2O2	204.2252	4	0.816
Methionine	amino acid	C5H11NO2S	149.2113	4	0.596
Glutamic Acid	amino acid	C5H9NO4	147.1293	4	0.588
Citrulline	amino acid derivative	C6H13N3O3	175.1857	4	0.7
Aspartic acid	amino acid	C4H7NO4	133.1027	4	0.532
Alanine	amino acid	C3H7NO2	89.09318	4	0.356
Histidine	amino acid	C6H9N3O2	155.1546	4	0.62
Glutamine	amino acid	C5H10N2O3	146.1445	4	0.584
4-guanidinobutyric acid	amino acid derivative	C5H11N3O2	145.1597	1.18	0.172

Hypoxanthine	nucleobase	C5H4N4O	136.1115	0.84	0.114
Uracil	nucleotide	C4H4N2O2	112.0868	0.64	0.072
Thymine	nucleotide	C5H6N2O2	126.1133	0.64	0.08
Guanine	nucleotide	C5H5N5O	151.1261	0.64	0.096
Cytosine	nucleotide	C4H5N3O	111.102	0.64	0.072
Adenine	nucleotide	C5H5N5	135.1267	0.64	0.086
Thymidine	nucleoside	C10H14N2O5	242.2286	0.52	0.126
Spermidine	osmolyte	C7H19N3	145.2459	0.52	0.076
Orotic acid	pyrimidine derivative	C5H4N2O4	156.0963	0.52	0.082
Inosine	nucleoside	C10H12N4O5	268.2261	0.52	0.14
Deoxyinosine	nucleoside	C10H12N4O4	252.2267	0.52	0.132
Cytidine	nucleoside	C9H13N3O5	243.2166	0.52	0.126
Choline	osmolyte	C5H14NO	104.1708	0.52	0.054
Adenosine	nucleoside	C10H13N5O4	267.2413	0.52	0.138
2'-Deoxyuridine	nucleotide	C9H12N2O5	228.202	0.52	0.118

Table B3. Exo-metabolite solution composition for SGW groundwater media.

APPENDIX C

CHARACTERIZATION OF PACKED BED REACTOR SYSTEM AT FIELD RELEVANT FLOW RATES

Experimental Justification

In order to better understand how cells move through and interact with porous media, it is necessary to understand how a solute flows through porous media. Triplicate up-flow packed bed reactors (PBRs) were inoculated with bromide at a concentration of 100 mg/L. A pulse inoculation method was used so that the porous media in the reactors was undisturbed. The packed bed reactors were filled with a sand mix that is representative of sediment found at the Oak Ridge National Laboratory Field Research Center (ORNL FRC). Two experiments were performed at two different field relevant flow rates and effluent samples were collected to construct a bromide breakthrough curve for each flow rate. Additionally, pressure readings were taken throughout the experiments to calculate the hydraulic gradient, hydraulic conductivity, and permeability for the reactors at the two flow rates.

Material and Methods

Experimental Plan

Once flow was established in triplicate reactors, reactors were inoculating with 3 mL of bromide at a concentration of 100 mg/L. Effluent samples were collected at different time points to measure the bromide concentration at each time point to construct a bromide breakthrough curve for two field relevant flow rates. The two flow rates of interest are 4.54 mL/hr and 11.32 mL/hr. Water was used for the media in the reactors and the media reservoir was constantly degassed with a gas mixture of 80% nitrogen, 20% carbon dioxide.

Reactor design and construction

The up-flow packed bed reactor system described here is designed for laboratory bench-top use and can maintain an anoxic environment for all components upstream of the reactor column, the reactor column itself, and the effluent line. The system can be run at varying flow rates, including low flow rates that are representative of the shallow subsurface environment. Each reactor system has sampling ports at the top and bottom for injector or sampling. The sampling ports allow for temporal sampling of the planktonic phase. The size of the reactor was designed for increased sampling volume needed for sampling the sand. A schematic of the system is shown in Figure C1.

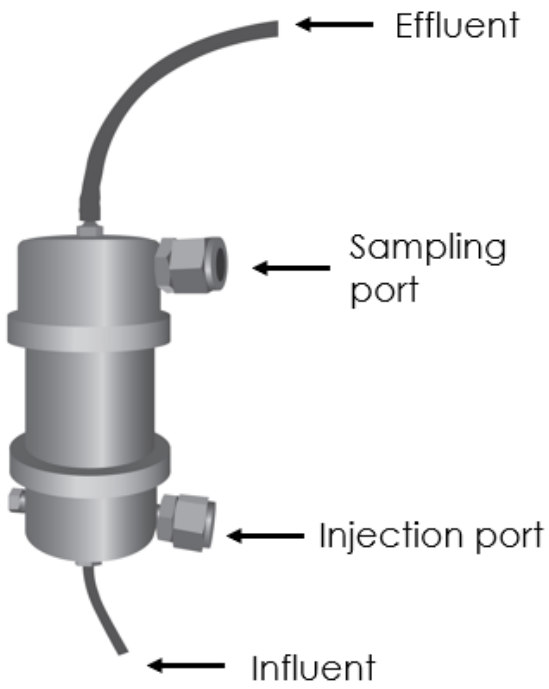

Figure C1. Diagram of the up-flow packed bed reactor designed and constructed. The reactor has an influent port at the bottom of the reactor and effluent exits the top of the reactor at the effluent port. Two septum ports were added to the reactor to easily inoculate the reactor and collect planktonic samples. The bottom septum port is used for inoculating the reactor and both ports can be used to collect planktonic samples.

The reactor column was constructed from type 316/316L stainless steel threaded pipe with a length of 3 inches, inner diameter of 2.067 inches, and a wall thickness of 0.154 inches. The threaded caps were 316 stainless steel with an outer diameter of 2.98 inches, a length of 1.77 inches, rated to a pressure of 150 psi. All components of the reactor body were bought from McMaster-Carr (Elmhurst, IL, USA). Holes were drilled into the side of both caps and 1/8-inch NPT threads were cut for the sampling port fittings. The bottom reactor cap (influent side) had two threaded holes, one located on the side for the sampling port and a second one located on the flat side of the cap for the influent port. The influent port was fitted with a 1/16-inch barbed fitting for flow and attached to size 13 Masterflex® Norprene tubing. The second hole on the bottom cap was fitted with a septum port fitting for sampling and injection. The top reactor cap had drilled holes, one located on the side for sampling and a second one located on the top for the effluent flow. The drilled hole located on the side was fitted with a septum port fitting for sampling. The top hole of the top cap was fitted with a ¼-inch barbed fitting for effluent flow and attached to size 25 Masterflex® Norprene tubing. The PBRs were packed with 380 g of 70 mesh sand that contains sand particles whose diameter ranged from 75 to 300 µm.

The liquid media reservoir is 2-liter glass carboy. The carboy is sealed with a butyl rubber stopper. The butyl rubber stopper was drilled to install a piece of glass tubing which is attached to Masterflex® Norprene tubing used to hold an oxygen-free gas purge. A second hole was drilled in the rubber stopper to hold 1/8-inch stainless steel tubing that is attached to Masterflex® Norprene tubing for the media influent line. The effluent flow was collected in 1 liter glass carboys.

Flow Rate Calculations

The flow rates used in this study were calculated using field relevant hydraulic properties. The flow rates were calculated using an average pore velocity equation that is based on Darcy's law where v_p is the average pore velocity, K is the hydraulic conductivity, $\Delta h/\Delta l$ is the hydraulic gradient and e is the porosity. The saturated hydraulic conductivity used for calculating the flow rates is 5.73E-05 m/s. The saturated hydraulic conductivity was used rather than unsaturated hydraulic activity because the saturated zone of the shallow terrestrial subsurface is the zone this study focused on. The range of porosity used for calculating the flow rates was 0.35 to 0.49. The hydraulic gradient used for calculating the flow rates was 0 to 0.035 m/m. Using these parameters, the range of flow rates is 4.54 mL/hr to 11.32 mL/hr.

$$v_p = \frac{(K) * (\frac{\Delta h}{\Delta l})}{e}$$

Unsat. Hydraulic conduct. (m/s) (K)	Sed	0.2-2.5 x 10^{-5}	Wilson & Luxmoore, 1988	Tension infiltrometer; geometric mean; n=39 obs.; field measure.; psi=0,2,5, 14cm
Sat. hydraulic conduct. (m/s) (K)	Sed	1x10^{-4} 5.73 x 10^{-5}	Wilson & Luxmoore, 1988 Collected 6/8/18	Tension infiltrometer; geometric mean; n=39 obs.; field measure.; psi=0,2,5, 14cm
Porosity (e)*	Sed	0.35-0.49	Howard 1997	Paraffin clod method
Gradient across site (m/m) ($\Delta h/\Delta l$)	GW	0.015 – 0.075 (horiz) 0.005-0.063 (vert.) 0.00-0.035	Schreiber et. al. 1998 Adams and McBride, Hazen Lab, measured weekly from Dec 2017 to March 2018	Range at one location; values may exceed this range, especially near streams

Table C1. Modified From Table 1 of Watson et. al, 2004. pg. 7. Data summaries for the FRC background area, Permeability of Saprolite.

Bromide Samples

Once flow was established in the reactors, 3 mL of bromide, at a concentration of 100 mg/L, were injected into each reactor. The bromide was injected into the reactors as a pulse over a time of 1 minute. 2 mL of effluent were collected from each reactor in a sterile

15 mL falcon tube for each time point listed in Tables C2 and C3. Samples were stored at -20 ℃. For the low flow rate experiment, samples were collected every 4 hours until hour 16. At hour 18, samples were collected every hour until hour 38. After hour 38, samples were collected every 4 hours until hour 54 (see Table C2). For the high flow rate experiment, samples were collected every 2 hours until hour 6. At hour 6, samples were collected every hour until hour 18. After hour 18, samples were collected every 2 hours until hour 30 (see Table C3). Bromide concentrations for each time point were determined using an ion chromatography instrument. A breakthrough curve for each flow rate was constructed using the bromide concentrations for each time point. Pressure readings were collected at every time point. Flow was measured gravimetrically at every time point.

Sample #	Time Point after injection (hr.)
0	0
1	4
2	8
3	12
4	16
5	18
6	19
7	20
8	21
9	22
10	23
11	24
12	25
13	26
14	27
15	28
16	29
17	30
18	31
19	32
20	33
21	34
22	35
23	36
24	37
25	38
26	42
27	46
28	50
29	54

Table C2. Sampling plan for the low flow rate experiment. The pumped was set to 5.2 mL/hour to achieve a desired flow rate of approximately 4.54 mL/hr.

Sample #	Time Point after injection (hr.)
0	0
1	2
2	4
3	6
4	7
5	8
6	9
7	10
8	11
9	12
10	13
11	14
12	15
13	16
14	17
15	18
16	20
17	22
18	24
19	26
20	28
21	30

Table C3. Sampling plan for the high flow rate experiment. The pumped was set to 12.8 mL/hour to achieve a desired flow rate of approximately 11.32 mL/hr.

Results

The average measured flow rate for reactor 1 was 4.64 ± 0.15 mL/hr. The average pressure difference for reactor 1 was 0.36 ± 0.05 psi. The theoretical residence time using the average measured flow rate is 22.1 hours, while experimental residence time was approximately 29 hours for reactor 1. The average measured flow rate for reactor 2 was 4.43 ± 0.12 mL/hr. The average pressure difference for reactor 2 was 0.41 ± 0.08 psi. The theoretical residence time using the average measured flow rate is 21.1 hours, while the

experimental residence time was approximately 38 hours for Reactor 2. The average measured flow rate for reactor 3 was 4.75 ± 0.13 mL/hr. The average pressure difference for reactor 3 was 0.39 ± 0.04 psi. The theoretical residence time using the average measured flow rate is 20.6 hours, while the experimental residence time was approximately 26 hours for Reactor 3. The peak of the bromide breakthrough curve for the average bromide concentrations for the low flow rate was 26 hours. The calculated hydraulic gradient for the reactors ranged from -1.99 to -2.16 m/m. The calculated hydraulic conductivities for the reactors ranged from 2.67E-07 to 3.19E-07 m/s. The calculated permeabilities for the three reactors ranged from 2.43E-14 to 2.90E-14 m^2.

Reactor	Measured Flow (mL/hr)	Measured Pressure, ΔP (psi)	Residence time (hr)
1	4.64 ± 0.15	0.36 ± 0.05	21.1
2	4.43 ± 0.12	0.41 ± 0.08	22.1
3	4.75 ± 0.13	0.39 ± 0.04	20.6

Table C4. Average measure flow rate, average measured pressure, and calculated residence time for each reactor for the low flow rate experiment.

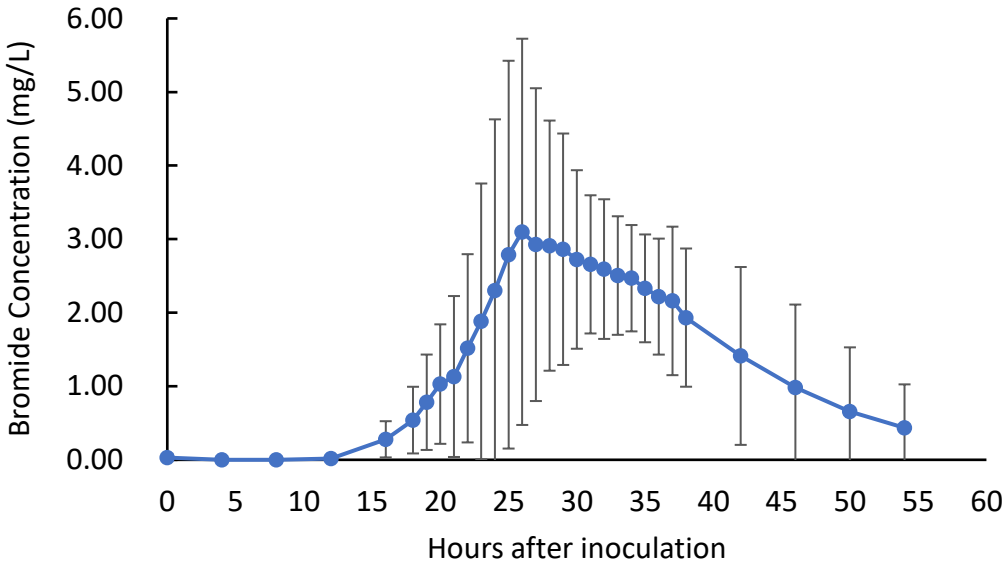

Figure C2. Average bromide concentrations of effluent samples over a period of 55 hours for the low flow rate. The data points are the averaged bromide concentrations of the three reactors.

Reactor	Average flow rate (mL/hr)	Pressure difference (psi)	Hydraulic gradient (m/m)	Hydraulic conductivity (m/s)	Permeability (m^2)
1	4.64	0.36	-1.99	3.19E-07	2.90E-14
2	4.43	0.41	-2.27	2.67E-07	2.43E-14
3	4.75	0.39	-2.16	3.01E-07	2.74E-14

Table C5. Calculated hydraulic gradient, calculated conductivity, and calculated permeability for each reactor at the low flow rate using the average flow rate and average pressure difference for each reactor.

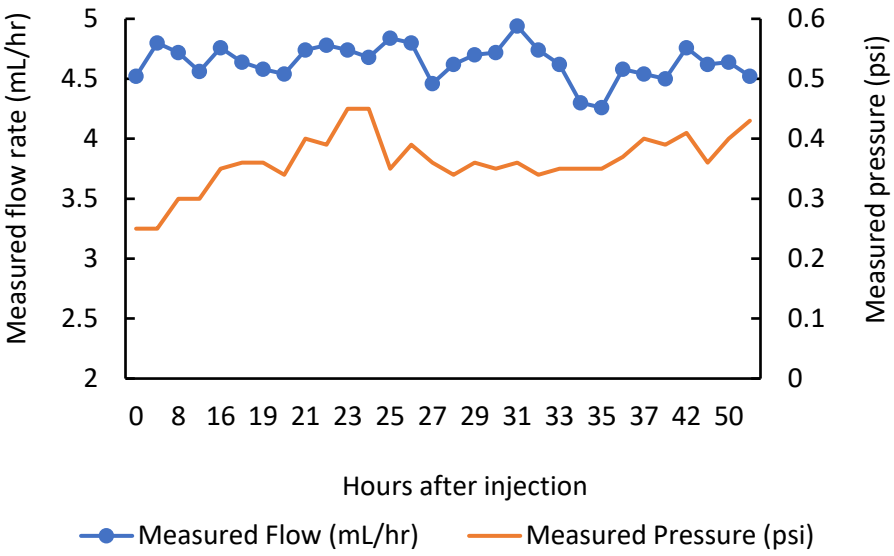

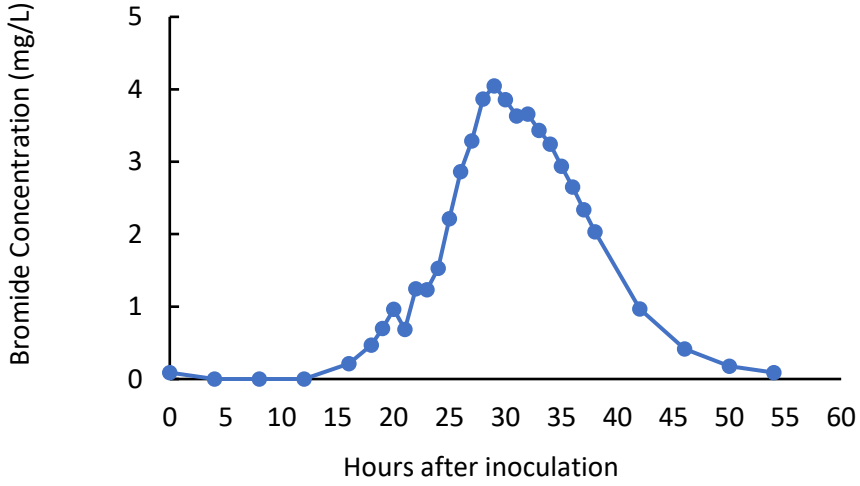

Figure C3. Individual measured flow rate, measured pressure difference and bromide breakthrough curve for reactor 1 at the low flow rate. The average measured flow rate for reactor 1 was 4.64 ± 0.15 mL/hr. The average pressure difference for reactor 1 was 0.36 ± 0.05 psi. The experimental residence time for Reactor 1 was 29 hours.

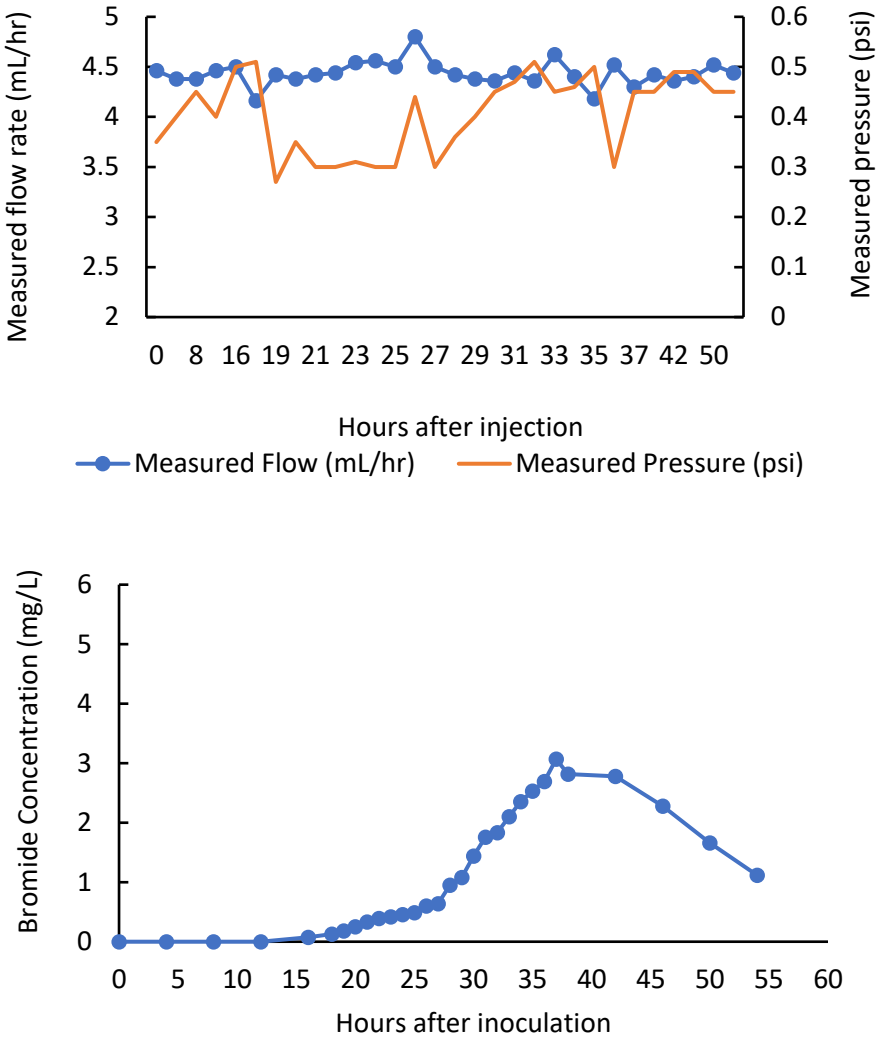

Figure C4. Individual measured flow rate, measured pressure difference and bromide breakthrough curve for reactor 2 at the low flow rate. The average measured flow rate for reactor 2 was 4.43 ± 0.12 mL/hr. The average pressure difference for reactor 2 was 0.41 ± 0.08 psi. The experimental residence time for Reactor 2 was 38 hours.

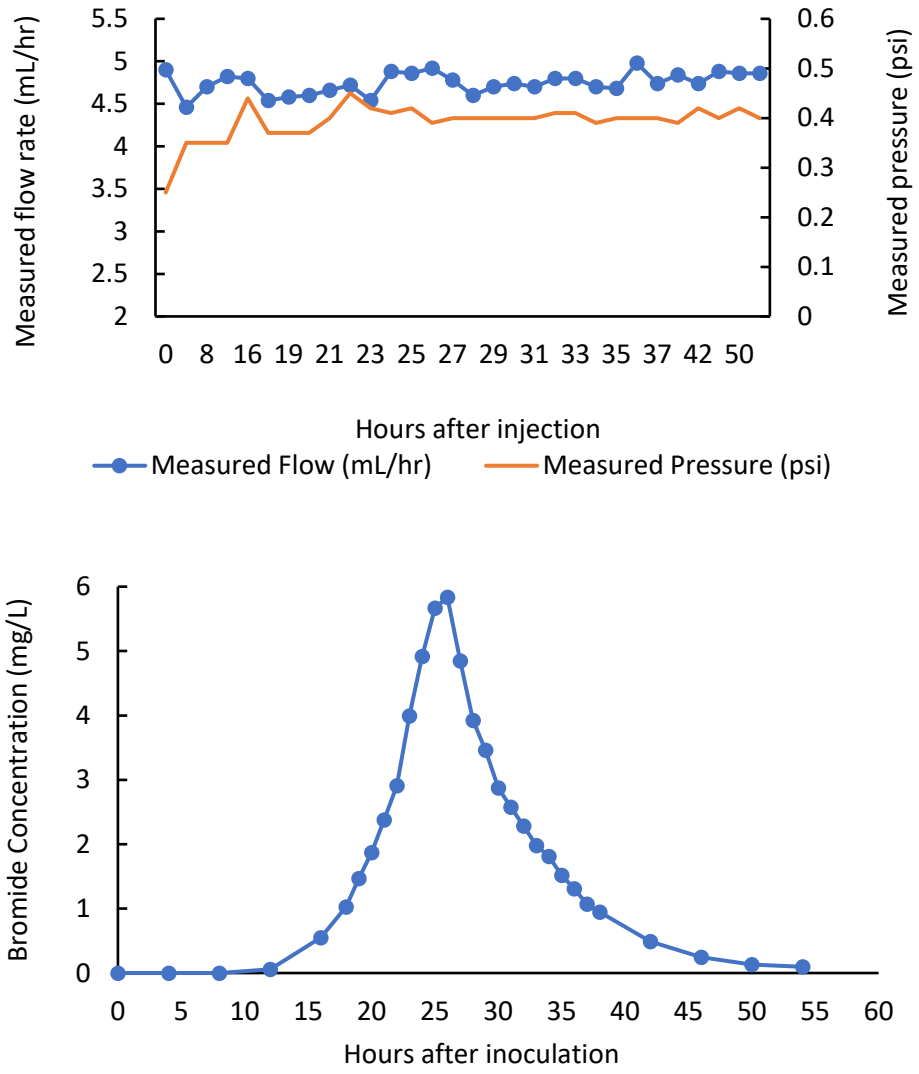

Figure C5. Individual measured flow rate, measured pressure difference and bromide breakthrough curve for reactor 3 at the low flow rate. The average measured flow rate for reactor 3 was 4.75 ± 0.13 mL/hr. The average pressure difference for reactor 3 was 0.39 ± 0.04 psi. The experimental residence time for Reactor 3 was 26 hours.

The average measured flow rate for reactor 1 was 11.69 ± 0.37 mL/hr. The average pressure difference for reactor 1 was 0.25 ± 0.06 psi. The theoretical residence time using the average measured flow rate is 8.4 hours, while the experimental residence time for reactor 1 was at hour 12 hours. The average measured flow rate for reactor 2 was 11.52 ±

0.60 mL/hr. The average pressure difference for reactor 2 was 0.39 ± 0.07 psi. The theoretical residence time using the average measured flow rate is 8.5 hours, while the experimental residence time for reactor 2 was at hour 12 hours. The average measured flow rate for reactor 3 was 11.71 ± 0.59 mL/hr. The average pressure difference for reactor 3 was 0.36 ± 0.05 psi. The theoretical residence time using the average measured flow rate is 8.4 hours, while the experimental residence time for reactor 3 was at hour 10 hours. The peak of the bromide breakthrough curve for the average bromide concentrations for the low flow rate was 11 hours. The calculated hydraulic gradient for the reactors ranged from -1.38 to -2.16 m/m. The calculated hydraulic conductivities for the reactors ranged from 1.16E-06 to 8.05E-07 m/s. The calculated permeabilities for the three reactors ranged from 1.05E-13 to 7.31E-14 m^2.

Reactor	Measured Flow (mL/hr)	Measured Pressure, ΔP (psi)	Residence time (hr)
1	11.69 ± 0.37	0.25 ± 0.06	8.4
2	11.52 ± 0.60	0.39 ± 0.07	8.5
3	11.71 ± 0.59	0.36 ± 0.05	8.4

Table C6. Average measure flow rate, average measured pressure, and calculated residence time for each reactor for the low flow rate experiment.

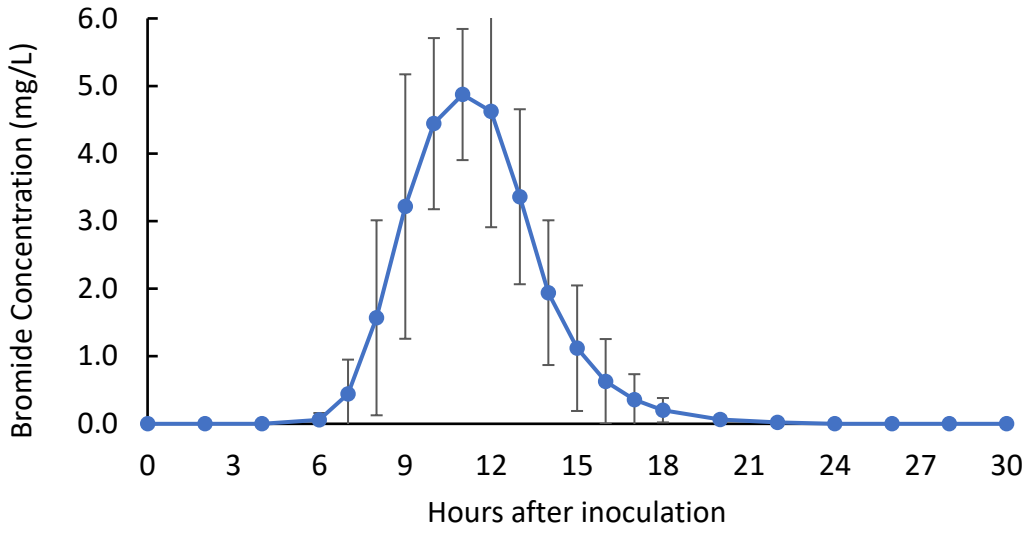

Figure C6. Average bromide concentrations of effluent samples over a period of 30 hours for the high flow experiment. The data points are the averaged bromide concentrations of the three reactors.

Reactor	Average flow rate (mL/hr)	Pressure difference (psi)	Hydraulic gradient (m/m)	Hydraulic conductivity (m/s)	Permeability (m^2)
1	11.69	0.25	-1.38	1.16E-06	1.05E-13
2	11.52	0.39	-2.16	7.31E-07	6.64E-14
3	11.71	0.36	-1.99	8.05E-07	7.31E-14

Table C7. Calculated hydraulic gradient, calculated conductivity, and calculated permeability for each reactor at the high flow rate using the average flow rate and average pressure difference for each reactor.

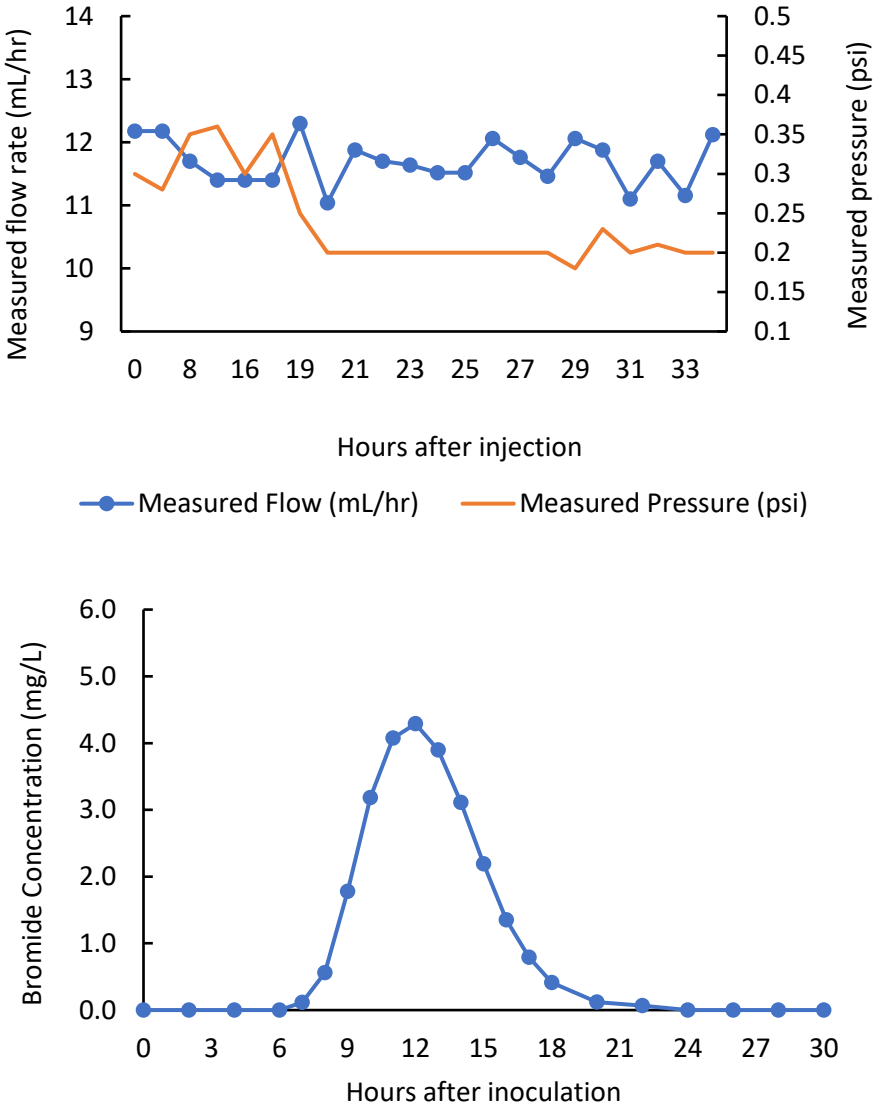

Figure C7. Individual measured flow rate, measured pressure difference and bromide breakthrough curve for reactor 1 at the high flow rate. The average measured flow rate for reactor 1 was 11.69 ± 0.37 mL/hr. The average pressure difference for reactor 1 was 0.25 ± 0.06 psi. The experimental residence time for Reactor 1 was 12 hours.

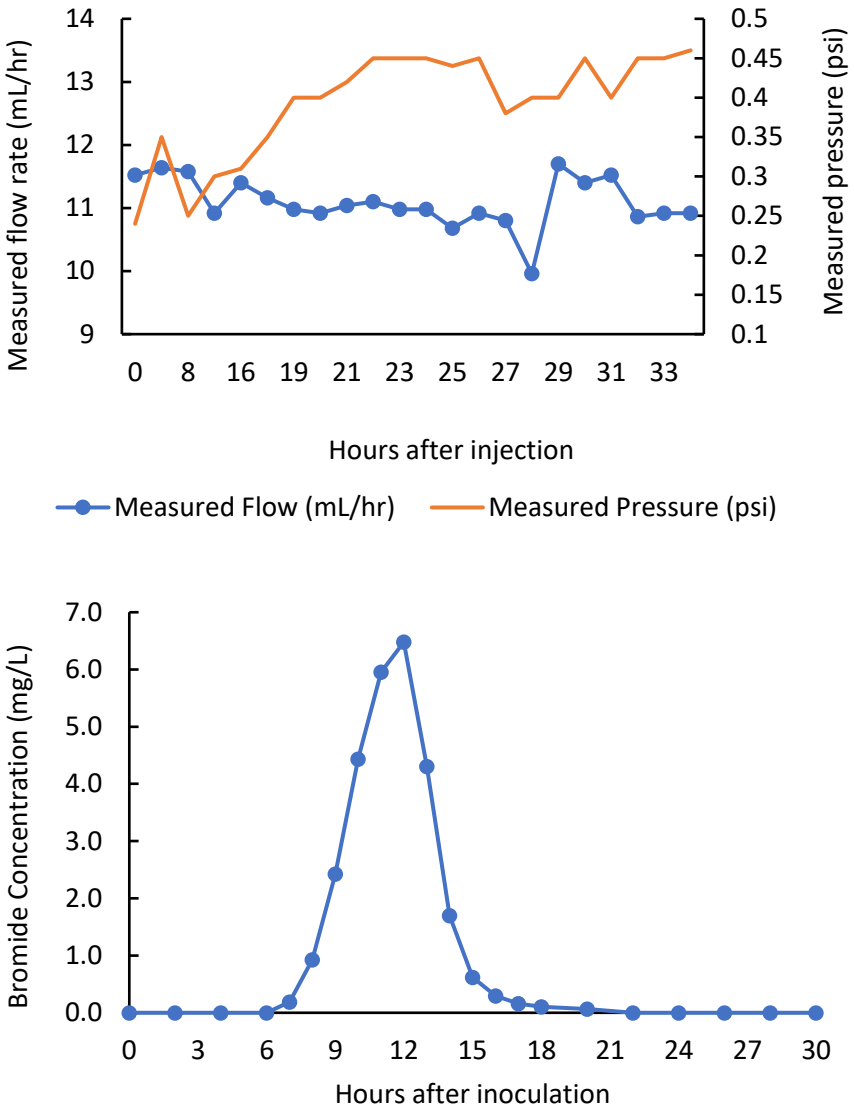

Figure C8. Individual measured flow rate, measured pressure difference and bromide breakthrough curve for reactor 2 at the high flow rate. The average measured flow rate for reactor 2 was 11.52 ± 0.60 mL/hr. The average pressure difference for reactor 2 was 0.39 ± 0.07 psi. The experimental residence time for Reactor 2 was 12 hours.

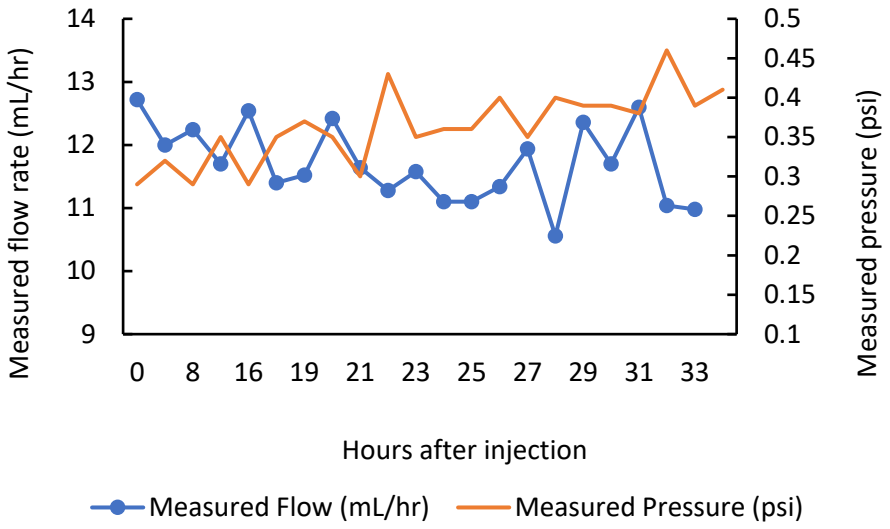

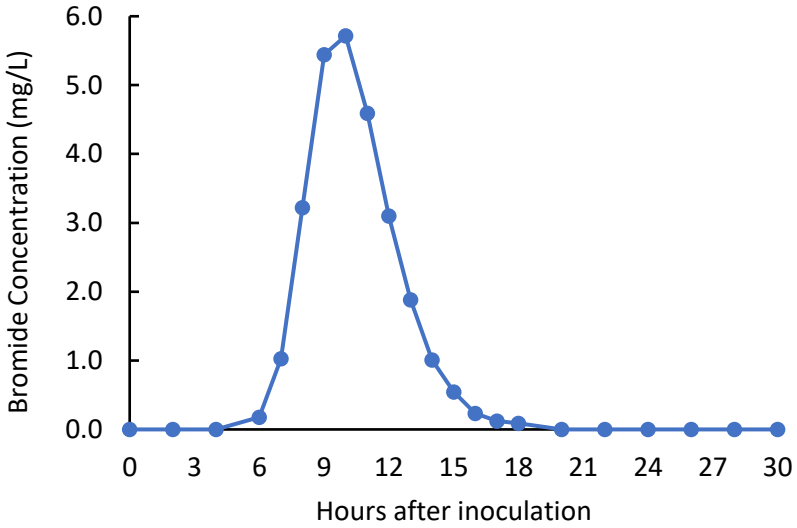

Figure C9. Individual measured flow rate, measured pressure difference and bromide breakthrough curve for reactor 3 at the high flow rate. The average measured flow rate for reactor 3 was 11.71 ± 0.59 mL/hr. The average pressure difference for reactor 3 was 0.36 ± 0.05 psi. The experimental residence time for Reactor 3 was 10 hours.

Discussion and Conclusions

The bromide breakthrough curves for both flow rates had a normal distribution. The variability for the average bromide concentration at different time points for both flow rates were likely due to the different porous media packing arrangement within the reactors. Although the reactors were packed with the same method throughout and packed with the same mass of sand, it is not possible to ensure the reactors have the same flow paths for media. Because of this, the effluent samples collected for both flow rates had varying bromide concentrations for the triplicate reactors at each flow rate. The peak of the bromide breakthrough curve for the averaged bromide concentrations for the low and high flow rate were 26 and 11 hours, respectively. However, when looking at the individual bromide breakthrough curves for each reactor, the peak time points varied more at the low flow rate than at the high flow rate. The peak concentrations occurred at 29, 38, and 26 hours for reactor 1, reactor 2, and reactor 3, respectively for the low flow rate. Whereas the peak concentrations occurred at 12, 12, and 10 hours for reactor 1, reactor 2, and reactor 3, respectively at the high flow rate. The variability of the peak time points for the low flow rate is likely due to local effects in the reactor that cause minor rearrangements of the flow paths due to capillary effects and surface tension effects within the reactor. When looking at the calculated hydraulic properties of the reactors (i.e., hydraulic gradient, hydraulic conductivity, and the permeability) both flow rates had hydraulic properties that are representative of what is seen at the FRC indicating the reactor system presented here emulates field relevant conditions.

Table 2.2 Range of Values of Hydraulic Conductivity and Permeability

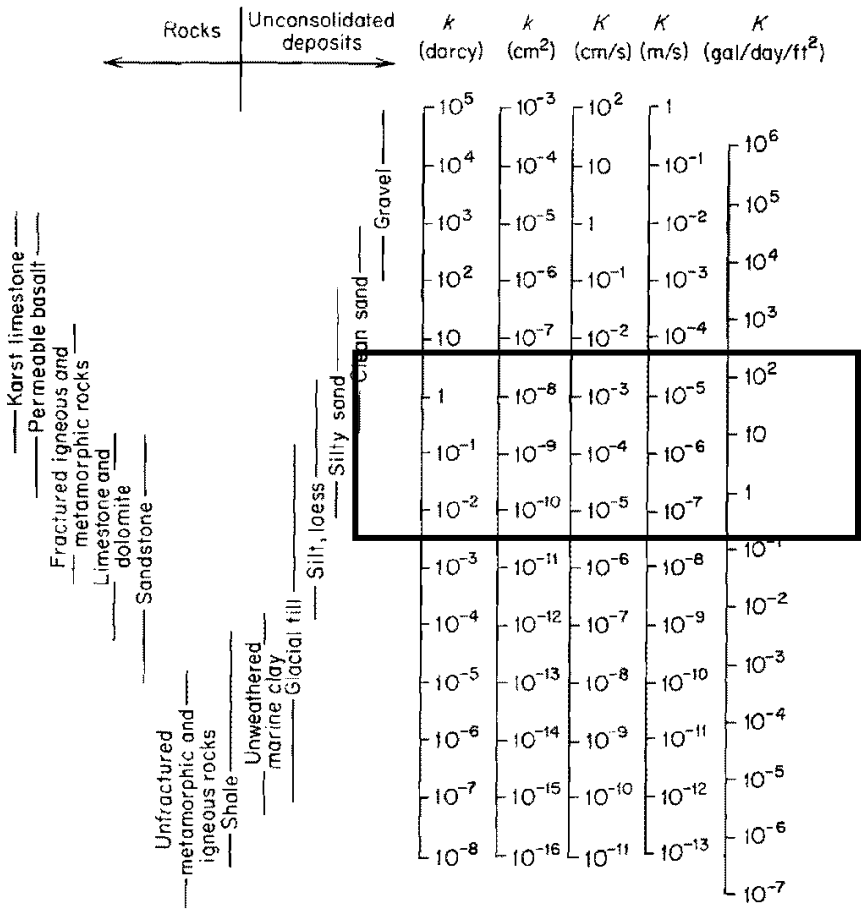

Figure C10. Range of values of hydraulic conductivity and permeability for different sediments found in the subsurface (Fetter, 2018).

APPENDIX D

FLOURESCENT MICROSPHERE BEAD DISTRIBUTION IN A POROUS MEDIUM REACTOR EMUALATING SHALLOW SUBSURFACE CONDITIONS

Experimental Justification

In order to better understand how cells move through and interact with porous media, it is necessary to understand how inert, non-charged particles distribute in a porous media environment. Triplicate up-flow packed bed reactors (PBRs) were inoculated with 1 µm fluorescent beads at a concentration of 1.05E+10 beads and with bromide at a concentration of 100 mg/L to compare breakthrough curves of a solute to an inert, non-charged particle. A pulse inoculation method was used so that the porous media in the reactors was undisturbed. The packed bed reactors were filled with 70 mesh sand that is representative of sediment found at the Oak Ridge National Laboratory Field Research Center (ORNL FRC). Two experiments were performed at two different field relevant flow rates and effluent samples were collected to construct a bromide breakthrough curve for each flow rate. Additionally, pressure readings were taken throughout the experiments to calculate the hydraulic gradient, hydraulic conductivity, and permeability for the reactors at the two flow rates.

Material and Methods

Experimental Plan

Once flow was established in triplicate reactors, reactors were inoculating with a mixture of bromide and 1 µm beads. Effluent samples were collected at different time points to measure the bromide concentration at each time point to construct a bromide breakthrough curve for two field relevant flow rates. The two flow rates of interest are 4.54 mL/hr and 11.32 mL/hr. UGA media used for the media in the reactors and the media reservoir was constantly degassed with a gas mixture of 80% nitrogen, 20% carbon dioxide.

Reactor design and construction

The up-flow packed bed reactor system described here is designed for laboratory bench-top use and can maintain an anoxic environment for all components upstream of the reactor column, the reactor column itself, and the effluent line. The system can be run at varying flow rates, including low flow rates that are representative of the shallow subsurface environment. Each reactor system has sampling ports at the top and bottom for injector or sampling. The sampling ports allow for temporal sampling of the planktonic phase. The size of the reactor was designed for increased sampling volume needed for sampling the sand. A schematic of the system is shown in Figure D1.

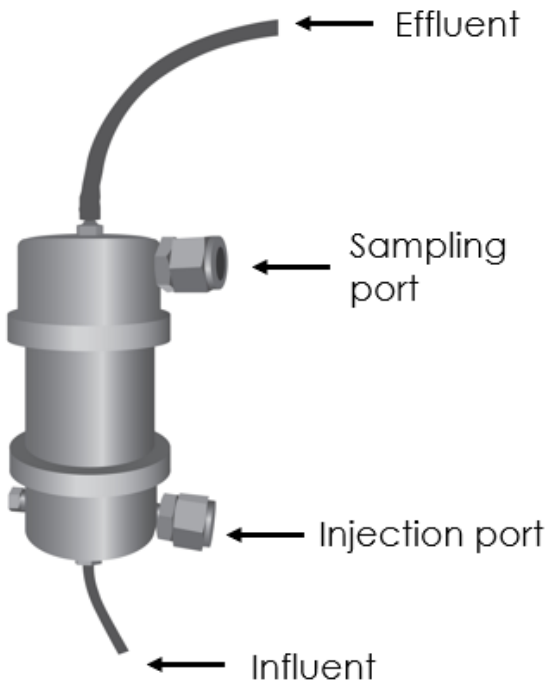

Figure D1. Diagram of the up-flow packed bed reactor designed and constructed. The reactor has an influent port at the bottom of the reactor and effluent exits the top of the reactor at the effluent port. Two septum ports were added to the reactor to easily inoculate the reactor and collect planktonic samples. The bottom septum port is used for inoculating the reactor and both ports can be used to collect planktonic samples.

The reactor column was constructed from type 316/316L stainless steel threaded pipe with a length of 3 inches, inner diameter of 2.067 inches, and a wall thickness of 0.154 inches. The threaded caps were 316 stainless steel with an outer diameter of 2.98 inches, a length of 1.77 inches, rated to a pressure of 150 psi. All components of the reactor body were bought from McMaster-Carr (Elmhurst, IL, USA). Holes were drilled into the side of both caps and 1/8-inch NPT threads were cut for the sampling port fittings. The bottom reactor cap (influent side) had two threaded holes, one located on the side for the sampling port and a second one located on the flat side of the cap for the influent port. The influent port was fitted with a 1/16-inch barbed fitting for flow and attached to size 13 Masterflex® Norprene tubing. The second hole on the bottom cap was fitted with a septum port fitting for sampling and injection. The top reactor cap had drilled holes, one located on the side for sampling and a second one located on the top for the effluent flow. The drilled hole located on the side was fitted with a septum port fitting for sampling. The top hole of the top cap was fitted with a ¼-inch barbed fitting for effluent flow and attached to size 25 Masterflex® Norprene tubing. The PBRs were packed with 380 g of a sand mix that contains sand particles whose diameter ranged from 75 to 300 µm.

The liquid media reservoir is 2-liter glass carboy. The carboy is sealed with a butyl rubber stopper. The butyl rubber stopper was drilled to install a piece of glass tubing which is attached to Masterflex® Norprene tubing used to hold an oxygen-free gas purge. A second hole was drilled in the rubber stopper to hold 1/8-inch stainless steel tubing that is attached to Masterflex® Norprene tubing for the media influent line. The effluent flow was collected in 1 liter glass carboys.

Flow Rate Calculations

The flow rates used in this study were calculated using field relevant hydraulic properties. The flow rates were calculated using an average pore velocity equation that is based on Darcy's law where v_p is the average pore velocity, K is the hydraulic conductivity, $\Delta h/\Delta l$ is the hydraulic gradient and e is the porosity. The saturated hydraulic conductivity used for calculating the flow rates is 5.73E-05 m/s. The saturated hydraulic conductivity was used rather than unsaturated hydraulic activity because the saturated zone of the shallow terrestrial subsurface is the zone this study focused on. The range of porosity used for calculating the flow rates was 0.35 to 0.49. The hydraulic gradient used for calculating the flow rates was 0 to 0.035 m/m. Using these parameters the range of flow rates is 4.54 mL/hr to 11.32 mL/hr.

$$v_p = \frac{(K) * (\frac{\Delta h}{\Delta l})}{e}$$

Unsat. Hydraulic conduct. (m/s) (K)	Sed	0.2-2.5 x 10^{-5}	Wilson & Luxmoore, 1988	Tension infiltrometer; geometric mean; n=39 obs.; field measure.; psi=0,2,5, 14cm
Sat. hydraulic conduct. (m/s) (K)	Sed	1x10^{-4} 5.73 x 10^{-5}	Wilson & Luxmoore, 1988 Collected 6/8/18	Tension infiltrometer; geometric mean; n=39 obs.; field measure.; psi=0,2,5, 14cm
Porosity (e)*	Sed	0.35-0.49	Howard 1997	Paraffin clod method
Gradient across site (m/m) (Δh/Δl)	GW	0.015 – 0.075 (horiz) 0.005-0.063 (vert.) 0.00-0.035	Schreiber et. al. 1998 Adams and McBride, Hazen Lab, measured weekly from Dec 2017 to March 2018	Range at one location; values may exceed this range, especially near streams

Table D1. Modified From Table 1 of Watson et. al, 2004. pg. 7. Data summaries for the FRC background area, Permeability of Saprolite.

Reactor Preparation

Prior to the experimental run of the reactor systems, all Norprene tubing, reactor columns, liquid media reservoir, and effluent carboys were autoclaved. After sterilization, the reactor system was constructed aseptically. The reactor system was purged of

atmospheric air, specifically targeting the removal of oxygen, using 80% N_2/20% CO_2. The pump was turned on to fill reactors with media before inoculating.

Pulse Inoculation

The bead concentration used to inoculate was be based on field relevant cell counts. The average cell count (total cell count) from the saturated zone is 2.78E+07 cells/gram sand. Thus, this number will be multiplied by the total mass of sand in the reactors to determine the initial concentration of beads for inoculating. The reactors were inoculated with a mixed solution of bromide at a concentration of 100 mg/L and 292 µL of the fluorescent microsphere bead solution at a concentration of 3.6E+07 beads/µL. The bromide, bead mixture was inoculated into the reactors as a pulse inoculation, inoculating the reactors over a time of 1 minute.

Bromide Samples

Once flow was established in the reactors, each reactor was inoculated with 3 mL of bromide at a concentration of 100 mg/L. The bromide was inoculated into the reactors as a pulse inoculation, inoculating the reactors over a time of 1 minute. 2 mL of effluent was collected from each reactor in a sterile 15 mL falcon tube for each time point listed in Tables D2 and D3. Samples were stored at -20 ℃. For the low flow rate experiment, samples were collected every 4 hours until hour 16. At hour 18, samples were collected every hour until hour 20. After hour 20, samples were collected every hour until hour 40 (see Table D2). For the high flow rate experiment, samples were collected every 2 hours until hour 6. At hour 6, samples were collected every hour until hour 18. After hour 18, samples were collected every 2 hours until hour 30 (see Table D3). Bromide samples were

ran on an ion chromatography instrument to measure the bromide concentration for each time point. A breakthrough curve for each flow rate was constructed using the bromide concentrations for each time point. Pressure readings were collected at every time point. Flow was measured gravimetrically at every time point.

Sample #	Time Point after injection (hr.)
0	0
1	4
2	8
3	12
4	16
5	18
6	20
7	21
8	22
9	23
10	24
11	25
12	26
13	27
14	28
15	29
16	30
17	31
18	32
19	34
20	35
21	36
22	37
23	38
24	39
25	40
26	44
27	48
28	52
29	56
30	60
31	64
32	68
33	72

Table D2. Sampling plan for the low flow rate experiment. The pumped was set to 5.2 mL/hour to achieve a desired flow rate of approximately 4.54 mL/hr.

Sample #	Time Point after injection (hr.)
0	0
1	2
2	4
3	6
4	7
5	8
6	9
7	10
8	11
9	12
10	13
11	14
12	15
13	16
14	17
15	18
16	20
17	22
18	24
19	26
20	28
21	30

Table D3. Sampling plan for the high flow rate experiment. The pumped was set to 12.8 mL/hour to achieve a desired flow rate of approximately 11.32 mL/hr.

Fluorescent Bead Samples

2 mL of effluent was collected from each reactor in a sterile 15 mL falcon tube for each time point listed in Tables D2 and D3. Samples were stored at 4 ℃. For the low flow rate experiment, samples were collected every 4 hours until hour 16. At hour 18, samples were collected every hour until hour 20. After hour 20, samples were collected every hour until hour 40 (see Table D2). For the high flow rate experiment, samples were collected every 2 hours until hour 6. At hour 6, samples were collected every hour until hour 18.

After hour 18, samples were collected every 2 hours until hour 30 (see Table D3). Fluorescent microsphere bead concentrations were determined using fluorescence activated cell sorting (FACS).

Epoxy embedding and imaging

Sand cores from each reactor were collected at the end of the experiment. Core were collected using a sterile 5-inch plastic core with a diameter of 1 inch. Once the cores were collected, each core was saturated with 2% paraformaldehyde and left at room temperature for 2 hours for fixation. After fixation, each core received a series of washes to remove moisture from the core. The cores were then saturated with LR white resin and placed in an incubator for 24 – 48 hours to allow the resin to set. Each of the LR white resin cores was cut into sections and imaged at multiple fields of view using Confocal Scanning Laser Microscopy. For each field of view, fluorescent images of the cells and reflection images of the exposed sand surface were taken using the same Z-stack depth. Reflection images of the sand particles were then overlaid with their corresponding fluorescent image in Imaris.

Results

The average measured flow rate for reactor 1 was 4.08 ± 0.25 mL/hr. The average pressure difference for reactor 1 was 0.28 ± 0.11 psi. The theoretical residence time using the average measured flow rate is 24 hours, while the experimental residence time for reactor 1 was at hour 25 hours. The average measured flow rate for reactor 2 was 4.56 ± 0.39 mL/hr. The average pressure difference for reactor 2 was 0.38 ± 0.08 psi. The theoretical residence time using the average measured flow rate is 21.4 hours, while the

experimental residence time for reactor 2 was at hour 18 hours. The average measured flow rate for reactor 3 was 4.57 ± 0.60 mL/hr. The average pressure difference for reactor 3 was 0.20 ± 0.05 psi. The theoretical residence time using the average measured flow rate is 21.4 hours, while the experimental residence time for reactor 3 was at hour 23 hours. The peak of the bromide breakthrough curve for the average bromide concentrations for the low flow rate was 25.

Reactor	Measured Flow (mL/hr)	Measured Pressure, ΔP (psi)	Residence time (hr)
1	4.08 ± 0.25	0.28 ± 0.11	24
2	4.56 ± 0.39	0.38 ± 0.08	21.4
3	4.57 ± 0.60	0.20 ± 0.05	21.4

Table D4. Average measure flow rate, average measured pressure, and calculated residence time for each reactor for the low flow rate experiment.

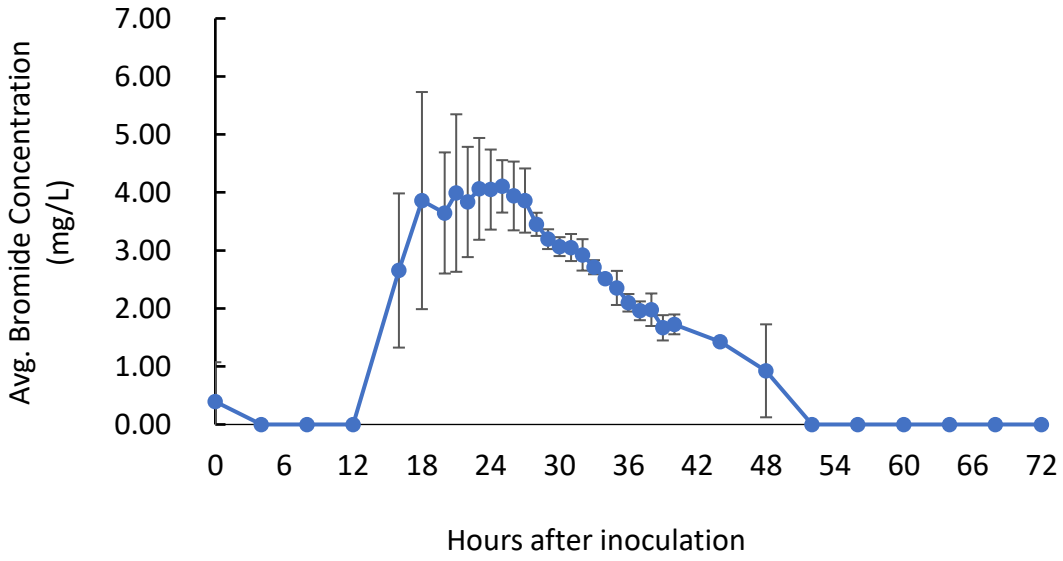

Figure D2. Average bromide concentrations of effluent samples over a period of 72 hours for the low flow experiment. The data points are the averaged bromide concentrations of the three reactors.

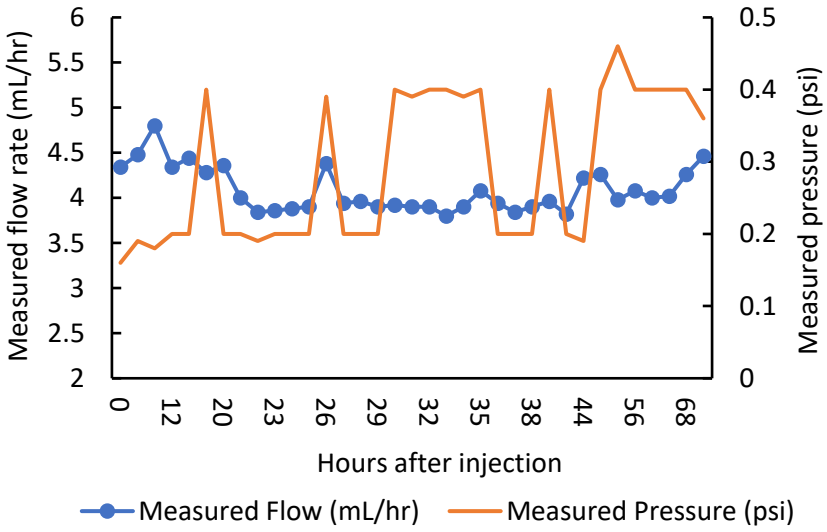

Figure D3. The average measured flow rate for reactor 1 was 4.08 ± 0.25 mL/hr. The average pressure difference for reactor 1 was 0.28 ± 0.11 psi. The experimental residence time for Reactor 1 was 25 hours.

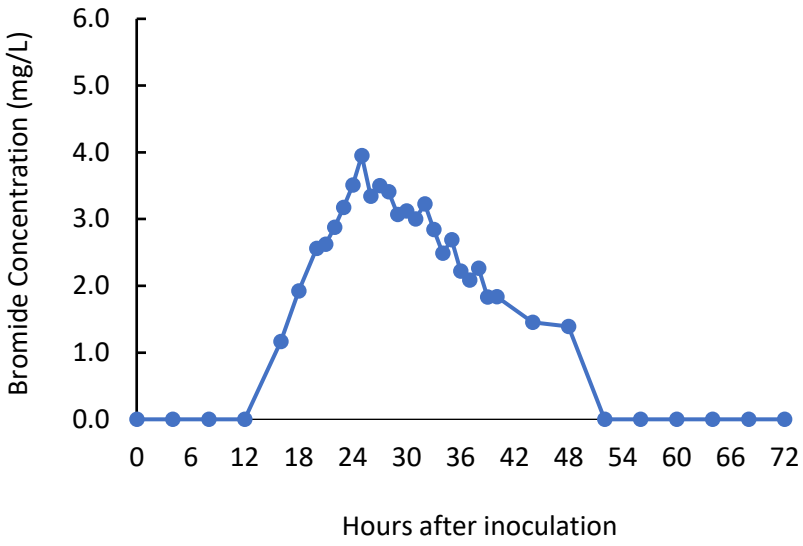

Figure D4. Bromide breakthrough curve for reactor 1. The calculated residence time using the average measured flow rate is 24 hours. The peak of the bromide breakthrough curve for reactor 1 is at hour 25 hours.

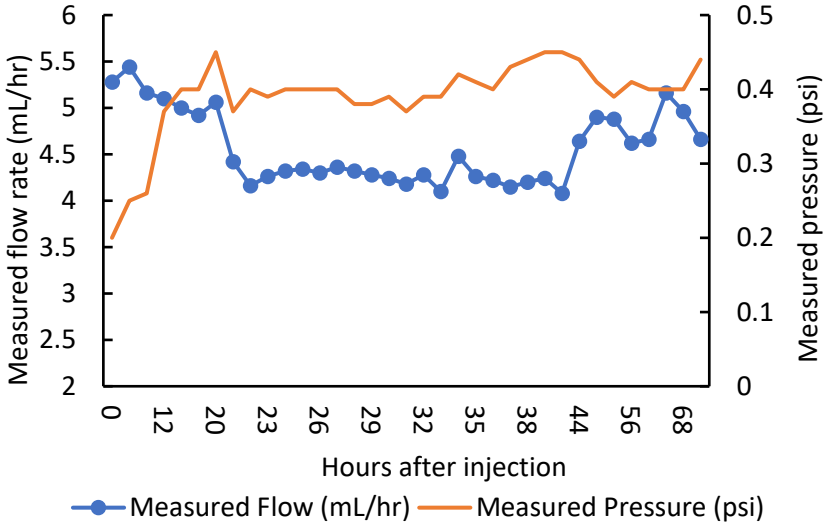

Figure D5. The average measured flow rate for reactor 2 was 4.56 ± 0.39 mL/hr. The average pressure difference for reactor 2 was 0.38 ± 0.08 psi. The experimental residence time for Reactor 2 was 38 hours.

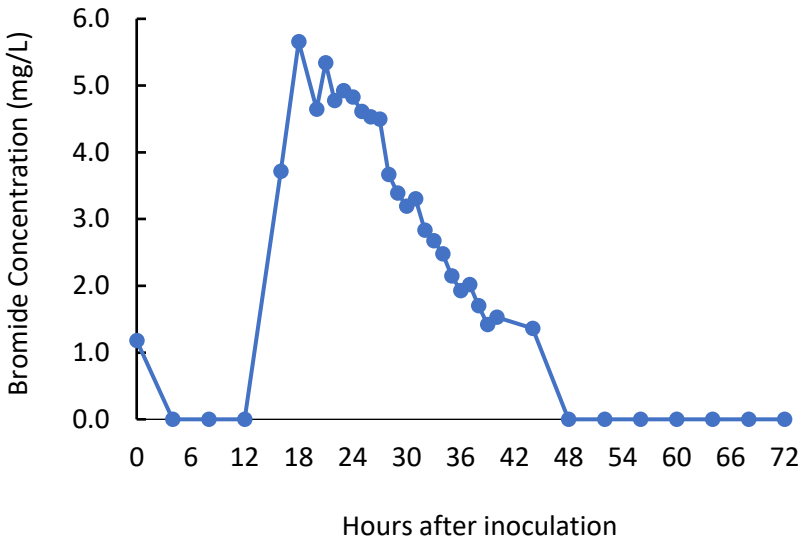

Figure D6. Bromide breakthrough curve for reactor 2. The calculated residence time using the average measured flow rate is 21.4 hours. The peak of the bromide breakthrough curve for reactor 2 is at hour 18 hours.

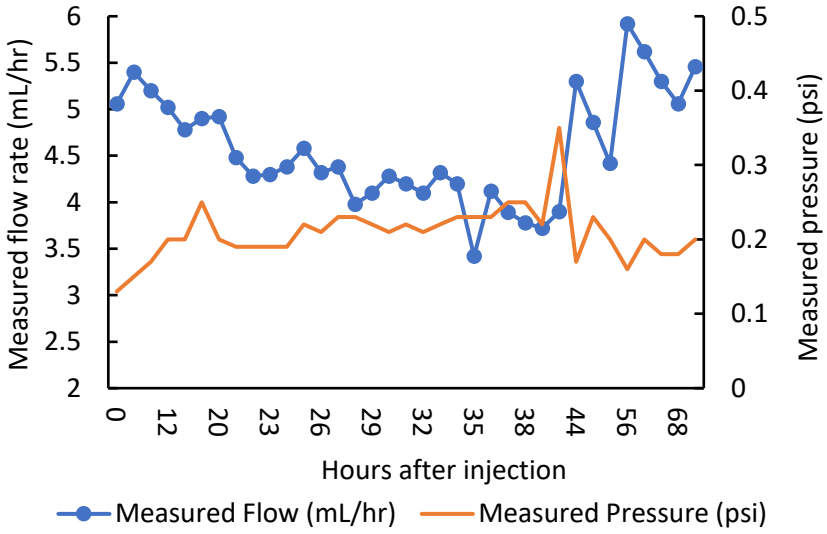

Figure D7. The average measured flow rate for reactor 3 was 4.57 ± 0.60 mL/hr. The average pressure difference for reactor 3 was 0.20 ± 0.05 psi. The experimental residence time for Reactor 3 was 23 hours.

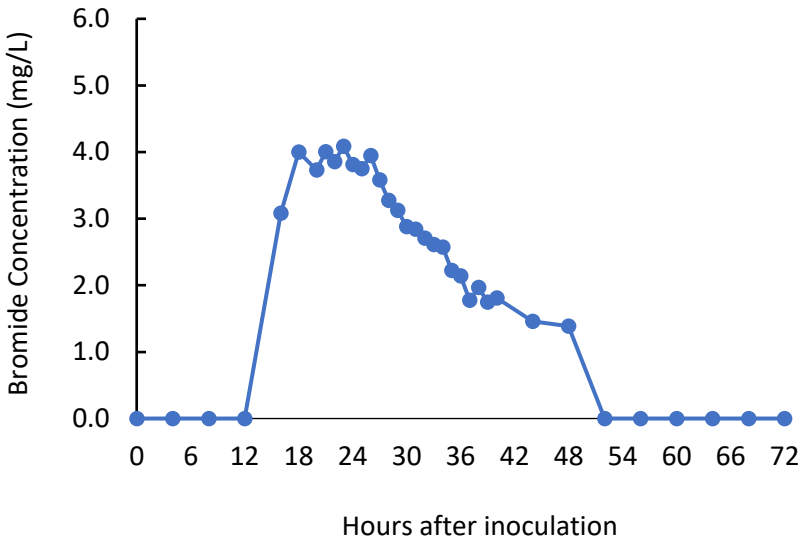

Figure D8. Bromide breakthrough curve for reactor 3.The calculated residence time using the average measured flow rate is 21.4 hours. The peak of the bromide breakthrough curve for reactor 3 is at hour 23 hours.

Discussion and Conclusions

Fluorescence activated cell sorting (FACS) was used to determine the fluorescent microsphere bead concentrations of the effluent samples collected. However, it was discovered that this method would not work. Effluent samples were ran on a BD Acurri C6 Plus FACs instrument and also filtered onto a 0.2 µm membrane for direct counts using microscopy. The results for a few samples can be seen in Table D5. As seen in Table D5, the results of the fluorescent microsphere bead concentrations are significantly different for the samples that were measured using both FACs and direct counts. Figure D9 shows an example of the 1 µm fluorescent microsphere beads that have been filtered onto a 0.2 µm membrane. Furthermore, resin sand cores were collected for the low flow rate experiment. The sand core was cut into different sections for imaging the bead distribution in the sand core. However, it was discovered that the resin degrades the plastic of the

fluorescent microsphere beads and thus they could not be imaged in the sand core. Different resins were tested for the sand cores but all resins tested degraded the plastic of the fluorescent microsphere beads. Figure D10 shows the process for obtaining and imaging the sand cores collected from the packed bed reactors.

Sample	FACS (beads/mL)	Direct count (beads/mL)
PBR 1_T10	492	1.36E+05
PBR 2_T10	5	1.21E+04
PBR 3_T10	33	1.24E+05

Table D5. Fluorescent microsphere bead concentrations using FACS and direct counts.

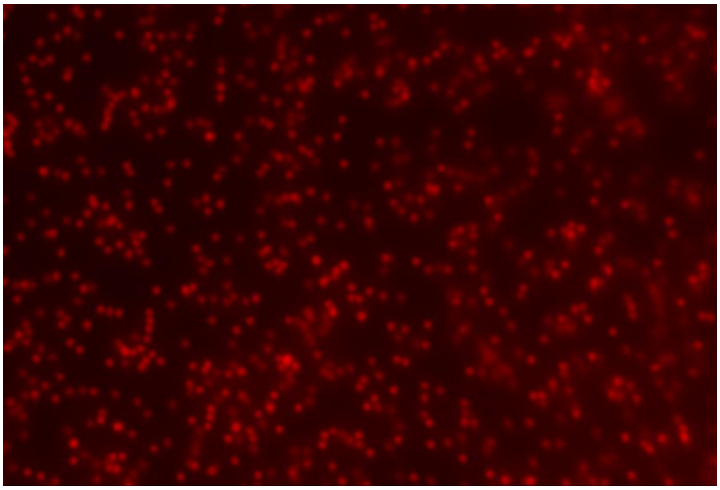

Figure D9. Image of 1 µm fluorescent microsphere beads filtered onto a 0.2 µm membrane.

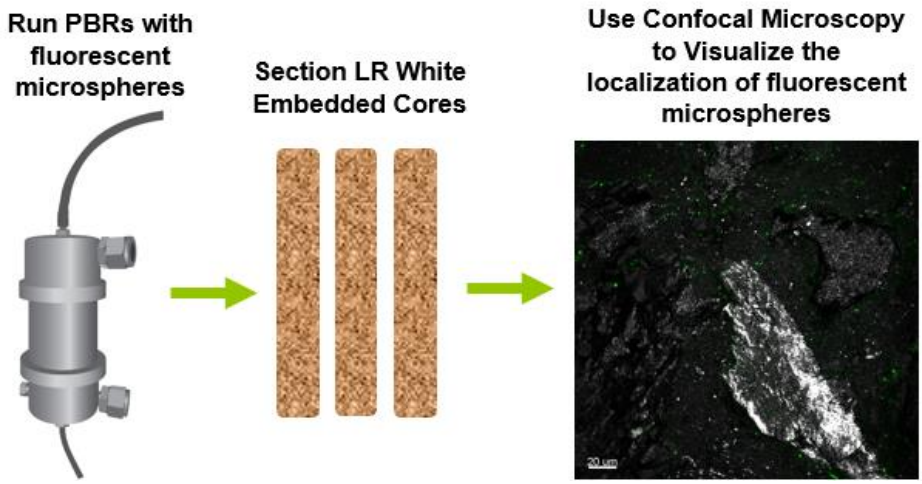

Figure D10. Process for collecting and imaging fluorescent microsphere beads in a sand core that has been washed with resin.

APPENDIX E

DETERMINING HOW INOCULATING METHODS INFLUENCE BIOFILM DISTRIBUTION IN A POROUS MEDIUM REACTOR

Experimental Justification

There are a range of methods used to inoculate reactors particularly for packed bed reactors, however, it is unknown what methods provide the best biofilm distribution in a porous media environment as well as which method is the most representative of cell distribution in the shallow subsurface environment. This study looks at six different inoculation strategies using a microorganism isolated from the Oak Ridge National Laboratory Field Research Center (ORNL FRC). Planktonic samples were collected every 48 hours for 240 hours. Destructive samples were collected after 240 hours.

Materials and Methods

Experimental Plan

Once flow was established in the reactors, reactors were inoculated with 6 different inoculation strategies. Porosity measurements were performed at the beginning and end of the experiment. Optical density, mutant library, protein, carbohydrate, dissolved oxygen, pH, dissolved organic carbon, nitrate, metabolite, and cell concentration samples were collected every 48 hours for 240 hours. Protein, carbohydrate, cell concentration, and mutant cell samples were collected from the sand fraction of the packed bed reactor. A LR white sand core was also collected at the end of the experiment. These samples were used to compare the different inoculation strategies.

Reactor design and construction

The up-flow packed bed reactor system described here is designed for laboratory bench-top use and can maintain an anoxic environment for all components upstream of the reactor column, the reactor column itself, and the effluent line. The system can be run at

varying flow rates, including low flow rates that are representative of the shallow subsurface environment. Each reactor system has sampling ports at the top and bottom for injector or sampling. The sampling ports allow for temporal sampling of the planktonic phase. The size of the reactor was designed for increased sampling volume needed for sampling the sand. A schematic of the system is shown in Figure E1.

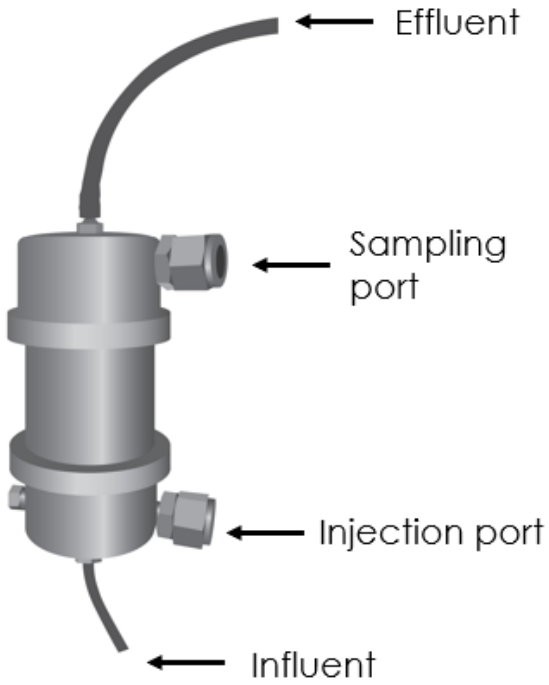

Figure E1. Diagram of the up-flow packed bed reactor designed and constructed. The reactor has an influent port at the bottom of the reactor and effluent exits the top of the reactor at the effluent port. Two septum ports were added to the reactor to easily inoculate the reactor and collect planktonic samples. The bottom septum port is used for inoculating the reactor and both ports can be used to collect planktonic samples.

The reactor column was constructed from type 316/316L stainless steel threaded pipe with a length of 3 inches, inner diameter of 2.067 inches, and a wall thickness of 0.154 inches. The threaded caps were 316 stainless steel with an outer diameter of 2.98 inches, a

length of 1.77 inches, rated to a pressure of 150 psi. All components of the reactor body were bought from McMaster-Carr (Elmhurst, IL, USA). Holes were drilled into the side of both caps and 1/8-inch NPT threads were cut for the sampling port fittings. The bottom reactor cap (influent side) had two threaded holes, one located on the side for the sampling port and a second one located on the flat side of the cap for the influent port. The influent port was fitted with a 1/16-inch barbed fitting for flow and attached to size 13 Masterflex® Norprene tubing. The second hole on the bottom cap was fitted with a septum port fitting for sampling and injection. The top reactor cap had drilled holes, one located on the side for sampling and a second one located on the top for the effluent flow. The drilled hole located on the side was fitted with a septum port fitting for sampling. The top hole of the top cap was fitted with a ¼-inch barbed fitting for effluent flow and attached to size 25 Masterflex® Norprene tubing. The PBRs were packed with approximately 315 g of 70 mesh sand that contains sand particles whose diameter ranged from 75 to 300 µm.

The liquid media reservoir was a 10-liter carboy that had a single media line and gas line connecting at the rubber stopper. The butyl rubber stopper was drilled to install a piece of glass tubing which is attached to Masterflex® Norprene tubing used to hold an oxygen-free gas purge. A second hole was drilled in the rubber stopper to hold 1/8-inch stainless steel tubing that is attached to Masterflex® Norprene tubing for the media influent line. The media line was split into 6 equal lines before the pump head as 6 reactors were used for this study. The effluent flow was collected in 2-liter glass carboys. SGW groundwater media was used for the experiment with constant gas flow at a mixture of 95% nitrogen, 5% oxygen. The flow rate used for this study was 3.31 mL/hr.

Component	Amount
KH_2PO_4	0.15 g/L
$NaNO_3$	0.425 g/L
$NaHCO_3$	2.5 g/L
Add after autoclaving:	
Wolfe's Vitamins	10 mL/L
Wolfe's Minerals	10 mL/L
Exo-metabolites 2X	20 mL/L

Table E1. SGW media used for this study.

Target Pore Velocity	Flow rate needed to achieve pore velocity
0.413 m/day	13.25 mL/hr
0.2065 m/day	6.63 mL/hr
0.10325 m/day	**3.31 mL/hr**

Table E2. Field relevant flow rates.

Reactor Preparation

Prior to the experimental run of the reactor systems, all Norprene tubing, reactor columns, liquid media reservoir, and effluent carboys were autoclaved. After sterilization, the reactor system was constructed aseptically. The reactor system was purged of atmospheric air, specifically targeting the removal of oxygen, using 95% N_2/5% O_2. The pump was turned on to fill reactors with media before inoculating. After the entire reactor system was filled with media, the pumped was paused and all three reactors were inoculated from the bottom sampling port with their respective inoculum sample. The pumped remained paused for 24 hours after inoculating the reactors to allow the bug trap inoculum to establish initial attachment to the porous medium. After 24 hours the pump was turned back on.

Inoculation

Six different inoculation strategies were tested in this study. The strategies different in volume and cell concentration. The volume of inoculation used were either 10% of the pore volume (10 mL) or 100% of the pore volume (100 mL). Three different cell concentrations were tested at each volume that was used. Table E3 lists the six different inoculation methods used for this study. *Cupriavidus* sp. strain 4G11 was grown in R2A media in a flask at 20 ºC for 24 hours. The culture was then spun down to collect a cell pellet. The cell pellet was resuspended in SGW groundwater to create the six different inoculation strategies. Once flow was established in the reactors, the flow was paused, and each reactor was inoculated with their corresponding inoculation strategy. Flow was turned back on 24 hours after inoculating the reactors to give the inoculum time for an initial attachment to the porous media.

Reactor	Inoculation Method & initial OD
1	10% of pore volume, OD = 1
2	100 % of pore volume, (1:10 dilution of OD = 1)
3	10% of pore volume, OD = 0.5
4	100 % of pore volume, (1:10 dilution of OD = 0.5)
5	10% of pore volume, OD = 0.1
6	100 % of pore volume, (1:10 dilution of OD = 0.1)

Table E3. Inoculation setup used for this study.

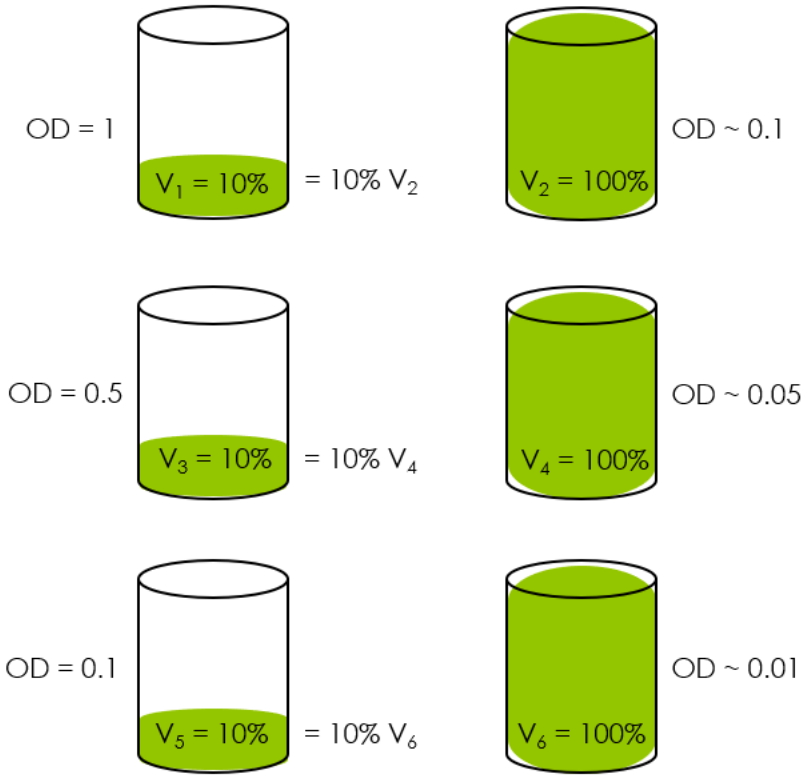

Figure E2. Diagram of inoculation setup for this study.

Reactor Breakdown and Sampling

Optical density, mutant library, protein, carbohydrate, dissolved oxygen, pH, dissolved organic carbon, nitrate, metabolite concentration, and cell concentration samples were collected every 48 hours for 240 hours. 1 mL of planktonic sample was collected for optical density (OD) measurements at each time point and measured at 600 nm. 1 mL of planktonic sample was collected for planktonic protein samples and were measured using the Qubit protein assay (Life Technologies, Carlsbad, CA). 1 mL of planktonic sample was collected for planktonic carbohydrate samples and was analyzed using a carbohydrate assay. Approximately 5 mL of planktonic sample was collected at each time point to measure dissolved oxygen (DO) and pH. A dual pH and DO probe was used to measure

the pH and DO for each time point. 1 mL of planktonic sample was collected for dissolved organic carbon (DOC) samples at each time point. The DOC samples were analyzed using a Formacs HT/TN (Skalar, Inc., Buford, GA, USA). Two mL of planktonic samples was collected at each time point for nitrate measurements. Nitrate samples were analyzed using an ion chromatography instrument (Dionex AS-DV Autosampler, Thermofisher Scientific, Waltham, MA, USA). One mL of planktonic sample was collected at each time point for cell concentration measurements. Formalin was added to the cell concentration samples and stored at 4 °C until analysis. Triplicate 1 mL planktonic samples for metabolite measurements were collected at each time point. Planktonic samples collected for metabolite measurements were filtered and stored at -80 °C until analysis. 5 mL of planktonic sample was collected at each time point for mutant library analysis at each time point. Mutant library samples were spun down and stored at -80 °C until analysis.

Porosity was measured at the beginning (initial porosity before reactor is filled and inoculated) and at the end of the experiment for each reactor. This gave an estimate of how much the porosity has changed in the reactor and some insight into how much biomass attached to the sand. Porosity was be measured by placing ~5 mL of sand in a graduated cylinder and removing all liquid from sand. Water was added to the sand until it reaches the top of the sand. Porosity will then be calculated using the following equation:

$$Porosity = \frac{mL\ of\ water\ added\ to\ sand}{mL\ of\ sand}$$

After 240 hours, the pumped was paused and the reactors were opened up to collect destructive samples. Four sand cores were collected from each reactor. The sand cores were

used for measuring attached protein, attached carbohydrate, attached mutant analysis and for a LR white sand core. The sand cores were collected using a sterile 5-inch steel tube with a diameter of 0.5 inches. Once the cores for the attached protein, attached carbohydrate, and attached mutant analysis were collected the core was divided into three sections (top, middle, and bottom) for a gradient analysis for each sample type. The sand collected for the gradient protein measurements were placed in a sterile 15 mL falcon tube for each reactor. The protein sand samples were stored in a 1:1 ratio of sand and sterile water. The protein samples were stored at -80 ℃ for 24 hours and then allowed to thaw at room temperature. After fully thawed, the samples were vortexed and placed back into the -80 ℃ freezer for an additional 24 hours. After 24 hours, the samples were allowed to thaw fully and vortexed. Ensuring the samples were tightly sealed, the protein samples were then placed in a water bath at 100 ℃ for 30 minutes and vortexed once more. Protein was measured using the Qubit protein assay (Life Technologies, Carlsbad, CA). The sand collected for each reactor was dried and weighed. The protein measurement was normalized to the sand weight. The sand collected for the gradient carbohydrate measurements were placed in a sterile 15 mL falcon tube for each reactor. The carbohydrate sand samples were stored in a 1:1 ratio of sand and sterile water. The samples were stored at -80 °C until analysis. The sand collected for the gradient mutant library measurements were placed in a sterile 15 mL falcon tube for each reactor. The samples were stored at -80 °C until analysis.

Epoxy embedding and imaging

Sand cores from each reactor were collected at the end of the experiment. Core were collected using a sterile 5-inch steel core with a diameter of 0.5 inch. Once the cores were collected, each core was saturated with 2% paraformaldehyde and incubated at room temperature for 2 hours (fixation). After fixation, each core received a series of washes to remove moisture from the core prior to embedding. The washes that are used for the cores are in the following order: 1X PBS, 50% 1X PBS/50%ethanold, 20% 1X PBS/80% ethanol, 100% ethanol, 50% ethanol/50% LR white epoxy. After the 50% ethanol/50% LR white epoxy wash, the cores were saturated with LR white resin (LR white hard grade, catalyzed, Electron Microscopy Sciences) and placed in an incubator for 24 – 48 hours to allow the resin to set. Each of the LR white resin cores was cut into sections and imaged at multiple fields of view using Confocal Scanning Laser Microscopy. Cores were stained with SYBR Green, a nucleic acid stain (Invitrogen; Life Technologies) 1X final concentration and were rinsed after staining with 0.2 µm filter sterilized DI water three times to remove any excess stain. Core samples were imaged with a Leica TCS SP5 II confocal microscope using a 63X water immersion objective, 0.9 NA, WD 2.2 mm. Fluorophore excitation lasers and emission bandwidths are as follows: SYBR Green (ex 497/em 520) 488 nm excitation, 500–550 nm emission collection; 235 autofluorescence, 561 nm excitation, 580–700 nm emission collection. Three randomly selected images were collected to enumerate cellular biomass (SYBR green, autofluorescence, reflection). For each field of view, fluorescent images of the cells and reflection images of the exposed porous material surface were taken using the same Z-stack depth. Reflection images of the particles were then overlaid with

corresponding fluorescent image in Imaris (version 9.3.0; Bitplane). The circumference of a particle, the number of cells along that circumference, and the distances between observed cells were then measured using the segmented line tool in ImageJ. To improve visibility of the cells along the outline of each sediment particle, both an overlaid reflection/fluorescent image and a plain fluorescent image were imported into ImageJ and layered using the "Overlay" tool. The fluorescent image was set to an opacity of 70%. Throughout the measuring process, the overlaid fluorescent image could be turned on and off to confirm cell placement along the sediment particle boundary. The data was tabulated in Excel and the average distance between cells along a given sediment particle was determined.

Results

The protein measurements for the gradient analysis for each reactor are shown in Figure E3. The reactors that were inoculated in a plug-flow style, inoculated with 10% of the pore volume, have a higher protein concentration in the bottom of the reactors. However, the protein concentration of the top section of the reactor volume is higher than the middle section of the reactor for reactors 1 (inoculation = 10% pore volume of an OD 1) and 5 (inoculation = 10% pore volume of an OD 0.1). Reactor 3 (inoculation = 10% pore volume of an OD 0.5) had a protein concentration of zero for the middle section. For reactors 2, 4, and 6, there is no trend in the distribution of protein in the gradient analysis. For reactor 2 (inoculation = 100% pore volume of an OD 0.1), the top section of the reactor has the highest concentration with the protein concentration decreasing with decreasing height. Unlike reactor 2, reactor 4 (inoculation = 100% pore volume of an OD 0. 5) and

reactor 6 (inoculation = 100% pore volume of an OD 0.01) have the highest protein concentration in the bottom section, similar to reactors 1, 3, and 5. However, for reactor 6 the protein concentration increases with increasing height in the reactor.

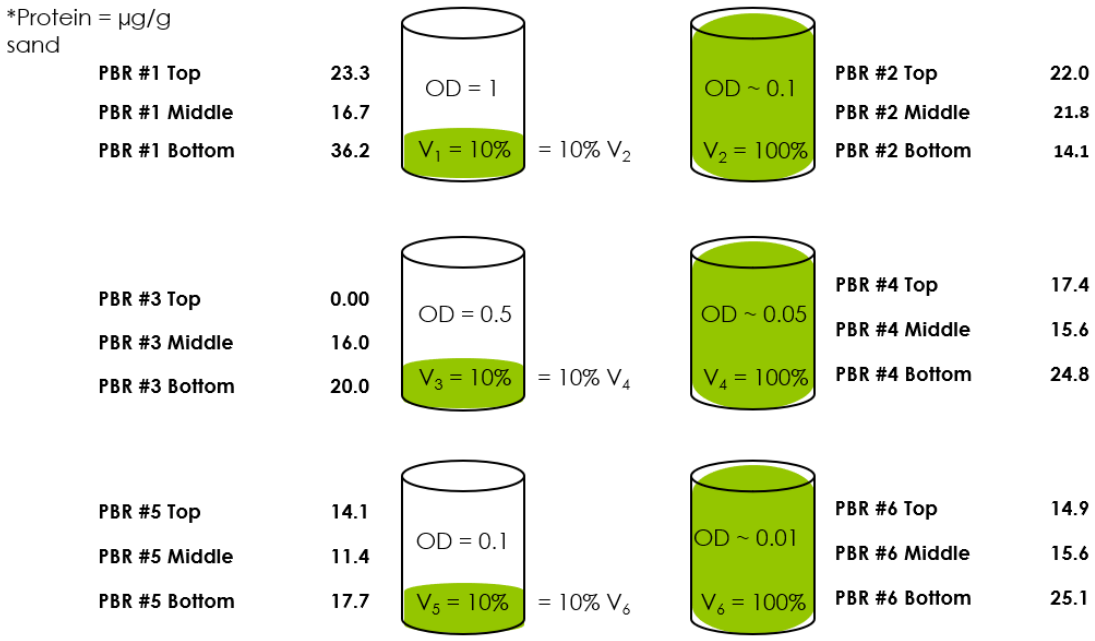

Figure E3. Protein measurements for each inoculation strategy tested.

DNA concentration and cell counts were performed on sand samples from reactors 2, 4, and 6 because these reactors had the highest protein concentration of all six reactors (shown in Figure E4). Although reactor 2 has a higher protein concentration in the top section, the DNA concentration was insufficient for an accurate measurement. However, for reactor 2 the DNA concentration for the middle section is smaller than the bottom section. Similar to reactor 2's protein concentration, the cell concentration increases with increasing height in the reactor. For reactor 4, the cell concentrations follow the same pattern as the protein concentration for the gradient analysis. However, the DNA concentrations are opposite of the protein concentrations for reactor 4. For reactor 6, the

cell concentrations follow the same pattern as the protein concentration for the gradient analysis with the highest concentration being in the bottom section and decreases with increasing height. For reactor 6, the DNA concentration is highest in the bottom section of the reactor.

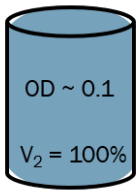

PBR #2	Protein (µg/g sand)	DNA (µg/mg sand)	Cells/mg sand
Top	22.0	-	4.93E+06
Middle	21.8	1.96E-06	3.22E+06
Bottom	14.1	1.474E-06	2.92E+06

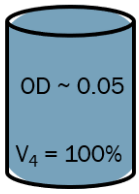

PBR #4	Protein (µg/g sand)	DNA (µg/mg sand)	Cells/mg sand
Top	17.4	5.789E-06	1.26E+06
Middle	15.6	2.709E-06	1.17E+06
Bottom	24.8	8.659E-06	1.28E+06

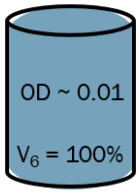

PBR #6	Protein (µg/g sand)	DNA (µg/mg sand)	Cells/mg sand
Top	14.9	2.454E-05	1.26E+06
Middle	15.6	3.535E-05	6.0E+06
Bottom	25.1	1.046E-05	1.14E+07

Figure E4. Protein (µg/g sand), DNA (µg/mg sand), and cells/g sand measurements for reactors 2, 4, and 6.

The measured optical density for planktonic samples from each reactor is shown in Figure E5. The optical densities for all six reactors decreased over time with the exception of reactor 2. The dissolved oxygen measured from planktonic samples for each reactor is shown in Figure E6. The dissolved oxygen did not follow a trend for any of the reactors. The measured pH from planktonic samples for each reactor is shown in Figure E7. The pH increased throughout the experiment for all six reactors. However, for reactor 6 the pH

initially dropped in the beginning of the experiment. The dissolved organic carbon (DOC) measured from planktonic samples for all six reactors is shown in Figure E8. The dissolved organic carbon increased throughout the experiment for all six reactors and eventually stabilized after 8 days for each reactor.

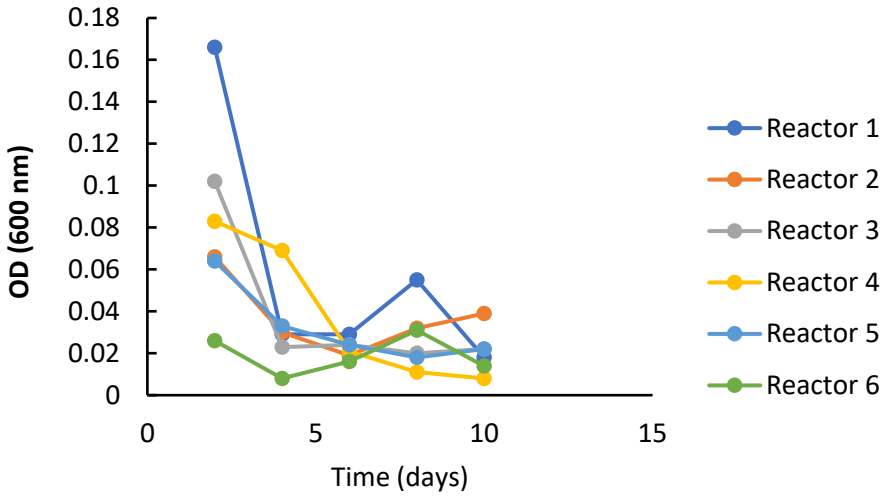

Figure E5. Optical density (OD) measurements for all six reactors at each time point.

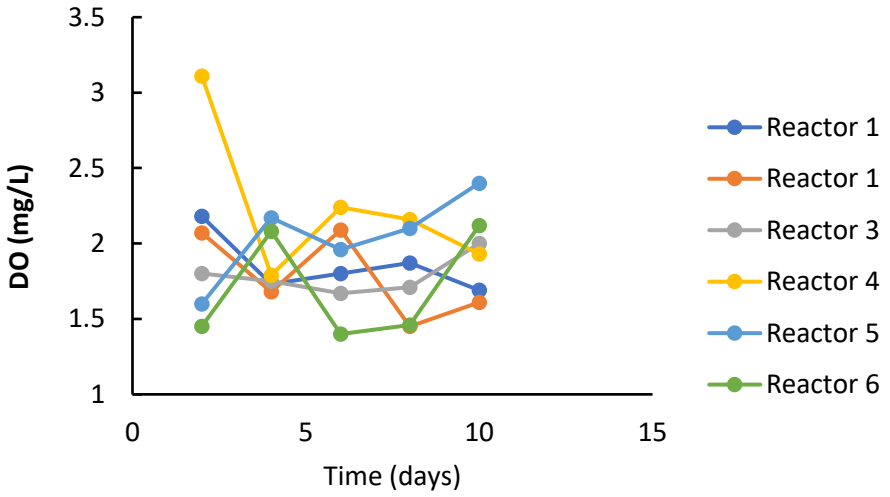

Figure E6. Dissolved oxygen (DO) measurements for all six reactors at each time point.

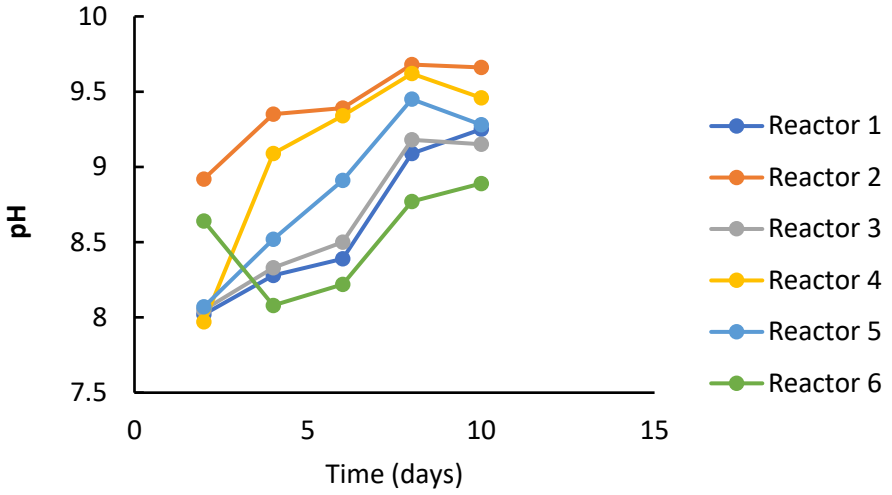

Figure E7. pH measurements for all six reactors at each time point.

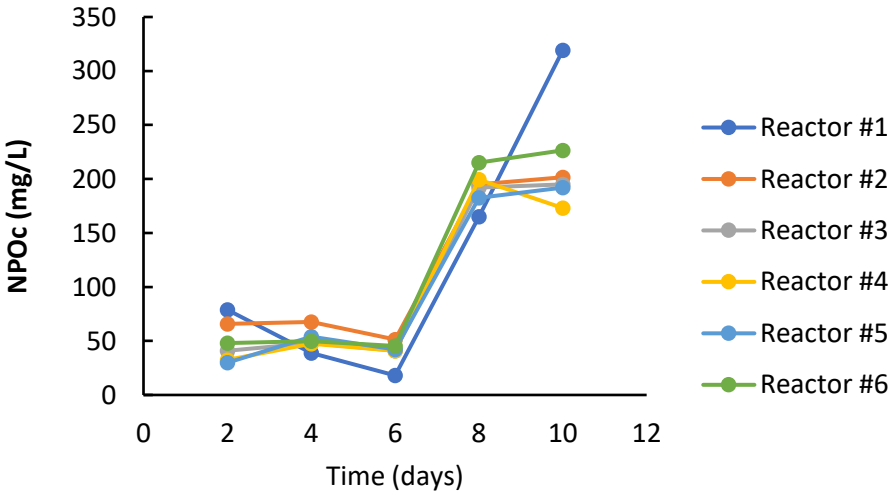

Figure E8. Dissolved organic carbon (DOC) measurements for all six reactors at each time point.

Discussion and Conclusions

There are a range of methods used to inoculate reactors particularly for packed bed reactors, however, it is unknown what methods provide the best biofilm distribution in a porous media environment as well as which method is the most representative of cell distribution in the shallow subsurface environment. This study looked at six different inoculation strategies using a microorganism isolated from the Oak Ridge National Laboratory Field Research Center (ORNL FRC). A more even distribution of biofilm occurs when the reactors are inoculated with 100% of the pore volume. When the reactors are inoculated in a plug-flow style with 10% of their pore volume, there is an uneven distribution of biomass with the majority of biomass distributing in the bottom section of the reactors where they were inoculated. Depending on the experiment, any of these inoculation methods could be used. The inoculation method would be dependent on the study at hand. Inoculating reactors with cell concentrations representative of the environment of interest would be more reproducible and accurate than using optical densities for starting inoculum.